UNDERSTANDING AGGREGATION OF SOLVATING EXTRACTANTS IN APPLIED SEPARATIONS

by

Anna G. Baldwin

© Copyright by Anna G. Baldwin, 2017

All Rights Reserved

A thesis submitted to the Faculty and the Board of Trustees of the Colorado School of Mines in partial fulfillment of the requirements for the degree of Doctor of Philosophy (Applied Chemistry).

Golden, Colorado

Date _____

Signed: _____
Anna G. Baldwin

Signed: _____
Dr. Jenifer C. Shafer
Thesis Advisor

Golden, Colorado

Date _____

Signed: _____
Dr. Thomas Gennett
Professor and Head
Department of Chemistry

ABSTRACT

Solvent extraction is an efficient and effective method for the industrial-scale recovery and purification of metals from mixed raw materials. Understanding the molecular-scale forces driving extraction remains an area of active research despite over 70 years of experience with industrial-scale solvent extraction processes. This thesis presents a series of studies on the extraction chemistry of two extractants relevant to applied separations. The extractant tributyl phosphate (TBP) is used in the Plutonium Uranium Reduction Extraction (PUREX) process for recovering uranium and plutonium from used nuclear fuel. The extractant N,N,N',N'-tetraoctyl diglycolamide (TODGA) is being considered for use in the Actinide Lanthanide Separation (ALSEP) process for separation and purification of lanthanides and minor actinides from PUREX process wastes.

Distribution data collected for the extraction of trace amounts of fission and corrosion products by TBP in the presence of bulk uranium were mostly consistent with extraction through a traditional solvation mechanism. The exeception was the decreased extraction of low valence transition metals with increasing uranium concentration, which suggests another extraction mechanism such as reversed micelle formation. Distribution data collected for lanthanides in a TODGA solvent extraction system were also consistent with a traditional solvation mechanism. The selectivity trend for TODGA across the lanthanide series was found to follow the amount of water co-extracted with each lanthanide, suggesting that the extraction of lanthanides by TODGA is impacted by species in the outer coordination sphere of the extracted complexes.

Diffusion NMR spectroscopy was used to determine the sizes and interactions of colloidal TBP aggregates in 20% TBP samples containing nitric acid, zirconium, and uranium. The aggregate sizes calculated from diffusion experiments were similar to those found previously using small angle neutron scattering (SANS). However, diffusion experiments suggested the

presence of repulsive interactions between aggregates, while prior SANS experiments suggested attractive interactions. Diffusion NMR spectroscopy, rheology, and SANS experiments with 30% TBP samples containing nitric acid, zirconium, and uranium also produced conflicting results when the TBP aggregates were assumed to be colloidal particles. These results suggest that understanding the extraction of metals by TBP on a molecular-scale requires treating TBP aggregates as molecular species.

TABLE OF CONTENTS

ABSTRACT iii

LIST OF FIGURES ix

LIST OF TABLES xi

ACKNOWLEDGMENTS xii

DEDICATION xiii

CHAPTER 1 INTRODUCTION 1

1.1 Industrial Solvent Extraction Processes: TBP and TODGA 4

1.2 Traditional Description of Extraction by Solvation 6

1.3 TBP Non-ideal Solution Behavior and Third Phase Formation 8

1.4 Colloidal and Molecular Approaches to Understanding Extracted Species . . . 11

1.5 Research Objectives and Thesis Summary 13

CHAPTER 2 DISTRIBUTION OF FISSION PRODUCTS INTO TRIBUTYL PHOSPHATE UNDER APPLIED NUCLEAR FUEL RECYCLING CONDITIONS 15

2.1 Abstract 15

2.2 Introduction 16

2.3 Experimental 18

2.3.1 PUREX Feed Simulant Composition 18

2.3.2 Materials 20

2.3.3 Radiotracer Production 21

2.3.4 Solvent Extraction Studies 21

2.3.5 Determination of Distribution Ratios . . . 23

2.4 Results and Discussion . . . 23

2.4.1 Fission and Corrosion Product Chemistry in the PUREX Process . . . 23

2.4.2 Distribution under Extraction Conditions . . . 24

2.4.3 Distribution under Stripping Conditions . . . 27

2.4.4 Impact of TBP Degradation Products on Trace Metal Extraction . . . 29

2.5 Conclusions . . . 29

2.6 Acknowledgements . . . 30

CHAPTER 3 THE IMPACT OF OUTER-SPHERE COORDINATION ON THE LANTHANIDE SELECTIVITY OF DIGLYCOLAMIDE EXTRACTANTS . . . 31

3.1 Abstract . . . 31

3.2 Introduction . . . 31

3.3 Experimental . . . 34

3.3.1 Solvent Extraction Studies . . . 34

3.3.2 Maximum Organic Phase Lanthanide Concentration . . . 35

3.4 Results and Discussion . . . 36

3.4.1 Limiting Organic Concentrations . . . 36

3.4.2 Distribution Data . . . 38

3.4.3 Trends in Water Co-extraction . . . 39

3.5 Conclusions . . . 42

CHAPTER 4 TRIBUTYL PHOSPHATE AGGREGATION IN THE PRESENCE OF METALS: AN ASSESSMENT USING DIFFUSION NMR SPECTROSCOPY . . . 44

4.1 Abstract . . . 44

4.2 Introduction 45
4.3 Experimental Section 49
4.3.1 Materials 49
4.3.2 Solvent Extraction Experiments 49
4.3.3 Pulsed-Field Gradient Stimulated Echo Experiments 52
4.4 Results and Discussion 55
4.4.1 Diffusion Coefficient and Inter-aggregate Interaction Models 55
4.4.2 Aggregate Sizes - Comparison of NMR and SANS 56
4.4.3 NMR Aggregate Sizes - Comparison Between Samples 59
4.4.4 Diffusion in the Third Phase 60
4.4.5 Aggregate Interactions 61
4.4.6 Repulsive Interactions: Ramifications for Scattering Interpretations . . 64
4.4.7 Potential Explanation for Repulsive Interactions 64
4.5 Summary and Conclusions 66
4.6 Acknowledgements 67
CHAPTER 5 THE STRUCTURE OF TRIBUTYL PHOSPHATE SOLUTIONS: NITRIC ACID, URANIUM (VI), AND ZIRCONIUM (IV) 68
5.1 Abstract 68
5.2 Introduction 69
5.3 Experimental Section 74
5.3.1 Materials 74
5.3.2 Sample Preparation and Characterization 74
5.3.3 Diffusion Coefficient Measurements 74

5.3.4 Viscosity Measurements . . . 75
5.3.5 SANS Measurements . . . 75
5.3.6 SANS Data Analysis . . . 77
5.3.7 Molecular Dynamics Simulations . . . 78
5.4 Results and Discussion . . . 79
5.4.1 Diffusion Data - Colloidal Interpretation . . . 79
5.4.2 Viscosity Data - Colloidal Interpretation . . . 81
5.4.3 SANS Data - Colloidal Interpretation . . . 82
5.4.4 Structures from Molecular Dynamics Simulations . . . 89
5.4.5 Diffusion Data - Molecular Interpretation . . . 92
5.5 Conclusions . . . 94
5.6 Acknowledgements . . . 94
CHAPTER 6 SUMMARY AND CONCLUSIONS . . . 96
6.1 Future Directions . . . 99
REFERENCES CITED . . . 102
APPENDIX A SELECTED METHODS . . . 116
A.1 Diffusion NMR Spectroscopy . . . 116
A.2 Small Angle X-ray and Neutron Scattering . . . 119
APPENDIX B SUPPORTING INFORMATION . . . 121
APPENDIX C COPYRIGHT PERMISSIONS . . . 124

LIST OF FIGURES

Figure 1.1 TBP and TODGA molecular structures 3

Figure 1.2 PUREX process schematic. 5

Figure 2.1 Trace metal distribution at 3 M HNO_3 26

Figure 2.2 Trace metal distribution at 0.1 M HNO_3 28

Figure 3.1 TODGA molecular structure 32

Figure 3.2 Lathanide ionic radii and TODGA distribution ratios 33

Figure 3.3 Lanthanide LOCs in TODGA 38

Figure 3.4 TODGA distribution ratio dependence on lanthanide concentration 39

Figure 3.5 Water co-extracted by TODGA with lanthanides 40

Figure 3.6 Trends in water and lanthanide extraction by TODGA 41

Figure 4.1 TBP molecular structure 46

Figure 4.2 Schematic TBP reversed micelle 47

Figure 4.3 STE-LED pulse sequence 53

Figure 4.4 NMR spectrum for TBP 54

Figure 4.5 NMR signal attenuation during diffusion measurements 54

Figure 4.6 TBP aggregate diameters from NMR and SANS 58

Figure 4.7 Effect of dilution on TBP diffusion 62

Figure 5.1 TBP molecular structure 69

Figure 5.2 Viscosity change with TBP concentration in Zr sample 82

Figure 5.3 Baxter model fit to SANS data 85

Figure 5.4 TBP aggregate sizes in samples with different TBP concentrations 87

Figure 5.5 MD simulation boxes of TBP/nitric acid 90

Figure 5.6 TBP species in MD simulations 90

Figure 5.7 TBP aggregation number distribution 91

Figure 5.8 Diffusion of TBP and nitric acid in 30% TBP samples 93

Figure A.1 NMR sample in a gradient coil 117

Figure A.2 Spin-echo pulse sequence 117

Figure A.3 Stimulated-echo pulse sequence 118

Figure A.4 Small angle scattering setup 120

LIST OF TABLES

Table 2.1 PUREX feed simulant composition 19

Table 2.2 PUREX feed simulant preparation 21

Table 2.3 Trace metal TBP distribution experimental conditions 22

Table 4.1 Diffusion sample compositions 51

Table 4.2 TBP diffusion results 63

Table 5.1 Diffusion and SANS sample compositions 76

Table 5.2 MD simulation compositions 79

Table 5.3 TBP aggregate sizes from the Stokes-Einstein and Wilke-Chang equations . 80

Table 5.4 SANS model parameters and percolation threshold 86

ACKNOWLEDGMENTS

First, I would like to thank my advisor, Dr. Jenifer C. Shafer, for her endless patience, kindness, and support. I am very grateful to have been one of the first students advised by such an exceptional and accomplished scientist. This thesis would not have been possible without her guidance.

I would also like to thank the engineers and scientists who helped me as I got to do some of the most fun research I could never have imagined when I started. I am grateful to Dr. Yuan Yang for her patient NMR spectroscopy instruction. I still have so much more to learn! Thank you to Dr. Ross J. Ellis for his mentorship at Oak Ridge National Laboratory and delightful discussions about solvent extraction. Thank you to my thesis committee for their input along the way, and for helping me avoid dead ends. And thank you to many others, who helped me find chemicals in strange labs or trained me on new equipment or pointed me in the direction of so many interesting ideas. This project has been successful because of the many ways they contributed.

For my niece and nephew, Riley and Zac, who are the future.

CHAPTER 1

INTRODUCTION

Solvent extraction is an important technique for separating components in a solution based on differences in their distribution between two immiscible solvents. Prior to the advances in nuclear technology that occurred in the 1940s, solvent extraction was primarily used for laboratory scale separations of organic compounds[1]. Its widespread use in large scale inorganic systems can be traced back to the design and construction of a uranium purification plant at the Mallinckrodt Chemical Works in St. Louis during World War II. This plant scaled up an analytical method for the determination of uranium that relies on the extraction of uranium by ether[2, 3]. At an industrial scale, solvent extraction has the benefit of being able to be run as a continuous, multistage process. The speed and effectiveness of such separations have made it an attractive choice for recovering pure metals from ores and other raw materials in the metallurgical industry. Recovery of these metals would otherwise require a series of selective batch precipitations and crystallizations, which have a low throughput and limited ability to produce metals of very high purity[4, 5].

Despite over 70 years of experience in the design and construction of solvent extraction plants, a comprehensive theoretical framework for predicting the thermodynamic properties of these systems at high solute and extractant concentrations remains an elusive goal. An accurate predictive model of metal partitioning under these conditions would allow for the design and optimization of process flowsheets with a minimum of liquid-liquid equilibrium distribution data, reducing the costs associated with the development of new extraction plants[6]. It could also be used to efficiently determine trace metal compositions of purified metals produced in different solvent extraction facilities using computational process modeling. This latter application is relevant to the field of nuclear forensics, where such trace metal compositions could be used to identify the origin of interdicted nuclear material

produced by solvent extraction[7]. The development of a rigorous thermodynamic model for predicting the behavior of solvent extraction systems requires a fundamental understanding of the composition, structures, and interactions of chemical species in both the aqueous and organic phases of a solvent extraction system. Thermodynamic models combining theoretical insight and experimental data have already been developed for predicting the behavior of aqueous phase species in concentrated systems[8–11]. However, no similarly well-developed correlations exist for organic phase species.

This research focuses on understanding the chemical behavior and structures of organic phase species in tributyl phosphate (TBP) and N,N,N',N'-tetraoctyl diglycolamide (TODGA) extraction systems under conditions similar to those that might be found in industrial scale processes. The chemical structures of these neutral solvating extractants are shown in Figure 1.1. TBP is the extractant used in the Plutonium Uranium Reduction Extraction (PUREX) process for selectively recovering uranium and plutonium from irradiated nuclear fuel[12]. The PUREX process was developed in the early 1950s, and is the predominant industrial-scale reprocessing method used in the nuclear industry. The more recently developed TODGA extractant is part of the class of neutral diglycolamide derivatives whose extraction behavior was first investigated in the early 2000s[13]. TODGA has a high affinity for trivalent f-block elements and has been proposed for use in the Actinide Lanthanide Separation (ALSEP) process for recovering minor actinides and lanthanides from PUREX raffinates[14]. TODGA may also have applications in the separation of light and heavy lanthanides[15].

A multipronged approach is used to understand the extraction chemistry of TBP and TODGA in systems with high aqueous phase concentrations of inorganic solutes and high organic phase concentrations of extractant. In the past, fundamental studies of molecular-scale solvent extraction behavior have focused on systems in which the concentrations of metal and extractant were on the order of one to ten mM. The results of these studies have been assumed to apply under concentrated conditions, although the evidence to support

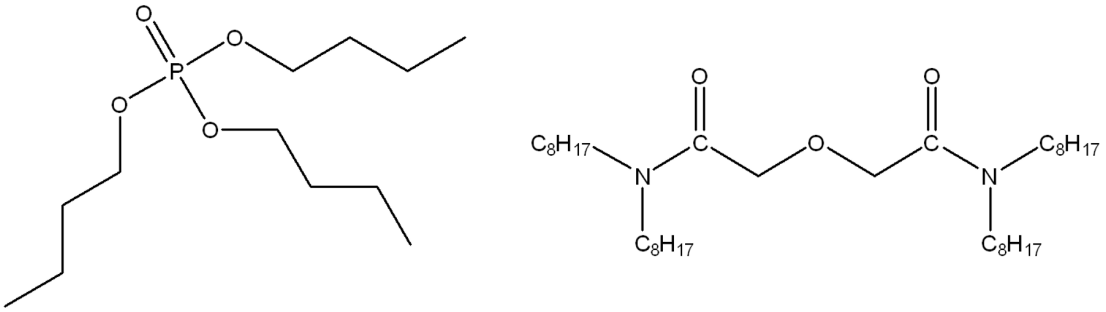

Figure 1.1: Tributyl phosphate (TBP), left, and N,N,N',N'-tetraoctyl diglycolamide (TODGA), right, are solvating extractants with applications in industrially-relevant separations processes.

such an extrapolation is limited. Here, the focus is on solvent extraction systems with metal and extractant concentrations that are on the order of ten to one hundred mM—one to two orders of magnitude greater than in many past studies. The examination of solvent extraction systems more closely approximating the concentrated conditions found in industrial processes eliminates the need to extrapolate from data collected under dilute conditions, and allows for a direct investigation of extraction chemistry in applied, industrial-scale separations.

The methods used to understand the extraction of metals by TBP and TODGA include both routine and state-of-the-art techniques. The bulk extraction chemistry of TBP and TODGA is understood using distribution studies and comprehensive chemical characterization of organic and aqueous phase samples at equilibrium under varying conditions of acid and metal loading. These methods have been used to understand solvent extraction of organic and inorganic compounds for over 100 years[16]. The microscopic structures of extracted species are investigated using diffusion nuclear magnetic resonance (NMR) spectroscopy, rheology, and small angle neutron scattering (SANS). These methods have been used for at least 40 years to characterize colloidal systems. Viscosity measurements of organic phase solvent extraction samples have been used over a similar period of time. However, the application of diffusion NMR spectroscopy and small angle scattering techniques to solvent extraction systems is a relatively recent development, occurring only within the last 20 years.

In brief, the sequence of work covered in this document proceeds from the use of established to more sophisticated techniques to advance the overall goal of understanding the molecular-scale forces and structures found in the organic phase of TBP and TODGA solvent extraction systems. The remainder of this chapter will cover essential background related to the extraction of inorganic species by TBP and TODGA. This includes the industrial applications of TBP and TODGA, the traditional understanding of their extraction mechanisms, and a survey of recent work. It ends with a listing of specific research objectives and a summary of the chapters making up the body of this thesis.

1.1 Industrial Solvent Extraction Processes: TBP and TODGA

Nuclear reprocessing is used to separate and recycle the components of used nuclear fuel that have potential for further use in energy generation. It also reduces the volume of radioactive waste that must be stored in long-term geological repositories. The PUREX and ALSEP processes were both developed to aid in the management of nuclear waste. In the PUREX process, an organic phase consisting of 30 v/v % TBP dissolved in an aliphatic hydrocarbon diluent preferentially extracts tetravalent plutonium and hexavalent uranium, leaving trace metal impurities behind in an immiscible aqueous phase[17]. This aqueous feed initially consists of irradiated nuclear fuel dissolved in molar nitric acid. A series of continuous, countercurrent solvent extraction steps follow, using process equipment such as mixer-settler banks or centrifugal contactors. After extraction, uranium and plutonium are stripped back into the aqueous phase one at a time by controlling the oxidation state of plutonium and the aqueous phase acidity. These separation steps result in two product streams of uranium and plutonium, which then undergo additional purification. Finally, these streams are converted to uranium and plutonium solids, often oxides. The PUREX process is shown schematically in Figure 1.2.

The waste stream that results from the PUREX process contains minor actinides, lanthanides, and transition metals. The volume of radioactive waste produced after PUREX reprocessing can be further reduced by separating and fissioning the minor actinides in fast

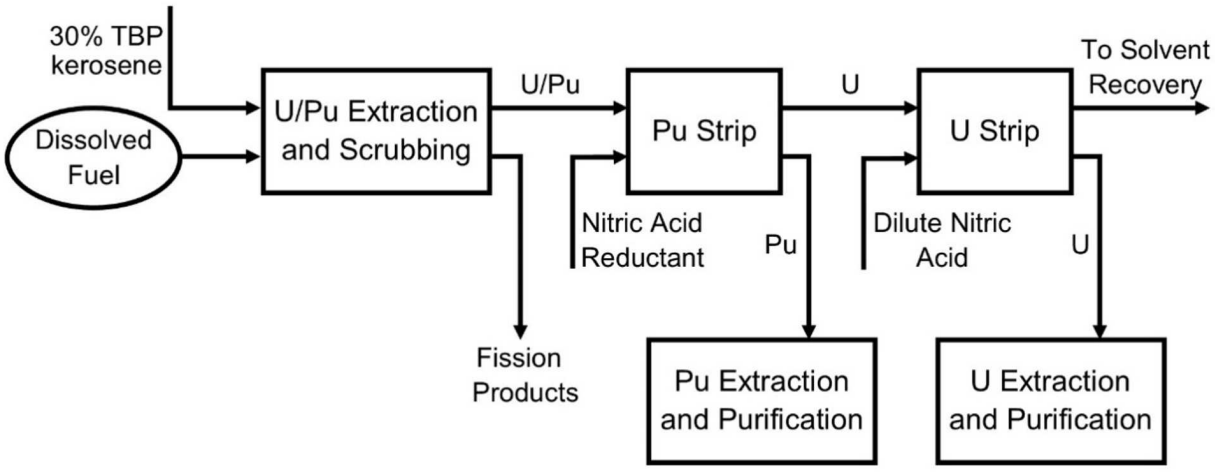

Figure 1.2: PUREX process schematic. Plutonium and uranium are often converted to their oxide forms after final purification.

reactors. However, trivalent lanthanides in PUREX wastes have chemistries similar to trivalent minor actinides but cannot be put in a fast reactor due to their significant nuclear interactions with neutrons. The established approach to the separation of these elements on an industrial scale requires two different solvent extraction processes - one to separate the trivalent lanthanides and actinides from the PUREX waste stream, and one to separate the minor actinides from the lanthanides. The proposed ALSEP process attempts to separate trivalent lanthanides and actinides from PUREX raffinates and each other in a single solvent extraction process.

In the ALSEP process, trivalent lanthanides and actinides are first separated from PUREX raffinates by extraction by TODGA or a similar diglycolamide derivative in the presence of an acidic organophosphorus extractant and an aliphatic hydrocarbon diluent[14]. TODGA has a high affinity for trivalent f-block elements, and is a particularly strong extractant for the lanthanides[13]. Initially, TODGA extracts both trivalent actinides and lanthanides from the PUREX raffinates into the organic phase, which is prevented from splitting into two organic phases by the acidic extractant. The minor actinides are then stripped from the organic phase by an aminopolycarboxylic acid and citrate buffered aqueous phase. This

aminopolycarboxylic acid complexes the minor actinides, which are not as strongly retained by the solvent as the lanthanides. The lanthanides are then stripped from the organic phase by a more strongly complexing aminopolycarboxylic acid capable of competing with the extracting power of TODGA, and the solvent is recycled.

1.2 Traditional Description of Extraction by Solvation

Traditionally, the extraction of inorganic species by neutral solvating extractants like TBP and TODGA has been considered to proceed through the formation of discrete stoichiometric solvates in the organic phase. This extraction mechanism can be understood as a series of steps in which water-solvated anions and cations associate in the aqueous phase to form neutral species, which are then solvated by unionized extractant molecules and transferred to the organic phase[18]. In the case of TBP and TODGA, the phosphate and amide groups belonging to each molecule are sufficiently basic to fully dehydrate the extracted metal, so that both extractants interact directly with the cation in the extracted complex. The number of TBP or TODGA molecules required to extract a mononuclear complex is dependent on the oxidation state of the metal according to the extraction equilibria shown in Equations 1.1–1.6.

$$M^{3+}{}_{(aq)} + 3\,{NO_3}^-{}_{(aq)} + 3\,TBP_{(org)} \rightleftharpoons M(NO_3)_3TBP_{3(org)} \tag{1.1}$$

$$M^{4+}{}_{(aq)} + 4\,{NO_3}^-{}_{(aq)} + 2\,TBP_{(org)} \rightleftharpoons M(NO_3)_4TBP_{2(org)} \tag{1.2}$$

$${MO_2}^{2+}{}_{(aq)} + 2\,{NO_3}^-{}_{(aq)} + 2\,TBP_{(org)} \rightleftharpoons MO_2(NO_3)_2TBP_{2(org)} \tag{1.3}$$

$$M^{3+}{}_{(aq)} + 3\,{NO_3}^-{}_{(aq)} + 3\,TODGA_{(org)} \rightleftharpoons M(NO_3)_3TODGA_{3(org)} \tag{1.4}$$

$$M^{4+}{}_{(aq)} + 4\,{NO_3}^-{}_{(aq)} + 3\,TODGA_{(org)} \rightleftharpoons M(NO_3)_4TODGA_{3(org)} \tag{1.5}$$

$${MO_2}^{2+}{}_{(aq)} + 2\,{NO_3}^-{}_{(aq)} + 3\,TODGA_{(org)} \rightleftharpoons MO_2(NO_3)_2TODGA_{3(org)} \tag{1.6}$$

The equilibria in Equations 1.1–1.6 were inferred from the chemical compositions of organic phases after being fully saturated with metal, and batch distribution studies under

highly dilute conditions.[19, 20] These latter studies were performed under the assumption that extracted species exist in solution as a limited number of distinct chemical species, analogous to traditional coordination compounds[19]. The compositions of these species were determined by measuring the distribution ratios of individual metals while varying the extractant concentration in the organic phase. The distribution ratio of a metal is its equilibrium organic phase concentration divided by its aqueous phase concentration. When the logarithm of the distribution ratio is plotted versus the logarithm of the extractant concentration, the slope of the resulting line corresponds to the number of extractant molecules in the extracted complex. This analysis requires assumptions of ideal solution behavior in the organic phase, constant activity coefficients of aqueous phase species, and a constant free extractant concentration in the organic phase[18].

The experimental conditions in these distribution studies were chosen to give validity to all of the necessary assumptions. Systems with low overall metal and extractant concentrations in the organic phase approximate ideal behavior, while the use of a large excess of extractant supports the assumption of a constant free extractant concentration. Constant aqueous phase activity coefficients can be assumed if a constant ionic strength is maintained in the aqueous phase. The stoichiometries of extracted species found using distribution studies can be verified by comparison with bulk composition measurements in metal-saturated systems, and have typically been assumed to apply to the concentrated systems used in industrial scale processes. Deviations from ideal behavior in concentrated systems are then attributed to non-ideality, rather than the formation of different extracted species[21]. If the degree of this non-ideality can be quantified, all of the thermodynamic properties of a solvent extraction system can be predicted, including equilibrium compositions and phase behavior.

Because of TBP's long history of use in the solvent extraction field, a substantial body of literature exists reporting equilibrium compositions of TBP solvent extraction systems under a wide variety of conditions. This includes distribution data for systems with high

concentrations of the major actinides as well as distribution data for trace amounts of nearly all of the elements in the periodic table. The distribution data trends for individual metals are consistent with the equilibria in Equations 1.1–1.6. However, there has not previously been distribution data available in the open literature for trace amounts of many fission product and corrosion impurities in the presence of bulk uranium, conditions similar to those found in the PUREX process. Such data could be used as further validation of these equilibria.

The amount of literature data available for solvent extraction systems in which TODGA is the only extractant is much less than that for TBP. While distribution data for trace amounts of many elements are available, there is a limited amount of distribution data available for concentrated systems. The distribution data that exist show that TODGA's affinity for the lanthanides increases across the series to gadolinium, beyond which the measured distribution ratios are approximately constant. Because of the great chemical similarity among the trivalent lanthanides and their steadily decreasing ionic radii, this behavior seems anomalous. It would be expected that there would be a consistent trend in distribution ratio across the series. The collection of TODGA distribution data for individual lanthanides from across the series at macroscopic concentrations could provide insight into the extraction mechanisms at work, as well as suggest a reason for the high selectivity of TODGA for the light lanthanides.

1.3 TBP Non-ideal Solution Behavior and Third Phase Formation

Organic phases in solvent extraction systems containing TBP in an aliphatic hydrocarbon diluent are observed to split into two liquid phases in equilibrium with the aqueous phase under conditions of high acid and metal loading. The upper, light organic phase consists primarily of diluent, while the middle, heavy organic phase consists primarily of extractant and extracted solutes. This phenomenon is referred to as third phase formation. In the traditional approach to solvent extraction, third phase formation was thought to occur because of the limited solubility of the extracted metal species in the nonpolar diluent. The

improved solubility of extracted metal species in nonpolar aromatic and polar solvents, such as alcohols, supports this hypothesis[22]. However, difficulties associated with determining the activities of organic phase species have made the development of a model capable of describing this phase transition within the framework of non-electrolyte solution theory alone a challenging task that has received limited attention in the literature. Most explanations for the molecular-scale forces responsible for third phase formation in the relevant literature have been limited to speculation supported by observations of macroscale phenomena.

A computational study by Colon *et al.* used thermodynamic modeling to predict metal partitioning under applied conditions in a TBP solvent extraction system also containing water, nitric acid, uranyl nitrate, and *n*-dodecane[23]. This approach predicted equilibrium phase compositions by minimizing the Gibbs free energy of the system, computed by modeling the activities of aqueous phase species using the Pitzer model and assuming that the organic phase behaves as an ideal mixture. When apparent thermodynamic parameters for organic phase species derived from equilibrium data are used in this model, it is able to accurately reproduce experimentally determined equilibrium aqueous and organic phase compositions. This modelling approach is effective as long as the system is not close to the third phase limit. However, the assumption of ideal behavior by organic phase species makes it incapable of describing the separation of the organic phase into two liquid phases.

Recently, progress has been made in explaining third phase formation in solvent extraction systems through the application of concepts and methods developed to describe the microscopic behavior of colloidal suspensions, a type of complex fluid. In 1991, Osseo-Asare suggested that TBP, which is a surface-active amphiphile like many inorganic extractants, might form water, acid, and metal-containing reversed micelles with TBP aggregation numbers greater than those determined in batch distribution studies under dilute conditions. In 1999, Erlinger *et al.* proposed that third phase formation observed in a diamide extractant organic phase could be attributed to substantial aggregation resulting from attractive interactions between acid and metal-containing reversed micelles in competition with dispersive

thermal energy. In order to analyze small angle X-ray scattering (SAXS) data for organic phase diamide samples, the samples were assumed to consist of reversed micelles modeled as monodisperse hard spheres interacting through surface adhesion. This interparticle interaction model, developed by Baxter in 1968, was used to determine the sizes of diamide aggregates and the strength of the attractive interactions between them by varying the values of the aggregate diameter and stickiness parameter, τ^{-1}, until a good fit to the data by the model was achieved. The stickiness parameter is directly proportional to the strength of the attractive interactions between adhesive hard spheres, such that higher values of τ^{-1} correspond to stronger attractive interactions.

Since 2003, the Baxter model has been used to interpret SAXS and SANS data for organic phase TBP samples containing water, nitric acid, and several metals[24–30]. The results for TBP aggregate sizes and interactions in these small angle scattering investigations have been consistent across samples containing different metals and inorganic acids, which were assumed to have been extracted in TBP reversed micelles modeled as monodisperse adhesive hard spheres. These SAXS and SANS experiments suggest that TBP aggregates consist of two to five TBP molecules interacting through a strong attractive surface potential with τ^{-1} values between approximately 6 and 12. Assuming a thin square well potential with a well width of 10% of the hard sphere diameter, this corresponds to well depths ranging from approximately 1.6 to 2.3 k_BT, with deeper well depths found in samples at compositions approaching third phase formation. This trend in the strength of the attractive interactions between aggregates supports the idea that third phase formation results from increasing attractive interactions with increasing metal and acid extraction.

While small angle scattering studies have been successful in determining an approximate empirical threshold value for τ^{-1} beyond which third phase formation takes place in TBP systems, they do not relate this phase transition to specific thermodynamic quantities characteristic of the components in these systems. The Baxter model is useful insofar as it suggests a mechanism for third phase formation, however, there is no way to predict this

phase boundary from the composition of a system. Given the identities of an extractant, diluent, and metal, the Baxter model does not suggest a way to predict the greatest concentration of metal that can be extracted into the organic phase before a third phase is formed by relating the τ^{-1} for a system to its composition. For the results of these small angle scattering experiments to have practical significance, they must be connected back to some fundamental property of the systems under investigation. The development of thermodynamic models for solvent extraction systems based on a molecular understanding of extraction requires still further experimental investigation. The most useful solvent extraction solution model would be able to quantify the activities of organic phase species in such a way that both extraction equilibria and the third phase transition could be predicted from a minimum of experimental data.

1.4 Colloidal and Molecular Approaches to Understanding Extracted Species

Relating the results of small angle scattering experiments to the structures formed by TBP in solution requires first, a general understanding of the species formed in solution and their dominant length-scales, and, second, a model that can be used to attribute bulk measurements of equilibrium phenomena, like small angle scattering patterns, to specific chemical species. The first requirement impacts the nature of the theoretical treatment needed to fulfill the second requirement because the simplest model capable of capturing the behavior of a solute depends on the size of the solute relative that of the solvent. Prior small angle scattering experiments with TBP solvent extraction samples have relied on the assumption that TBP extracted species are colloidal. TBP species were treated as mesoscopic particles suspended in a continuum fluid, similar to reversed micelles or macromolecules. This assumption allows small angle scattering data to be interpreted with relative ease using simplified particle scattering models. However, the justification for using this approach relies almost entirely on speculation that such structures may exist, rather than material evidence that they do[31, 32].

One way to establish that organic phase TBP samples are colloidal systems is to compare the results of different experimental methods for a set of identical samples, interpreting the data from a colloidal perspective. This is the approach used in this thesis. The theoretical treatment of colloidal systems is relatively straightforward because they fall in the hydrodynamic regime. A simplified model of particles moving in a hydrodynamic field can be used to relate experimentally-accessible quantities in systems in the hydrodynamic regime to molecular-scale forces and structures. The hydrodynamic field in this model represents the solvent. If the experimental results for different experimental methods using a colloidal approach are in agreement, this suggests that the colloidal treatment of TBP extracted species is valid. However, if the results are contradictory, this suggests that considering organic phase TBP solvent extraction samples as molecular solutions may be a more appropriate model to use in understanding small angle scattering data and extraction by TBP in general.

The theoretical treatment of molecular solutions is much more challenging than the treatment of colloids. This is because of the need to explicitly address the interactions among the different species in a molecular solution, which strongly impact their equilibrium properties. The shapes of the solvent and solute molecules, the directionality and strength of their interactions, and the mass densities of each type of molecule impact chemical behavior and structures in these systems. Models relating small angle scattering and other experimental measurements to molecular-scale phenomena must take these attributes into account. Because of this complexity, all-atom molecular dynamics (MD) simulations are the most effective means of modeling behavior in molecular solutions. However, MD models must be rigorously developed and validated before they can be used to relate molecular-scale phenomena to experimental observations. Regardless, if TBP does not form colloidal species, such computational methods will be important in understanding solvent extraction at a fundamental level.

1.5 Research Objectives and Thesis Summary

The primary objectives of the work described in this thesis and their underlying hypotheses are as follows:

Objective 1: Collect distribution data in TBP and TODGA solvent extraction systems under concentrated conditions that have not been previously characterized in the literature.

Hypothesis 1.1: The extraction of trace metals by TBP and lanthanides by TODGA adhere to a traditional solvation mechanism.

Hypothesis 1.2: The selectivity of TODGA for the light lanthanides results from outer coordination sphere effects.

Objective 2: Compare the results of diffusion NMR spectroscopy and SANS studies of organic phase TBP samples interpreted from a colloidal perspective.

Hypothesis 2.1: Like small angle scattering techniques, diffusion NMR spectroscopy can be used to characterize the nitric acid, uranium (VI) nitrate, and zirconium (IV) nitrate species extracted by TBP.

Objective 3: Assess the use of colloidal models to describe organic phase TBP samples by comparing the results of diffusion NMR spectroscopy, rheology, and SANS studies of samples under concentrated (PUREX-like) conditions.

Hypothesis 3.1: Nitric acid, uranium (VI) nitrate, and zirconium (IV) nitrate are extracted by TBP as colloidal species under PUREX-like conditions.

Chapters 2 and 3 describe batch distribution studies performed to determine the distribution ratios of metals in industrially-relevant solvent extraction systems under applied

conditions. For TBP, this refers to the distribution of fission and corrosion product impurities under representative PUREX conditions. For TODGA, this means the extraction of macroscopic amounts of lanthanides by a concentrated TODGA organic phase. Chapter 4 describes the use of diffusion NMR spectroscopy to characterize TBP structures formed in samples assuming the existence of colloidal aggregates. The results of this NMR spectroscopy investigation are compared with prior SANS experiments using similar samples. Chapter 5 compares the results of diffusion NMR spectroscopy, rheology, and SANS investigations interpreted from a colloidal perspective. Conflicts among the results of these experimental methods suggest that TBP solutions should not be treated as colloids, a conclusion supported by MD simulations. The final chapter integrates the results of these studies, and provides suggestions for future work.

CHAPTER 2

DISTRIBUTION OF FISSION PRODUCTS INTO TRIBUTYL PHOSPHATE UNDER APPLIED NUCLEAR FUEL RECYCLING CONDITIONS

Modified from a paper published in *Industrial & Engineering Chemistry Research*[1]

Anna G. Baldwin[2], *Nicholas J. Bridges*[3], *Jenifer C. Braley*[4]

2.1 Abstract

Tributyl phosphate (TBP) is an important industrial extractant used in the Plutonium Uranium Redox Extraction (PUREX) process for recovering uranium and plutonium from used nuclear fuel. Distribution data have been assessed for a variety of fission and corrosion product trace metals at varying uranium concentrations under representative PUREX extraction (3 M HNO_3) and stripping (0.1 M HNO_3) conditions. As might have been anticipated, the extraction of most trace metals was found to decrease or remain constant with increasing uranium concentration. In contrast, the extraction of some low valence transition metals was found to increase with increasing uranium concentration. The increase in extraction of low valence transition metals may be related to TBP forming reverse micelles instead of recovering uranium as a classical $UO_2(NO_3)_2(TBP)_2$ coordination complex. The low valence transition metals may be being recovered into the cores of the reverse micelles. Also unanticipated was the lack of impact the TBP degradation product, dibutyl phosphate (DBP), had on the recovery of metals in batch distribution studies. This is possibly related to the batch contacts completed in these experiments not adequately recreating the multi-

[1]Adapted with permission from *Industrial & Engineering Chemistry Research* **2016** *55* (51), 13114-13119. Copyright 2016 American Chemical Society.
[2]Primary author and researcher
[3]Co-author, Savannah River National Laboratory
[4]Corresponding author and advisor

stage aspects of industrial-scale uranium extraction done using mixer settlers or centrifugal contactors.

2.2 Introduction

The extractant tributyl phosphate (TBP) has been used for the industrial-scale recovery of actinides in nearly all stages of the nuclear fuel cycle over the past 60 years[33]. In that time, a substantial amount of TBP extraction data has been published under numerous experimental conditions[34]. Extraction studies have examined the partitioning of various metals and metal compositions[35–40], the impact of acid types and concentrations[41], and diluents[42]. Data collected in support of industrial-scale processes used to separate uranium from used nuclear fuel for recycling have focused on the combined extraction behavior of high concentrations of uranium, low concentrations of plutonium and select problematic fission products[17, 43–45]. Similarly, TBP extraction data collected in support of nuclear waste remediation processes have focused on the recovery of a variety of fission and corrosion products in the presence of very low concentrations of uranium[46]. As a whole, these data have been essential to the scale-up of solvent extraction processes involving TBP. However, the solvent extraction behavior of many fission and corrosion products simultaneously recovered in the presence of bulk uranium remains an area where data is lacking in the open literature.

The design and predictive modeling of industrial scale solvent extraction processes rely on data collected under conditions closely approximating those found in the final process. Industrial-scale solvent extraction processes using TBP for uranium recovery have been refined to the extent that the recovery of poorly extracted, low-concentration metals in the presence of bulk uranium may need to be assessed to further optimize these separations[47]. A predictive understanding of fission and corrosion products recovery by TBP in these processes also has application in the field of nuclear forensics. Uranium is used in the manufacture of nuclear weapons, and high-purity uranium products are often the result of processes using TBP as an extractant. Trace metal fingerprints arising from the minimal partitioning of fission and corrosion products could be characteristic of the processes used in the

production of any uranium-containing material[7]. Fully understanding these trace metal partitioning patterns may help determine the history of recovered, illegally-trafficked uranium. Ideally, these trace metal fingerprints would be determined through direct chemical analysis of product samples. However, in the case where such samples are difficult to obtain or nonexistent, predictive process modeling could be used to determine characteristic trace metal compositions of uranium products from different industrial processing facilities.

Tributyl phosphate is used for the separation and purification of uranium as part of the Plutonium Uranium Reduction Extraction (PUREX) process[12, 48–50]. In a typical PUREX process, uranium and plutonium in used nuclear fuel are separated from fission and corrosion product impurities in a series of continuous, countercurrent solvent extraction stages. A high concentration of nitric acid is used both to dissolve the nuclear fuel and as a salting-out agent to facilitate the extraction of uranium and plutonium nitrate by the organic phase containing 30 v/v% TBP in a long-chain aliphatic hydrocarbon diluent. A low concentration of nitric acid is used in the stripping and recovery of these purified metals back into the aqueous phase following reduction of plutonium to the trivalent state. In the course of several treatment and recycle steps, the TBP extractant is exposed to high levels of radioactivity and a high concentration of acid. The exposure of TBP to these acid and radiation conditions results in degradation products which are known to impact the decontamination of the plutonium and uranium products[51–53]. The primary degradation product is dibutyl phosphate (DBP), an organic-soluble cation exchange extractant. Limited data also exists regarding the extraction chemistry of trace metals in the presence of DBP under PUREX relevant conditions. This information is also crucial to accurate predictive modeling of PUREX-type processes.

In this work, the extraction behavior of selected trace metals in the presence of bulk uranyl nitrate under representative PUREX conditions were determined using multiple radiotracers simultaneously in a series of batch extraction experiments. A PUREX feed simulant was designed and produced based on previously published calculations of nuclear fuel composition

arising from a typical nuclear power reactor. Changes in the distribution ratios of the metals in this simulant with varying organic phase uranium concentrations and aqueous nitric acid concentrations were explored. Finally, data on the effect of the TBP degradation product, DBP, on trace metal distribution ratios under extraction and stripping conditions were collected.

2.3 Experimental

2.3.1 PUREX Feed Simulant Composition

The PUREX feed simulant is a combination of fission and corrosion product radiotracers, and bulk uranyl nitrate. The calculated composition of pressurized water reactor (PWR) Zircaloy-4 clad UO_2 fuel at approximately 3% enrichment after 20 MWd/kgM burnup was used as the basis for choosing representative fission products. This has been calculated previously by Guenther *et al.* using the ORIGEN2 computer program[54]. Only elements with a concentration greater than 10^{-5} g/g U were included in the simulant. Fission product gases, such as xenon or krypton, were not included, nor were palladium and rhenium because of their high cost and previously reported minor extraction by TBP[40]. The important corrosion products chromium, manganese, iron, and nickel were identified from Izumida *et al.* and are consistent with PUREX raffinate compositions given in Choppin *et al.*[55, 56]. These corrosion products were included in the simulant.

The final choice of fission and corrosion product radiotracers used in the PUREX feed simulant took into account the availability of strong, unique gamma peaks after neutron activation of each element, and their importance in the PUREX process. Table 2.1 shows the final composition of the PUREX feed simulant used in these studies, the anticipated trace metal and uranium concentrations in a typical PUREX feed, utilized radioisotopes, half-lives, and unique gamma peak energies. The activities of the radiotracers used in the PUREX simulant were kept approximately equal to maintain a low detector dead time while also ensuring that each unique peak had sufficient counts. As a result, the concentrations

Table 2.1: PUREX feed simulant elemental composition, radiotracers, and comparison with a typical PUREX feed stream.

Element	*Radioisotope*	*Half-life*	*Gamma Peak (keV)*	*Typical PUREX (mM)*	*PUREX Simulant (mM)*
Cr	^{51}Cr	27.7 days	320.1	0.58	2.51
Fe	^{59}Fe	44.6 days	1099.2	11.10	12.54
Rb	^{86}Rb	18.7 days	1076.6	0.52	12.54
Sr	^{85}Sr	64.9 days	514.0	1.20	1.25
Zr	^{95}Zr	64.0 days	724.2	4.87	25.07
Mo	^{99}Mo	66 hours	181.1	4.17	1.50
Ru	^{103}Ru	39.26 days	497.1	2.41	0.63
Cs	^{134}Cs	2.05 years	604.7	2.57	0.13
La	^{140}La	40.22 hours	487.0	1.06	0.0075
Ce	^{143}Ce	33 hours	293.3	2.03	0.35
Sm	^{153}Sm	46.8 hours	103.2	0.64	0.00075
U	^{235}U	7.04×10^8 years	185.7	1,800	0 - 1,000

of trace metals deviate in most cases from those found in a typical PUREX feed. These differences would be expected to have minimal impact on the distribution ratios measured due to their overall low concentrations. However, future work could benefit from using real used nuclear fuel in the measurement of trace metal distribution ratios under PUREX conditions.

2.3.2 Materials

All chemicals were used as received without further purification. All metal compounds used were of analytical grade. Chromium, iron, rubidium, strontium, and cesium stock solutions were prepared by dissolving their respective solid nitrates in 0.01 M HNO_3. The stock solution containing molybdenum (VI) was prepared by dissolving solid ammonium molybdate in 0.01 M HNO_3. The ruthenium (III) nitrosyl nitrate stock solution was prepared by dissolving solid ruthenium nitrosyl nitrate in 0.01 M HNO_3. Lanthanum (III) and samarium (III) nitrate stock solutions were prepared by dissolving the solid oxides in concentrated nitric acid. A cerium (III) nitrate stock solution was prepared by dissolving solid cerium (IV) oxide in nitric acid and reducing the metal to cerium (III) with hydrogen peroxide. The stock solution of zirconium nitrate was made from hydrous zirconium oxide as described in Chiarizia *et al.* using zirconium (IV) chloride as a starting material[27]. The details of these stock solutions are summarized in Table 2.2. Stock solution of ACS grade uranyl nitrate hexahydrate (International Bio-Analytical Industries, Inc., Boca Raton,FL) at varying concentrations of HNO_3 (3, 0.01, and 0.001 M) were used in the preparation of aqueous solutions.

Organic phases were prepared using 99+% tributyl phosphate from Acros Organics, 97% dibutyl phosphate from Acros Organics, and 99+% *n*-dodecane from Alfa Aesar, as specified. The TBP was washed with 0.1 M NaOH for solvent extraction experiments involving the addition of dibutyl phosphate to the organic phase. The purpose of this wash was to remove acidic impurities (including DBP) from the TBP before adding in the desired amount of DBP. Aqueous phases were prepared using metal stock solutions, ACS grade nitric acid from

Macron Fine Chemicals and degassed, ultrapure (18 MΩ-cm) water.

Table 2.2: Chemicals used in the preparation of the PUREX feed simulant and irradiation times.

Element	*Starting Material*	*Irradiated Form*	*Stock Solution (M)*	*Irradiation Time (hr)*
Cr	$Cr(NO_3)_3 \cdot 9\,H_2O$	Liquid	1	3
Fe	$Fe(NO_3)_3 \cdot 9\,H_2O$	Solid	2.4	8
Rb	$RbNO_3$	Liquid	2	3
Sr	$Sr(NO_3)_2$	Solid	1.2	8
Zr	$ZrO_2 \cdot n\,H_2O$	Solid	0.3	8
Mo	$(NH_4)_2MoO_4$	Liquid	1	3
Ru	$RuNO(NO_3)_3$	Liquid	1	3
Cs	$CsNO_3$	Liquid	0.2	3
La	La_2O_3	Liquid	0.01	3
Ce	CeO_2	Liquid	0.47	3
Sm	Sm_2O_3	Liquid	0.001	3

2.3.3 Radiotracer Production

All radiotracers were produced by neutron irradiation of solid or solution-phase samples of individual metals at the United States Geological Survey TRIGA Reactor (GSTR) in Denver, CO. Specifics about the neutron fluence and irradiation positions have been provided previously[57]. Metals irradiated as solids were dissolved in 0.01 M HNO_3 after irradiation to yield stock solutions at the concentrations given in Table 2.2, except for zirconium which was dissolved in 8 M HNO_3. For metals irradiated as liquids, stock solutions at the concentrations given in Table 2.2 were irradiated directly. Irradiation times are also given in Table 2.2.

2.3.4 Solvent Extraction Studies

Distribution ratios of the trace metals in the PUREX feed simulant under representative PUREX conditions were determined using batch solvent extraction studies at ambient temperature (22 ± 1 °C). All batch extractions were run using 30% TBP in *n*-dodecane previously equilibrated with an aqueous phase containing only nitric acid. Nitric acid, uranium, and DBP concentrations were varied as shown in Table 2.3. The high nitric acid conditions

simulate the extraction step of the PUREX process. The low nitric acid conditions simulate the stripping step. Extraction in the PUREX process is usually run at approximately 70% saturation of the organic phase[17]. This saturation level corresponds to an initial aqueous uranium concentration of 0.42 M in these batch extraction experiments. The variation in the uranium concentration is inclusive of the conditions under which PUREX takes place, but allows for observation of the effect of different uranium concentrations. Similarly, the variation in concentration of DBP used here is inclusive of PUREX conditions. The DBP concentration in a typical PUREX stream has been previously determined to be approximately 170 ppm[58].

Table 2.3: Experimental matrix showing conditions under which trace metal distribution ratios were determined.

Unit Operation	*Initial HNO_3 (M)*	*Initial U (M)*	*Additional DBP (ppm)*
Extraction	3	0 - 0.6	0
Stripping	0.1	0 - 1.0	0
Extraction	3	0.4	0 - 400
Stripping	0.1	0.4	0 - 400
Stripping	0.01	0.4	0 - 400

For each experimental condition, 5 mL volumes of the organic and aqueous phases were used. Immediately before contact, 20 μL of a combined radiotracer solution containing the fission and corrosion product elements given in Table 2.3 was added to the aqueous phase. The organic and aqueous phases were contacted by vortex mixing for 15 minutes. The phases were separated by centrifugation. Subsamples of each phase were collected and counted on a well-type high-purity germanium detector (Canberra GCW2523, FWHM resolution is 1.25 keV at 122 keV). A typical 4 mL organic phase sample was counted for 20 to 24 hours. A typical, 500 μL aqueous phase sample was diluted up to a total volume of 4 mL to give a sample geometry consistent with the organic phase samples and counted for approximately an hour. Equilibrium organic uranium concentrations were determined by using a calibration curve unique to the well-detector used.

2.3.5 Determination of Distribution Ratios

Gamma spectra of each equilibrium solvent extraction phase were analyzed to give the peak areas of each radioisotope's unique gamma peak. The average dead time for aqueous samples was 2.6%. The average dead time for organic samples was 1.0%. Only peaks with at least 1,000 counts, which corresponds to a counting error of 3%, were used. The count rate was then calculated from the count time and peak area. The count rates associated with each radioisotope were decay corrected to give their count rates at the time of phase separation by centrifugation. These were then adjusted for the different sample volumes collected from each phase to give the specific count rates in each phase. These count rates were then divided to give the distribution ratio (D) of each trace metal, as shown in Equation 2.1:

$$D = \frac{C_{org}}{C_{aq}} \tag{2.1}$$

where C_{org} is the decay-corrected count rate in the organic phase, and C_{aq} is the decay-corrected count rate in the aqueous phase. The relative uncertainty in the distribution ratio was calculated by adding the relative standard deviations of the counts measured for each organic and aqueous phase sample.

2.4 Results and Discussion

2.4.1 Fission and Corrosion Product Chemistry in the PUREX Process

The chemical states of all ions in the PUREX feed simulation solution were chosen to simulate those found in real PUREX processes. The PUREX feed simulant fission products with the most complex solution chemistry are ruthenium and zirconium. The solution chemistry of these metals in nitric acid have been studied extensively because of their established roles as problematic impurities in the PUREX process[59]. Ruthenium is known to exist in dissolved nuclear fuel primarily as various nitro- and nitrato- ruthenium (III) nitrosyl complexes whose speciation is time- and concentration-dependent. Each species is extracted substantially differently by TBP[60]. Likewise, the speciation of zirconium (IV) in dissolved nuclear fuel is dependent on the history of the solution. Zirconium is known to polymerize

in nitric acid solution particularly under conditions of low acid or high metal concentration. Zirconium monomers are relatively well-extracted by TBP, while polymers are effectively inextractable[53]. Rather than explore the effects of all the different potential ruthenium and zirconium species on the distribution of these metals, these experiments were designed to improve the reproducibility of ruthenium and zirconium extraction by timing dilution of the ruthenium and zirconium stocks identically between batch extraction experiments. The radiotracer spikes were added immediately (<10 minutes) before contacting the organic and aqueous phases.

All other metals have stable solution chemistry in nitric acid solution. Molybdenum (VI) exists as the molybdate ion in dissolved reactor fuel. The lanthanides exist as mononuclear species in the trivalent state. While some cerium (IV) may form on dissolution of nuclear fuel, cerium is found as cerium (III) in PUREX process streams. The transition metals — chromium (III), iron (III), rubidium (I), strontium (II), and cesium (I) — are found as mononuclear species in their respective dominant oxidation states[59].

2.4.2 Distribution under Extraction Conditions

The extraction of metals by TBP is commonly understood to proceed through the solvation of a neutral metal salt according to the equilibrium relationships given in Equations 2.2 to 2.4[61]. The negative dipole on the phosphoryl oxygen of TBP interacts with the positively charged metal cation, resulting in the formation of a metal solvate. The nonpolar butyl tails of TBP keep the resulting metal solvate dissolved in the aliphatic hydrocarbon diluent.

$$M^{3+}{}_{(aq)} + 3\,NO_3{}^-{}_{(aq)} + 3\,TBP_{(org)} \rightleftharpoons M(NO_3)_3TBP_{3(org)} \tag{2.2}$$

$$M^{4+}{}_{(aq)} + 4\,NO_3{}^-{}_{(aq)} + 2\,TBP_{(org)} \rightleftharpoons M(NO_3)_4TBP_{2(org)} \tag{2.3}$$

$$MO_2{}^{2+}{}_{(aq)} + 2\,NO_3{}^-{}_{(aq)} + 2\,TBP_{(org)} \rightleftharpoons MO_2(NO_3)_2TBP_{2(org)} \tag{2.4}$$

The distribution of trace fission and corrosion products under representative PUREX extraction conditions (3 M HNO_3 in the aqueous phase) with increasing uranium concentration in the organic phase is given in Figure 2.1. The extraction of ruthenium (III) nitrosyl, zirconium (IV), the lanthanides (III), and the molybdate anion were found to decrease with increasing uranium concentration. This would be expected given the high affinity of TBP for uranium (VI) and the limiting concentrations of TBP relative to uranium and other fission or corrosion products. As the amount of uranium increases in the solvent extraction system, it displaces other metals from TBP extracted complexes. In contrast, the extraction of mono-, di-, and trivalent transition metals appears to increase with increasing uranium concentration, suggesting a different mechanism for their extraction. If the extraction of these metals were dependent on the same interaction between the phosphoryl oxygen of TBP and the metal cation, a decrease in their extraction with increasing uranium concentration would be observed. The observed minimum in the chromium distribution ratio curve could be the result of both TBP extraction mechanisms. The decrease in distribution ratio could result from competition for TBP between uranium and chromium at low uranium concentrations, followed by an increase in the distribution ratio as chromium starts to be extracted by the same mechanism as the rest of the low valence transition metals.

Given the extremely low concentrations of the mono-, di-, and trivalent transition metals in the organic phases of these solvent extraction systems, the possibility exists that metal recovery is occurring due to physical entrainment of the metal in the organic phase. The low valence transition metals are at micromolar concentrations in the organic phases of these solvent extraction systems. For comparison, at 25 °C, the solubility of water in pure *n*-dodecane is 65 mg/kg solvent, which corresponds to a concentration of around 3 mM[62]. The extracted metals may not be associated with the TBP extractant, but could instead be independently associated with either the *n*-dodecane diluent or the free water in the organic phase. However, this does not explain the apparent dependence of the extraction of these metals on the uranium concentration.

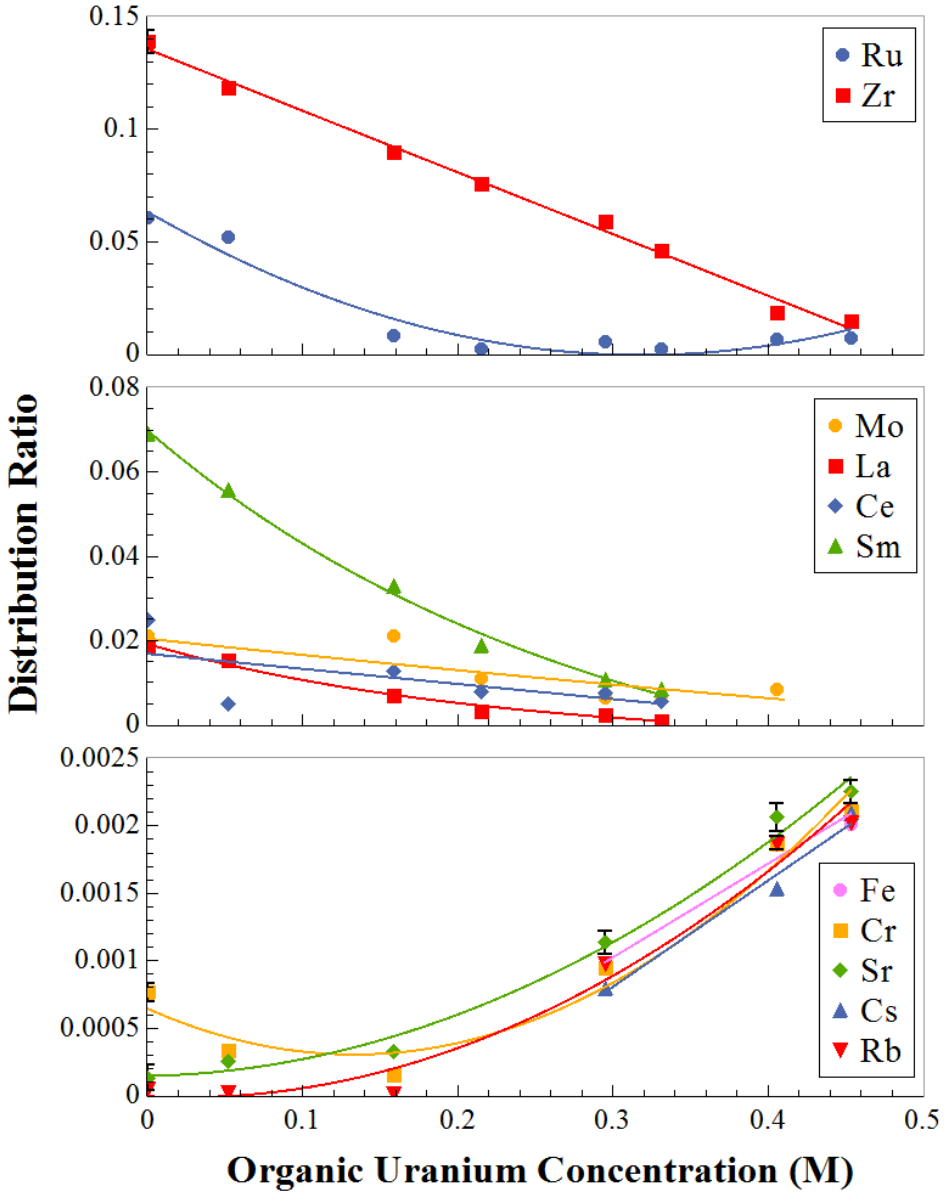

Figure 2.1: Trace metal extraction distribution ratios measured under extraction conditions. Error bars are counting error, and are smaller than the marker if not visible.

Alternatively, these low valence transition metals may be being co-extracted with uranium in the core of the reversed micellar structures formed in solution by TBP. Tributyl phosphate is a surface-active amphiphile with a polar head and nonpolar tails that are necessary for metal extraction. Such molecules are known to self-assemble into complex structures in solution, including reversed micelles[31]. Tributyl phosphate has been noted to form reversed micellar structures in the presence of high concentrations of polar solutes, where the polar solutes are located in the core of the micelle[24, 25, 27]. The low valence transition metals may have sufficiently small hydrated radii, where the bulk of the hydrated radii are made up of metal ion and not long range ordered water, that they are being co-extracted as part of uranium-containing TBP reversed micelles[63]. Such a mechanism would explain the observed increase in extraction of these metals with extracted uranium.

2.4.3 Distribution under Stripping Conditions

The distribution of trace fission and corrosion products under representative PUREX stripping conditions (0.1 M HNO_3 in the aqueous phase) with increasing uranium concentration in the organic phase is given in Figure Figure 2.2. The behavior of these metals under stripping conditions is consistent with expectations. Measured distribution ratios remained low for all metals and either stayed substantially the same or decreased with increasing uranium concentration in the organic phase. Ruthenium was the only metal with appreciable distribution ratios at a low nitric acid concentration. This behavior has been observed previously and attributed to reduced competition for free TBP between ruthenium nitrosyl nitro- and nitrato- complexes and nitric acid at low nitric acid concentrations. These data indicate that if most of these trace metals were in the organic phase following the extraction step of the PUREX process, they would be quantitatively stripped into the aqueous phase along with the uranium product. The lone exception is ruthenium, which would be partially retained in the solvent, possibly contributing to its identity as a problematic trace metal impurity in the PUREX process.

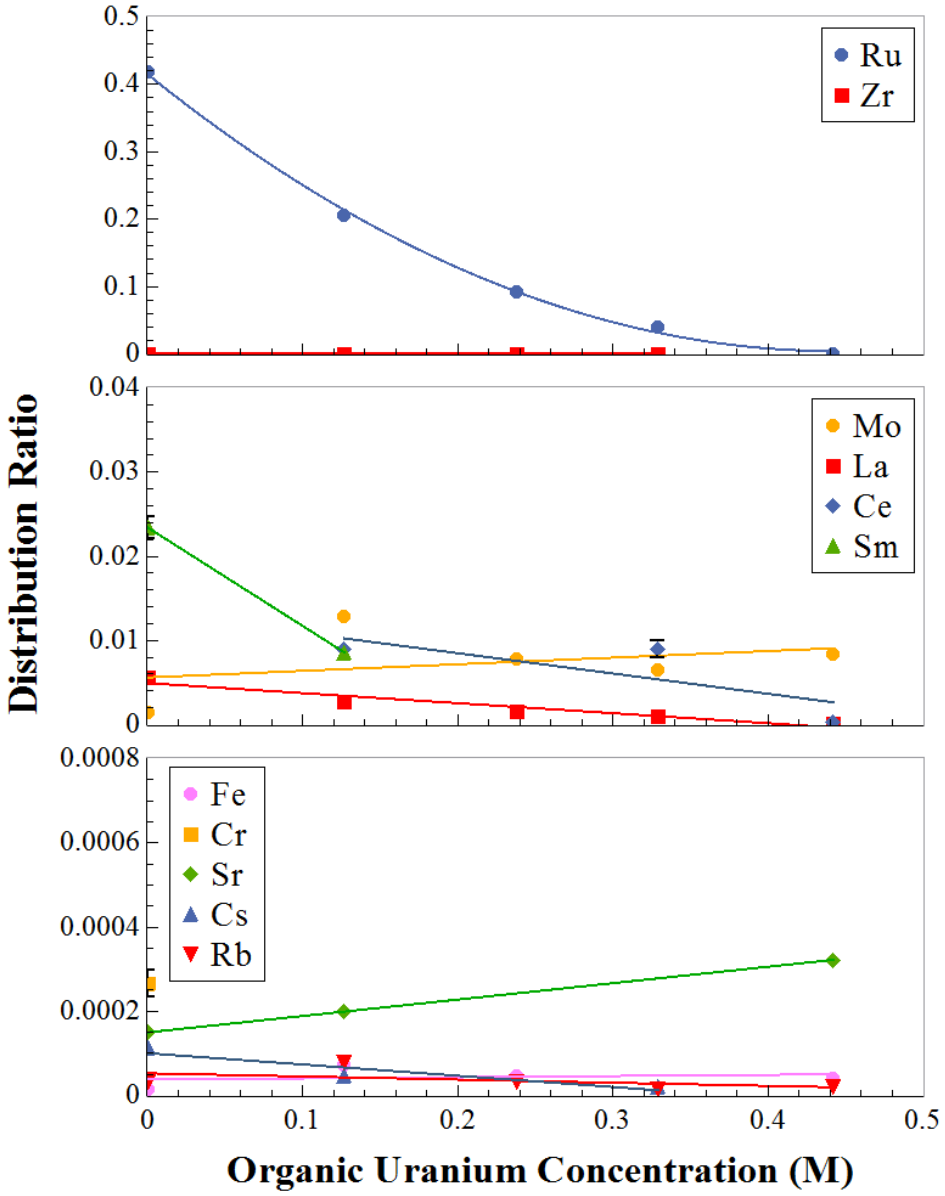

Figure 2.2: Trace metal extraction distribution ratios measured under stripping conditions. Error bars are counting error, and are smaller than the marker if not visible.

2.4.4 Impact of TBP Degradation Products on Trace Metal Extraction

The primary product of the hydrolytic and radiolytic degradation of TBP is DBP, which behaves as a strong ion-exchange extractant. As a much stronger extractant than TBP, DBP is known to extract some transition metals better than TBP, and to retain these metals under stripping conditions[52, 64]. A secondary product is monobutyl phosphate (MBP), which does not compete with the extraction of metals by TBP and is somewhat soluble in the aqueous phase. A series of experiments exploring the addition of small, PUREX process-relevant amounts of DBP (0 to 400 ppm) added to the organic phase under representative PUREX extraction and stripping conditions showed that there was no observable effect of DBP on metal extraction in batch distribution experiments. These results are provided in Appendix B as part of the supporting information.

The presence of TBP degradation products in the PUREX process is known to reduce decontamination of uranium and plutonium streams over the course of several solvent cycles through retention of trace metal impurities in the organic phase. The effect of trace metal accumulation cannot be explored by single batch extraction experiments, which do not reproduce the effect of many solvent extraction stages and cycles. In the batch extractions completed here, the high concentrations of uranium used likely suppressed the expected increase in metal uptake by the organic phase, particularly zirconium[52]. The effects of TBP degradation products on trace metal extraction behavior might better be explored in a multi-stage bench-scale bank of mixer-settlers or centrifugal contactors like those used in the PUREX process. Recycle of the same solvent stream through a series of solvent extraction cycles could shed light on the effect of TBP degradation products on trace metal partitioning.

2.5 Conclusions

Trace metal extraction data for TBP systems containing bulk uranium have not been extensively explored in the past, despite their potential importance to optimizing separations

processes and modeling characteristic trace metal signatures for nuclear forensics applications. The PUREX process for recovering uranium and plutonium from used nuclear fuel is one of the most important industrial-scale processes using TBP as an extractant. In this work, batch distribution studies have been completed under representative PUREX extraction and stripping conditions to find the distribution ratios of select fission and corrosion product trace metals in the presence of uranium. Metal extraction decreases for most of these metals with increasing uranium concentration, as would be expected given the commonly-understood mechanism of TBP extraction. However, under extraction conditions, the distribution ratios of some low valence transition metals were found to increase with increasing uranium concentration. This anomalous behavior must be taken into account when modeling trace metal extraction in the PUREX process.

Batch distribution studies of TBP systems with added DBP were unable to demonstrate the impact of DBP on the extraction of trace metals. This was unexpected because previous studies on the impact of DBP on metal extraction by TBP in the absence of uranium indicated that TBP and DBP extract some metals better than TBP alone[52, 64]. The observed lack of impact of small amounts of DBP on trace metal partitioning is likely because a single batch solvent extraction experiment cannot capture the effects of multistage solvent extraction cycles on extraction behavior. This would be an appropriate area for further consideration, as well as other experiments assessing the possibility of entrainment versus reverse micellar recovery of low valence transition metals.

2.6 Acknowledgements

This invited contribution is part of the I&EC Research special issue for the 2017 Class of Influential Researchers.

This material is based upon work supported by the U.S. Department of Homeland Security under Grant Award Number, 2012-DN-130-NF0001. The views and conclusions contained in this document are those of the authors and should not be interpreted as representing the official policies, either expressed or implied, of the U.S. Department of Homeland Security.

CHAPTER 3

THE IMPACT OF OUTER-SPHERE COORDINATION ON THE LANTHANIDE SELECTIVITY OF DIGLYCOLAMIDE EXTRACTANTS

3.1 Abstract

The extraction of adjacent lanthanides by the solvating extractant tetraoctyl diglycolamide (TODGA) has been explored in distribution studies using a 0.25 M TODGA in *n*-dodecane organic phase and aqueous phases with macroscopic amounts of lanthanides from across the series in nitrate media. The limiting organic concentrations (LOCs) of La, Pr, Sm, Gd, Dy, and Tm form an "S"-shaped curve when plotted against atomic number. The distribution ratios for La, Pr, Sm, and Gd increase with decreasing ionic radius, and decrease with increasing metal concentration, consistent with established extraction behavior. The amount of water co-extracted with each lanthanide was found to increase with decreasing ionic radius, from La to Gd, after which it levels off. This trend is similar to the trend observed for the extraction of the lanthanides by TODGA across the series, and suggests a relationship between co-extracted water and lanthanide extraction.

3.2 Introduction

The trivalent *f*-block elements are difficult to separate from one another due to their similar charge densities and near-identical chemistries. Amide extractants were originally considered for use in the separation of *f*-block elements after being described by Siddall in 1960[65]. Neutral diglycolamide extractants were first explored as alternatives to bidentate malonamide ligands in the early 2000s[13]. Both classes of extractant are fully incinerable, making them attractive for applications in the management of high level radioactive waste. However, the additional ether oxygen in tridentate diglycolamide extractants greatly increases their affinity for trivalent lanthanides and actinides over bidentate malonamide ligands. While the extraction capabilities of numerous different diglycolamides have been

explored in the literature, most work has focused on N,N,N',N'-tetraoctyl diglycolamide (TODGA), shown in Figure 3.1, due to its low solubility in water, high solubility in organic diluents, and high affinity for trivalent f-block elements[66]. Work with these extractants has focused on the utility of diglycolamides in the separation of trivalent actinides from lanthanides. However, the high affinity of diglycolamide extractants for trivalent lanthanides suggests that they may also have applications in the separation of adjacent lanthanides.

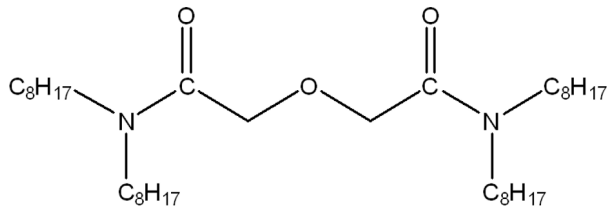

Figure 3.1: Molecular structure of the solvating extractant N,N,N',N'-tetraoctyl diglycolamide (TODGA).

Traditional approaches to the solution-phase separation of adjacent lanthanides have focused on the effect of the contraction of trivalent lanthanides' ionic radii on their inner-sphere coordination environment[67]. The trivalent lanthanides are hard acids with very similar chemical and physical properties[63], making this small decrease in size across the series, shown in Figure 3.2, the primary difference that can be leveraged to accomplish mutual separations in lanthanide mixtures. The primary effect of this contraction is the increased strength of ion-dipole interactions between the lanthanides and extractant molecules with increasing atomic number. In a solvent extraction system, this corresponds to slightly better extraction of the heavier lanthanides. However, this simplistic understanding of the extraction chemistry of the lanthanides fails to include the possible effects of interactions occurring beyond the first coordination sphere. Determining the nature of these interactions, which are most effectively probed at high metal concentrations, may be essential to designing efficient lanthanide separation processes.

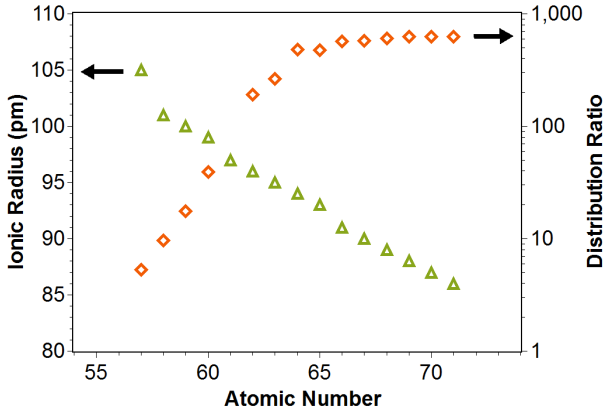

Figure 3.2: The ionic radii of the lanthnides decrease steadily across the series[63]. Extraction of the lanthanides by TODGA increases from the light to mid-lanthanides, after which it levels off[66].

The affinity of TODGA for the trivalent lanthanides does not follow a linearly increasing trend across the lanthanide series as would be expected if the strength of the Coulombic interactions between the lanthanide and extractant were the only property impacting extraction. Instead, distribution data show a steady increase in extraction across the light lanthanides and a break in this trend at Gd beyond which metal distribution is effectively constant (Figure 3.2)[66]. In a previously reported study, this trend was attributed to a similar but much less pronounced break in the energy difference between an aqueous-solvated lanthanide ion and a diglycolamide-solvated lanthanide ion, measured relative the energy of lanthanum solvation[68]. This difference is referred to as the aqueous-phase selectivity, and takes into account only the energetics of inner sphere coordination. However, the weak agreement between the experimental distribution data and aqueous-phase selectivities suggests that there are additional factors affecting the observed selectivity trend that have not yet been identified.

Prior work looking at the structure of diglycolamide-lanthanide complexes has determined that the extractant amide and ether groups are directly coordinated to the central metal cation in a tridentate fashion, while charge neutralizing anions are located in the outer-sphere of the complex. This structure has been determined in the solid state for lanthanide

and actinide nitrates[69, 70], and verified for solution-phase species in solvent extraction samples[68, 71]. The calculation of aqueous-phase selectivities does not take these outer-sphere anions into account. However, the behavior of outer-sphere species may provide an additional basis for the observed selectivity.

The purpose of this work is to expand understanding of the trend in lanthanide extraction across the series by the neutral diglycolamide extractant, TODGA, at high metal concentrations. The extraction behavior of TODGA was investigated by measuring the equilibrium organic and aqueous phase compositions of solvent extraction systems containing macroscopic amounts of La, Pr, Sm, Gd, Dy, and Tm. The maximum concentration of each lanthanide that could be extracted into the organic phase before it splits into two phases was also determined for these metals. This concentration is referred to as the limiting organic concentration (LOC) of the metal. Solvent extraction studies performed at high metal concentrations could give further insight into the nature of TODGA extracted complexes and trends in lanthanide selectivity.

3.3 Experimental

Stock solutions of approximately 0.5 M $La(NO_3)_3$, $Pr(NO_3)_3$, $Sm(NO_3)_3$, $Gd(NO_3)_3$, $Dy(NO_3)_3$, and $Tm(NO_3)_3$ were prepared by dissolving 99.9% pure solid lanthanide nitrate hydrates from Sigma Aldrich in 0.001 M HNO_3, to prevent hydrolysis. A stock solution of 3 M $NaNO_3$ was prepared by dissolving ACS grade $NaNO_3$ in water. All solutions were standardized by inductively coupled plasma optical emission spectroscopy (ICP-OES) prior to use. TODGA was used as received from Marshallton Research Laboratories, and dissolved in 99+% *n*-dodecane from Alfa Aesar to make a 0.25 M stock solution.

3.3.1 Solvent Extraction Studies

The 0.25 M TODGA solution was pre-equilibrated with water prior to all distribution experiments. Aqueous solutions at the desired lanthanide concentration were prepared from stock solutions, such that the equilibrium aqueous phase concentration of NO_3^- under each

experimental condition remained constant at 0.5 M NO_3^-. For each extraction sample, equal volumes of an aqueous and organic phase were combined in a plastic centrifuge tube and contacted on a vertical rotating wheel in a thermostated incubator maintained at 21 °C. Samples were allowed to rotate until equilibrium was reached, at least one hour. Samples were centrifuged for five minutes at 3000 rpm to separate the phases, and aliquots taken from each phase for analysis.

Metal concentrations in both phases were determined using ICP-OES. Aqueous phase samples were prepared for analysis by adding a small sample of the separated aqueous phase aliquot directly to a 4% HNO_3 solution. Organic phase samples were prepared by stripping the metal from the organic phase aliquot three times with equal volumes of 0.01 M HNO_3. These solutions were combined and the HNO_3 concentration adjusted to 4% HNO_3 for analysis by ICP-OES.

Organic phase water concentrations were determined using a Metrohm 831 Karl-Fischer coulometer.

All metal and water analyses were performed in duplicate. The estimated uncertainty in the measured metal concentrations is 2%. The estimated uncertainty in the measured water concentrations is 2%.

3.3.2 Maximum Organic Phase Lanthanide Concentration

To determine the maximum amount of each lanthanide that could be dissolved in the organic phase before the appearance of a third phase, solvent extraction studies were performed as described in the previous section. A range of initial aqueous phase lanthanide concentrations was used such that a third phase was observed for at least one of the concentrations. For La, the third phase appeared as a thin liquid phase located above the aqueous phase and below the larger organic phase. For the other lanthanides, the third phase appeared as a pale white gel or waxy solid in the upper organic phase. The initial aqueous phase concentrations were refined until the organic phase limit was determined to within an initial aqueous phase concentration of 2 mM. Once the conditions under which the

LOC was reached were determined, ICP-OES was used to find the organic phase lanthanide concentrations.

3.4 Results and Discussion

The investigated solvent extraction systems consisted of an organic phase with 0.25 M TODGA dissolved in an *n*-dodecane diluent contacted with a 0.001 M HNO_3 aqueous phase containing macroscopic amounts of $NaNO_3$ and lanthanides from across the series. The organic phase TODGA concentration was chosen to be high enough that it could reasonably be considered for use in an industrial-scale operation, where a high saturation of the organic phase by metal is desired. The aqueous phase composition was chosen to minimize the impact of competitive extraction on the system. A salting out agent in the aqueous phase is required to obtain approximately 50% extraction of the light lanthanides by a 0.25 M TODGA organic phase. Nitric acid, a salting out agent used in applied separations, competes with metals for extractant, adding an additional experimental parameter that must be considered. In these experiments, a background electrolyte consisting of approximately 0.5 M $NaNO_3$ was used to improve the extraction of the lanthanides without Na^+ being extracted. A small amount of nitric acid was added to the aqueous phase to prevent hydrolysis of the metals, for a final acid concentration of 0.001 M HNO_3.

3.4.1 Limiting Organic Concentrations

According to solvent extraction[20] and EXAFS studies[68], trivalent lanthanides are likely extracted as a 1:3 metal to TODGA species according to the following equilibrium relationship:

$$M^{3+}{}_{(aq)} + 3\,{NO_3}^-{}_{(aq)} + 3\,\mathrm{TODGA}_{(org)} \rightleftharpoons M(NO_3)_3\mathrm{TODGA}_{3(org)} \tag{3.1}$$

This equation suggests a theoretical value for the maximum concentration of metal that can be extracted into a 0.25 M TODGA organic phase. A fully saturated organic phase would have a 0.083 M metal concentration, corresponding to all TODGA molecules being a part of a

trimeric extracted metal species. However, like other neutral solvating extractants, TODGA is known to form a third phase before this saturation concentration can be reached[72]. Third phase formation in a solvent extraction system occurs when the organic phase splits into an upper, diluent-rich organic phase, and a heavy, extractant- and metal-rich organic phase in equilibrium with the aqueous phase. Third phase formation is correlated with high metal concentrations in the organic phase.

The limiting organic concentration (LOC) is defined as the greatest concentration of metal that can be extracted into an organic phase before a third phase is formed. The LOCs of six metals from across the light, middle, and heavy lanthanides (La, Pr, Sm, Gd, Dy, and Tm) were found by incrementally changing the initial aqueous phase concentrations of each metal. The result is an "S"-shaped curve, shown in Figure 3.3, in which the LOC starts at a high concentration and decreases slowly across the light lanthanides, rapidly across the early-middle lanthanides, then levels off beginning at the late-middle lanthanides. The point of inflection of this curve roughly corresponds to Nd, and the complete leveling-off of the LOCs takes place at Gd. The leveling off of the LOC takes place at the same point in the series at which metal extraction is also observed to level off. However, the "S"-shape does not correspond to other important reported physical or chemical attributes of the lanthanide ions in solution[63], suggesting that this trend is not the result of a direct interaction between the metal ion and extractant. Rather, it may be the result of outer-sphere coordination effects.

La comes the closest to the theoretical limit of saturation of the organic phase before forming a third phase at an organic concentration of 0.077 M, followed by Pr at 0.070 M. The remaining lanthanides reach the LOC at concentrations much less than the theoretical saturation point of the organic phase. The closeness of the LOC to the saturation concentration of the organic phase validates the formation of the 1:3 metal to TODGA species for La and Pr, and suggests that the 1:4 metal to TODGA species is not favored in these systems.

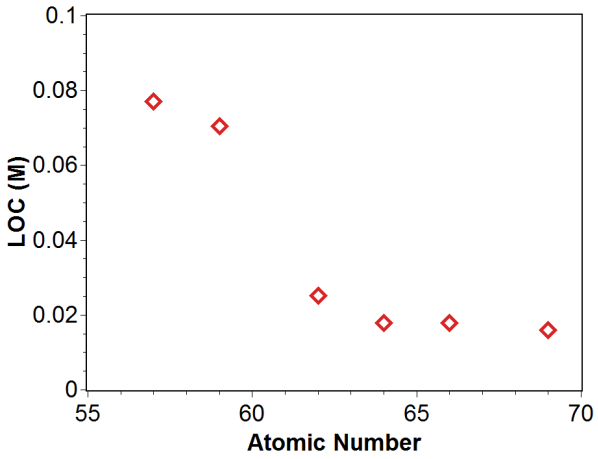

Figure 3.3: Lanthanide LOCs in a TODGA solvent extraction system form an "S"-shaped curve when plotted against atomic number.

3.4.2 Distribution Data

The distribution ratio, D, is a measure of metal extraction, and is calculated as shown in Equation 3.2, where the organic phase concentration of a metal, $[M]_{org}$ is divided by the aqueous phase concentration, $[M]_{aq}$.

$$D = \frac{[M]_{org}}{[M]_{aq}} \tag{3.2}$$

In the absence of confounding factors like competitive extraction, distribution ratios are expected to decrease with increasing metal concentration as saturation of the organic phase is approached. This trend is observed in the distribution ratio values shown in Figure 3.4. The distribution ratios of La, Pr, Sm, and Gd decrease exponentially with increasing metal concentration in the system until the LOC is reached. The heavy lanthanides Dy and Tm are sufficiently well-extracted that their aqueous phase concentrations were undetectable by ICP-OES, preventing the calculation of distribution ratios for these metals. Because of the high recovery of the heavy lanthanides, the leveling off of the distribution ratio from Gd onward that has been observed in dilute extraction experiments could not be verified for concentrated systems. However, the distribution data collected for La, Pr, Sm, and Gd under concentrated conditions follow the same trend as that observed in dilute systems. For

a given equilibrium organic phase concentration of metal, the distribution ratio increases with increasing atomic number.

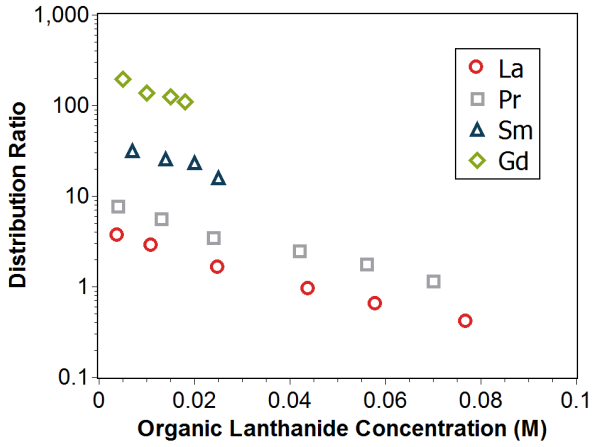

Figure 3.4: The distribution ratios of the lanthanides are inversely proportional to concentration and ionic radii.

3.4.3 Trends in Water Co-extraction

The amount of water co-extracted with each lanthanide is shown in Figure 3.5. The point at zero lanthanide concentration in the organic phase corresponds to the equilibrium composition of a 0.25 M TODGA phase contacted with a 0.5 M $NaNO_3$ and 0.001 M HNO_3 aqeuous phase. As expected, the amount of Na extracted into the organic phase was undetectable by ICP-OES. The water concentration in the equilibrium organic phase increases with increasing metal concentration at different rates depending on the identity of the co-extracted metal. The equilibrium organic phase water concentration increases at the slowest rate with increasing La concentration, followed by Pr, Sm, and Gd. At Gd the amount of co-extracted water stops increasing, such that the increase in water concentration with metal concentration is the same for Gd, Dy, and Tm.

For a constant organic phase lanthanide concentration, the observed trend in water co-extraction follows the distribution ratio trend across the lanthanides. The number of water molecules co-extracted with each lanthanide ion in the organic phase increases steadily to

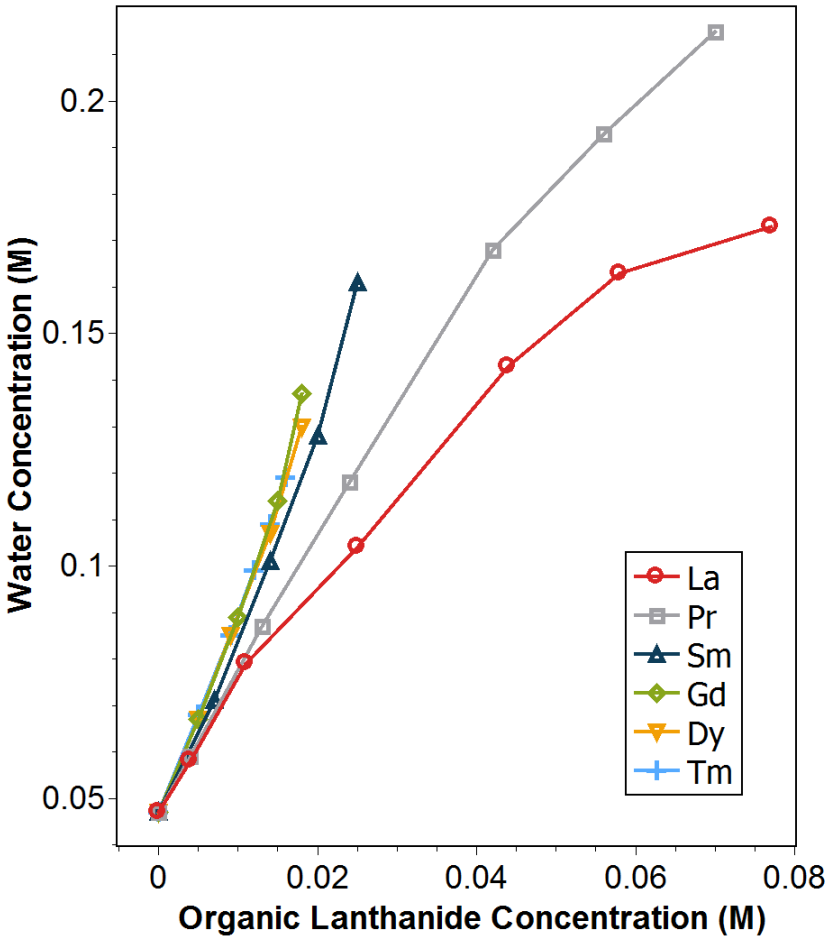

Figure 3.5: The amount of water co-extracted with each lanthanide increases with increasing metal concentration. At a given metal concentration, it increases and levels off across the series. Error bars have been omitted for clarity. Lines are included to guide the eye and do not represent a model fit.

Gd, beyond which it remains approximately constant. Figure 3.6 shows the increase in the organic phase water concentration for a constant lanthanide concentration of 0.014 M. These values were determined from linear interpolation of the data shown in Figure 3.5. This trend compares favorably with the trend in distribution ratios across the lanthanide series, also shown in Figure 3.6. Such close agreement between these data suggests a relationship between the water co-extracted with a metal and how well that metal is extracted by TODGA. However, the exact nature of this relationship is unclear.

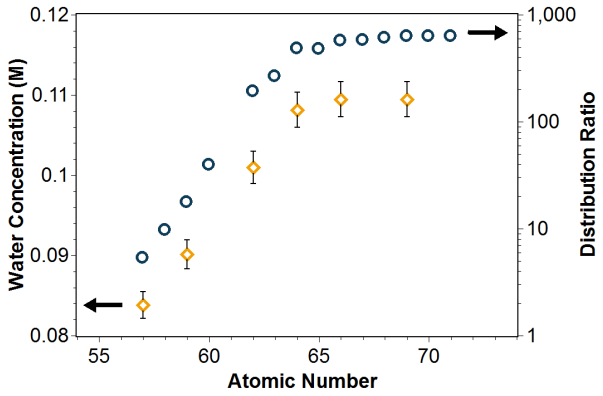

Figure 3.6: The expected concentration of water in an equilibrium organic phase with a 0.014 M lanthanide concentration increases for the light lanthanides and levels off for the heavy lanthanides. This trend in water co-extraction appears to closely follow the trend in lanthanide extraction by TODGA.

Water is not a part of the inner coordination sphere of TODGA-extracted trivalent lanthanides. A time resolved laser-induced fluorescence spectroscopy (TRLFS) study on the complexation of Eu by TODGA demonstrated that water is not coordinated to the metal[73]. This finding was validated by solution-phase EXAFS studies of TODGA-extracted Pr, Nd, Eu, Yb, and Lu, which showed the inner coordination sphere of these ions saturated by the ligand[68]. These findings, as well as the low concentration of water in the organic phase without metals, means that this water is likely being co-extracted in the outer coordination sphere of the lanthanides, suggesting a link between the outer-sphere coordination chemistry of the lanthanides and their extraction by TODGA. Such outer-sphere effects have been con-

sidered as an explanation for the extraction chemistry of a malonamide extractant, although the explicit molecular origins of these effects were not identified[74].

In the case of TODGA, the observed trend in extraction across the lanthanide series could be explained by a decrease in the organic phase solubility of the extracted complexes beyond Gd due to their higher water content. To be soluble in the organic phase, TODGA complexes must be net neutral species. However, the inner coordination sphere of an extracted trivalent lanthanide is fully saturated by TODGA molecules, meaning that charge neutralizing nitrate anions must be electrostatically associated in the outer coordination sphere. These nitrate ions could be interacting strongly enough with water molecules to pull them into the organic phase with the extracted lanthanides. As the radii of the lanthanides contract across the series, the hydrocarbon chains of the coordinated TODGA molecules could become more crowded, pushing the nitrate anions farther away from the metal center and beyond the steric protection of TODGA's nonpolar tails. This could increase the polar surface of the nitrate available to interact with water, and, as a result, the amount of water associated with the extracted complex. Any increase in the extraction of lanthanides by TODGA beyond Gd, which would be expected if extraction was only impacted by inner sphere coordination effects, could potentially be offset by the decrease in organic phase solubility of species with more associated water, leading to the observed trend in extraction.

3.5 Conclusions

The trivalent lanthanides are difficult to separate because of similarities in their physical and chemical properties. Most mutual separation processes take advantage of the small decrease in ionic radius that occurs across the lanthanide series. In solvent extraction systems, this decrease would be expected to result in steadily increasing extraction across the series. However, this trend is not observed with TODGA, for which lanthanide extraction has been observed to increase across the light to middle lanthanides, then remain constant across the heavy lanthanides. In this work, distribution studies in TODGA extraction systems with high lanthanide concentrations were used to explore the basis for this observed extraction

trend. The LOCs of La, Pr, Sm, Gd, Dy, and Tm form an "S"-shaped curve. The distribution ratios of La, Pr, Sm, and Gd increase with decreasing ionic radius, and decrease with increasing metal concentration. These trends are consistent with the previously established TODGA extraction mechanism. Finally, the amount of water extracted with each lanthanide was found to closely follow the extraction trend for lanthanides across the series, suggesting a relationship between water and lanthanide extraction by TODGA. This behavior could be explained by the competing effects of improved extraction with decreasing ionic radius and diminished solubility of the extracted complex with increasing amounts of co-extracted water.

CHAPTER 4

TRIBUTYL PHOSPHATE AGGREGATION IN THE PRESENCE OF METALS: AN ASSESSMENT USING DIFFUSION NMR SPECTROSCOPY

Modified from a paper published in *The Journal of Physical Chemistry B*[1]

Anna G. Baldwin[2], *Yuan Yang*[3], *Nicholas J. Bridges*[4], *Jenifer C. Braley*[5]

4.1 Abstract

Diffusion nuclear magnetic resonance (NMR) spectroscopy was used to find the inter-aggregate interactions and sizes of tributyl phosphate (TBP) aggregates containing varying concentrations of uranium or zirconium and HNO_3 in an *n*-dodecane diluent. The average diffusion coefficients of TBP species were measured using a pulsed-field gradient stimulated echo experiment with a longitudinal eddy-current delay (STE-LED). Inter-aggregate interactions were determined by measuring the diffusion coefficient of TBP in a sample after a series of dilutions with *n*-dodecane. The interaction-independent infinite dilution diffusion coefficient was also calculated from these measurements. The sizes of TBP aggregates were calculated from the infinite dilution diffusion coefficient using the Wilke-Chang equation. Interactions between TBP aggregates were observed to correspond to a hard sphere potential with a repulsive component. Aggregate sizes found by NMR were comparable to literature values found using small angle neutron scattering. The diffusion of TBP in heavy organic third phases indicates that the third phase may be a bicontinuous structure like that found in traditional surfactant systems.

[1]Adapted with permission from *The Journal of Physical Chemistry B* **2016** *120* (47), 12184-12192. Copyright 2016 American Chemical Society.
[2]Primary author and researcher
[3]Co-author, NMR research scientist
[4]Co-author, Savannah River National Laboratory
[5]Corresponding author and advisor

4.2 Introduction

Solvent extraction is an important chemical separation process with applications in many different industries. Solvent extraction separates components by leveraging differences in their solubilities between two immiscible liquid phases, usually a less-dense organic and a more-dense aqueous phase. For solvent extraction processes targeting metals, a metal extractant in the organic phase must be hydrophobic enough to be insoluble in the aqueous phase yet polar enough to interact with the metal of interest. As a result, extractants used in the separation and purification of metals are usually amphiphiles consisting of a polar headgroup attached to nonpolar hydrocarbon tails[75]. The polar headgroup interacts with the extracted ionic species while the nonpolar hydrocarbon tails prevent the extracted metal species from being soluble in the aqueous phase.

One of the most industrially-relevant metal extractants is tributyl phosphate (TBP), a neutral solvating extractant used to separate plutonium and uranium from used nuclear fuel in the Plutonium Uranium Redox EXtraction (PUREX) process[12, 48–50]. The structure of TBP is shown in Figure 4.1. TBP has a density close to that of water and is usually dissolved in kerosene, an inert hydrocarbon diluent, to facilitate disengagement of the organic phase[76]. Under conditions of high acid and metal loading, TBP and other neutral extractants are prone to the formation of liquid third phases, a problematic phenomenon not usually observed in extraction systems containing acidic extractants[77, 78]. Third phase formation interferes with solute recovery, and refers to the appearance of a second, heavy organic phase consisting primarily of extracted species in equilibrium with a light, diluent-rich organic phase and the aqueous phase.

Historically, the extraction mechanisms of metals in solvent extraction systems have been investigated through batch distribution studies at low solute and extractant concentrations[16, 18, 61]. By analogy with traditional coordination compounds, extracted species were assumed to exist in solution as a limited number of discrete stoichiometric solvates[19]. The compositions of these solvates were determined by relating the metal concentration in each

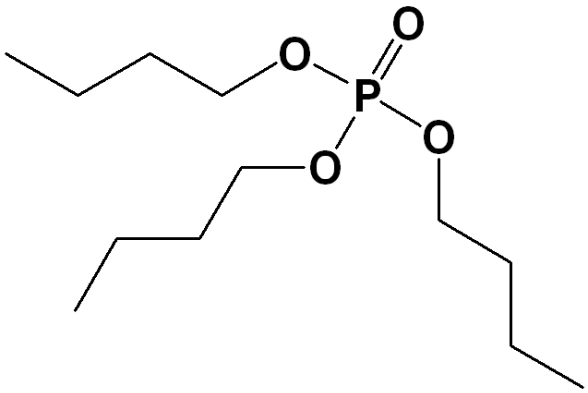

Figure 4.1: Molecular structure of tributyl phosphate (TBP).

liquid phase to experimental variables based on equilibrium extraction relationships and the law of mass action. These studies were run under dilute conditions to eliminate the effects of the activities of extracted species on the thermodynamic constants governing the extraction equilibria. The small, discrete species found under dilute conditions have been assumed to exist under the highly concentrated conditions in industrial-scale processes. Deviations from ideal behavior in these concentrated systems were then attributed to non-ideality rather than the formation of different extracted species[21]. However, this understanding of the organic phase does not explain third phase formation, leading to the need for an improved understanding of the molecular-scale forces at work in solvent extraction systems.

Interest in understanding the fundamental chemistry of solvent extraction, particularly under applied separation conditions, has encouraged the application of the characterization tools of colloid chemistry to determine the structure of the organic phase. In 1991, Osseo-Asare suggested that solvating metal extractants, which are usually surface-active amphiphiles, might form reversed micellar aggregates like those found in more traditional surfactant systems at high concentrations of acid and metals[31]. A simplified representation of such a proposed structure is shown in Figure 4.2. This important parallel between colloid chemistry and solvent extraction provided the impetus for small angle X-ray scattering (SAXS) and small angle neutron scattering (SANS) studies of the morphology of organic

phase species in solvating extractant systems[24–27, 30, 32, 79, 80]. These studies indicate the formation of extractant aggregates containing more extractant molecules than had been found as part of the coordination compounds whose stoichiometries were established by dilute batch distribution studies.

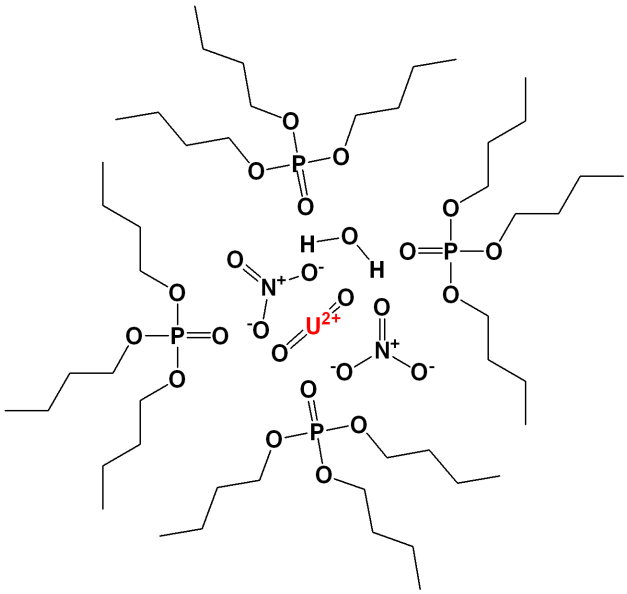

Figure 4.2: A simplified representation of the proposed structure of metal-containing reversed micellar TBP species.

Neutron and X-ray scattering are techniques used to probe the structure of nanoscale particles in solution. In these techniques, a beam of either X-ray or neutron radiation is passed through a sample and the resulting interference pattern is collected. These scattering data are then either directly fit by an appropriate theoretical model or indirectly analyzed by computing the Fourier transform of the scattering data and reversing correlation averaging to yield particle size, shape, and interaction information[81, 82]. Recent work has used scattering patterns derived from molecular dynamics simulations of sample systems in the interpretation of experimental small angle scattering data[83–85]. The primary difference between SAXS and SANS is in the nature of the interactions of X-ray and neutron radiation with the sample. X-rays are scattered by areas of electron density, while neutrons interact with atomic nuclei. However, mathematically identical principles of radiation scattering are

used to analyze the resulting experimental intensity data[86]. As a result, both SAXS and SANS scattering patterns suffer from the same fundamental inability to uniquely define the shapes and interactions of particles in a sample. The analysis of small angle scattering data requires making general assumptions about the shapes of the particles in solution and the types of interactions expected between them to get quantitative structural information[87]. These assumptions must be made based on information from independent methods.

An independent, alternative method for gaining particle size and interaction information is pulsed-field gradient nuclear magnetic resonance (PFG-NMR) spectroscopy, which can be used to measure the self-diffusion coefficients of molecular aggregates in solution. PFG-NMR is an established method for directly measuring the average diffusion coefficients of colloidal particles containing NMR-active nuclei[88–91]. It measures the change in the intensity of the NMR signal of a sample with either changing applied magnetic field gradient pulse strength or diffusion time. This change in intensity is then related to the diffusion coefficients of species in the sample. The diffusion coefficient of a species is directly related to its size and the nature of its interactions with other components in the system. Diffusion coefficient data can be used to determine the volumes of diffusing species using models relating the diffusion coefficient and aggregate size. The impacts of the assumptions used in models relating the diffusion coefficient and aggregate size may be substantially less than those used in small angle scattering data fitting. For example, Chiarizia *et al.*, used a non-interacting ellipsoidal model and an adhesive hard sphere model to fit scattering data measured for samples containing TBP and zirconium[27]. The resulting model fits were equally good. However, the aggregate volumes calculated using these two models differ by nearly two orders of magnitude. In contrast, aggregate volumes calculated from diffusion data may be off by as much as 12%, on average[92]. Because it provides complementary information, diffusion NMR spectroscopy can be used as an important supplement to small angle scattering experiments.

In this work, the use of PFG-NMR to determine the size and interparticle interactions of metal-containing extractant aggregates is described for the first time in the literature. The extraction systems under consideration contain TBP and either uranyl or zirconium nitrate. The results of PFG-NMR experiments are compared with prior small angle scattering investigations of the same systems.

4.3 Experimental Section

4.3.1 Materials

All organic solutions were prepared using 99+% tributyl phosphate from Acros Organics and 99+% *n*-dodecane from Alfa Aesar. All aqueous solutions were prepared using ACS grade nitric acid from Macron Fine Chemicals and degassed, ultrapure (18 MΩ-cm) water. A stock solution of zirconium nitrate (0.601 ± 0.001 M $Zr(NO_3)_4$, 6.0 ± 0.1 M HNO_3) was prepared from hydrous zirconium oxide as described in Chiarizia *et al.*[27], using reactor grade (99.5+%) zirconium (IV) chloride (Alfa Aesar) as a starting material. A stock solution of uranyl nitrate (1.40 ± 0.01 M $UO_2(NO_3)_2$, 3.0 ± 0.1 M HNO_3) was prepared using ACS grade uranyl nitrate hexahydrate (International Bio-Analytical Industries, Inc., Boca Raton, FL). These metal stock solutions were diluted with water and nitric acid as needed to obtain aqueous solutions of the desired metal and acid concentrations. All reagents were used as received, without further purification.

4.3.2 Solvent Extraction Experiments

All batch solvent extractions were performed at 21 ± 0.5 °C using equal volumes of aqueous and pre-equilbrated organic phases. Organic phase solutions were initially prepared with 20 v/v% TBP in *n*-dodecane. This organic phase was then contacted with an equal volume of a nitric acid solution at the same concentration as that used in the batch extraction to produce a pre-equilibrated organic phase. The aqueous phases used in the batch extractions initially contained either 5 or 10 M HNO_3 and 0.06 - 0.24 M $Zr(NO_3)_4$ or 0.4 - 0.51 M $UO_2(NO_3)_2$. These systems were chosen because SANS comparison data exist for

them in the literature. Equal volumes of these aqueous and pre-equilibrated organic phases were contacted for 15 minutes on a vortex mixer. Samples were centrifuged at 2000 RPM to separate the phases. Pure organic phase samples were taken and kept neat or diluted 3:1, 1:1, or 1:3, giving samples for NMR analysis with approximately 0.2, 0.15, 0.1, and 0.05 solute fractions, respectively. The average diffusion coefficients of TBP aggregates in these samples were measured by PFG-NMR experiments. Samples from both the organic and aqueous phases were taken for further chemical analysis, as described below.

Zirconium concentrations in the organic and aqueous phases were found using a ^{95}Zr radiotracer produced by neutron irradiation of the same stock of hydrous zirconium oxide used in the preparation of the zirconium nitrate stock solution[57]. It was assumed that the extraction of the radiotracer would be directly proportional to that of the non-radioactive zirconium. This assumption was verified by comparing the distribution of the ^{95}Zr radiotracer to the distribution of non-radioactive zirconium, which was quantified using neutron activation analysis. The zirconium concentrations could then be found from the specific radioactivity of organic and aqueous phase samples from a batch extraction experiment identical to that used in the preparation of NMR diffusion samples, to which a 10 μL spike of the zirconium radiotracer had been added. A well-type high purity germanium detector was used to determine the radioactivity of the samples. Uranium concentrations were found directly by the same method, using the ^{235}U peak at 186 keV. Organic phase water concentrations were found using a Mettler-Toledo DL39 coulometric Karl-Fischer titrator. Nitric acid concentrations were determined by potentiometric titration, as described elsewhere[27]. All chemical analyses were done in triplicate. The experimental error is the average relative standard deviation of these measurements. It was assumed that the TBP concentration in the organic phase remained constant over the course of each batch extraction experiment.

A heavy organic phase sample containing zirconium was prepared by contacting an aqueous phase containing 10 M HNO_3 and 0.24 M $Zr(NO_3)_4$ with a pre-equilibrated organic

Table 4.1: Initial aqueous phase and equilibrium organic phase compositions. Samples for NMR diffusion measurements were taken from the equilibrium organic phase.

Sample	*Initial Aqueous*			*Equilibrium Organic*				
	$[HNO_3]^a$ *(mol/L)*	$[Zr]^b$ *(mol/L)*	$[U]^b$ *(mol/L)*	$[TBP]^c$ *(mol/L)*	$[HNO_3]^a$ *(mol/L)*	$[H_2O]^d$ *(mol/L)*	$[Zr]^b$ *(mol/L)*	$[U]^b$ *(mol/L)*
5a	5.1	0	0	0.73	0.660	0.131	0	0
Zr5b	5.1	0.060	0	0.73	0.697	0.128	0.0097	0
Zr5c	4.8	0.24	0	0.73	0.659	0.126	0.026	0
10a	10.3	0	0	0.73	0.859	0.081	0	0
Zr10b	10.3	0.0060	0	0.73	0.864	0.084	0.0053	0
Zr10c	10.3	0.014	0	0.73	0.865	0.085	0.012	0
U10b	10.6	0	0.40	0.73	0.280	0.061	0	0.23
U10c	10.8	0	0.51	0.73	0.529	0.055	0	0.25

[a]Average uncertainty 4%; [b]Average uncertainty 2%; [c]Estimated uncertainty 2%; [d]Average uncertainty 1%

phase consisting of 20 v/v% TBP in n-dodecane, as in previous batch extractions. The resulting heavy organic phase was sampled, and the diffusion of the TBP species was measured by PFG-NMR. The chemical composition of the heavy organic phase sample was not determined.

All sample compositions determined are given in Table 4.1.

4.3.3 Pulsed-Field Gradient Stimulated Echo Experiments

The average diffusion coefficients of TBP-containing species were found using a ^{1}H NMR pulsed-field gradient stimulated echo (STE) experiment[93] with a longitudinal eddy-current delay (LED)[94] on a 400 MHz Bruker AVANCEIII NMR spectrometer with a 5 mm Bruker single-axis DIFF60 Z-diffusion probe. In the STE-LED experiment, an initial 90° RF pulse rotates the magnetization from the $z-$axis to the $x-y$ plane, after which a magnetic field gradient pulse of strength G and duration δ is applied. This gradient pulse effectively "marks" the positions of ^{1}H nuclei along the $z-$axis of the sample by causing the magnetization of nuclei in identical chemical environments to lose phase coherence depending on their location along the $z-$axis. A second 90° RF pulse stores the magnetization in the $z-$direction, which is then subject to longitudinal relaxation. A third 90° RF pulse restores the magnetization to the $x-y$ plane with the signs of the phase angles reversed, after which a second gradient pulse is applied. The magnetization is again stored in the $z-$direction by the application of a fourth 90° RF pulse while eddy currents induced by high gradient pulses are allowed to decay for a time t_e, after which a fifth and final 90° RF pulse restores the transverse magnetization for measurement of the stimulated echo signal. The amplitude of this signal can be related to the self-diffusion coefficient of a species by the Stejskal-Tanner equation:

$$S(G) = S(0)\, e^{-\gamma^2 \delta^2 G^2 D\left(\Delta - \frac{\delta}{3}\right)} \tag{4.1}$$

where S is the intensity of the NMR signal at a given magnetic field gradient strength (G), γ is the gyromagnetic ratio of the ^{1}H nucleus, δ is the gradient pulse length, Δ is the diffusion time, and D is the diffusion coefficient. The STE-LED experiment used in this work varied

the strength of the applied magnetic field gradient while keeping all other experimental parameters constant. The resulting NMR signal intensity for the desired chemical species was then plotted versus the magnetic field gradient strength. The self-diffusion coefficient was calculated by fitting the Stejskal-Tanner equation (Equation 4.1) to this data. The STE-LED pulse sequence is shown in Figure 4.3.

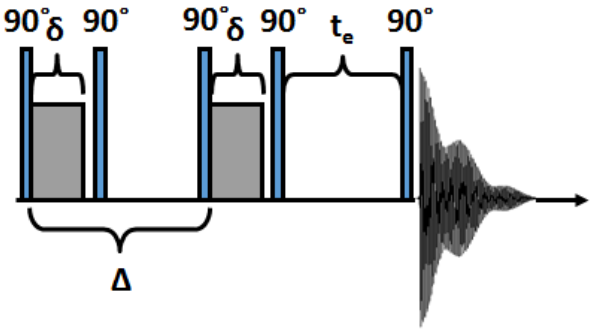

Figure 4.3: Schematic representation of the STE-LED pulse sequence used to measure the diffusion coefficient of TBP aggregates.

All diffusion measurements were made at 25.0 ± 0.1 °C, using a diffusion time of 20 ms, a gradient pulse duration of 1 ms, a 90° RF pulse duration of 5 μs, and an eddy current delay of 5 ms. Each experiment consisted of 16 gradient steps with a maximum gradient strength between 270 and 320 G/cm, chosen to correspond to at least 95% attenuation of the stimulated echo signal. Each gradient step consisted of 16 averaged scans collected with a repetition time of 5000 ms. TBP diffusion was measured using the attenuation of the ^{1}H peak at 4.3 ppm, which corresponds to the protons bound to the carbon immediately adjacent to the butoxy oxygens of TBP[95]. Figure 4.4 shows a 1-D ^{1}H NMR spectrum of a sample containing only TBP and *n*-dodecane (no deuterated solvents) measured with the solid-state diffusion probe used in all diffusion experiments. The spectra of the TBP samples at different gradient strengths for a typical STE-LED experiment are shown in Figure 4.5.

A line was fit to the measured diffusion coefficients at varying solute fractions to obtain the infinite dilution diffusion coefficient and unitless interaction parameter, α, given in Equa-

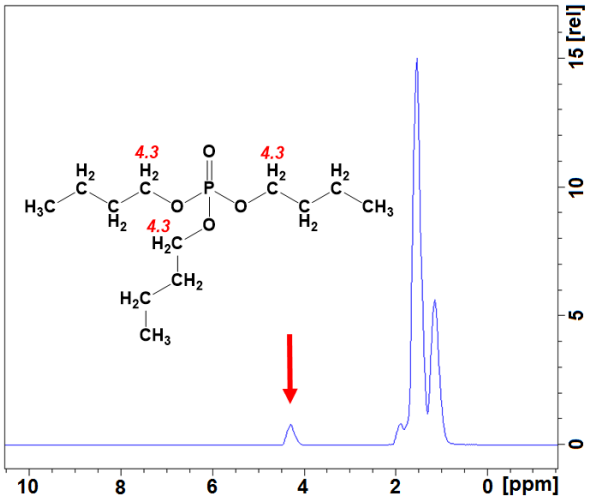

Figure 4.4: The diffusion coefficient of TBP aggregates was measured by following the attenuation of the TBP peak at 4.3 ppm. Overlapping TBP and n-dodecane peaks are found between 1 and 2 ppm.

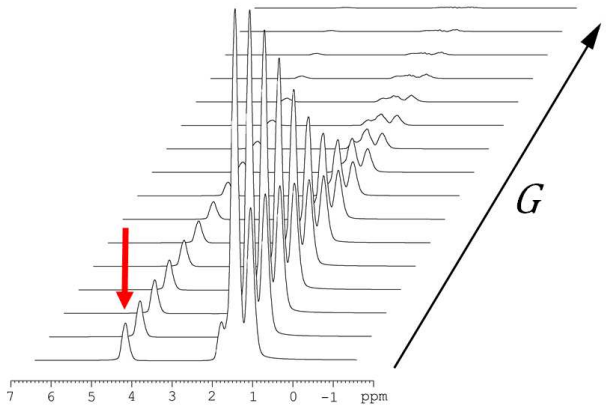

Figure 4.5: Attenuation of the TBP and n-dodecane peaks occurs with increasing gradient strength.

tion 4.2. Aggregate volumes were calculated from the Wilke-Chang equation (Equation 4.3) using the infinite dilution diffusion coefficients of TBP species, a viscosity of 1.331 cP for the *n*-dodecane solvent at 25 °C[96], and a solvent association parameter of 1. Average TBP aggregation numbers were calculated using the sample compositions and molar volumes. For each experimental condition, a single set of dilution samples were analyzed. Diffusion measurements were done in duplicate, due to the low variability of this measurement. The experimental error associated with a given system was estimated at 1.6% from the relative standard deviation of the average diffusion measurements of triplicate batch extraction experiments under a single set of conditions.

4.4 Results and Discussion

4.4.1 Diffusion Coefficient and Inter-aggregate Interaction Models

At a given temperature, the diffusion coefficients of colloidal particles are affected by the solvent viscosity, the sizes and shapes of the solvent molecules, the sizes and shapes of the particles, and interparticle interactions resulting from obstruction by other diffusing particles or electrostatic potentials[97]. The impact of interparticle interactions can be eliminated by measuring the diffusion coefficient of a sample at different solute fractions upon dilution with fresh solvent, assuming a decrease in solute concentration is the only effect of this dilution[98]. The change in the diffusion coefficient with solute fraction (φ) can be approximated by a line under dilute conditions, and fit by Equation 4.2 to yield the infinite dilution diffusion coefficient (D_0) and an interaction parameter, α. The interaction parameter, α, corresponds to the second virial coefficient of the system and directly reflects the combined effects of two-body and hydrodynamic interactions[99]. The linear approximation for the relationship between the diffusion coefficient and solute volume fraction is accurate to a volume fraction of approximately 0.2, after which higher order terms in the virial expansion become relevant as three- or four-body interactions begin to increase in magnitude[100]. D_0 is only dependent on the hydrodynamic radii of the diffusing particles, while α reflects the nature of the interparticle interactions. In the case of reversed micelles, this parameter is

usually negative due to the combination of hard sphere and attractive interactions between micelles. Neglecting the effect of interparticle interactions in reversed micellar systems leads to an overestimation in the size of the reversed micelles.

$$D = D_0 (1 + \alpha\varphi) \tag{4.2}$$

The Stokes-Einstein equation is often used to relate diffusion coefficients of species in dilute solution to the hydrodynamic radii of the diffusing particles[101]. However, due to the solvent continuum assumption used in its derivation, this relationship is poor for systems in which the solute radius is less than two to three times that of the solvent, as might be found in solvent extraction systems[102]. The Wilke-Chang correlation was developed for application to systems in which the solute and solvent are similar in size[92]. It is shown in Equation 4.3:

$$D_0 = 7.4 \times 10^{-8} \frac{\sqrt{\chi M_B} T}{\mu V_A^{0.6}} \tag{4.3}$$

where D_0 is the diffusion coefficient under dilute conditions, χ is the solvent association parameter, M_B is the molar mass of the solvent, T is the temperature, μ is the solvent viscosity, and V_A is the volume of the diffusing solute. The value for χ reflects the degree of association of the solvent through intermolecular interactions like hydrogen bonding. It is 2.6 for water and 1.0 for non-associating solvents like heptane.

4.4.2 Aggregate Sizes - Comparison of NMR and SANS

The average volumes of TBP aggregates were calculated using the Wilke-Chang equation from the infinite dilution diffusion coefficients at each experimental condition. These volumes are given in Table 4.2. An average TBP aggregation number was calculated from the average aggregate volume, the chemical compositions of the samples, and the molecular volumes of the system components. The molecular volumes of TBP, HNO_3, and H_2O used were 273.87, 43.26, and 18.02 cm^3/mol, respectively[24, 103]. Because the molecular volume of $Zr(NO_3)_4$ has not been determined, the known molecular volume of $ZrCl_4$ (83.14

cm^3/mol) was used as a reasonable estimate[27]. The molecular volume of $UO_2(NO_3)_2$ used was 70.70 cm^3/mol[24]. For purposes of comparison with SANS data, the hydrodynamic radii of these aggregates were calculated from the Wilke-Chang volume by assuming the aggregates were spherical. The corresponding hydrodynamic diameters of TBP aggregates containing zirconium or uranium determined using NMR diffusometry are compared to the scattering diameters determined using SANS in Figure 4.6. While the SANS diameters for TBP aggregates containing zirconium were determined in *n*-octane, experimental evidence suggests that the choice of aliphatic hydrocarbon diluent does not affect the average aggregate size for a given sample composition. The distribution behavior of metals prior to third phase formation has been observed to be independent of diluent chain length, as have the stoichiometries of extracted species under dilute conditions.[77, 78] NMR experimental uncertainty and SANS fitting errors have not been included as error bars in Figure 4.6 because they are smaller than the markers. It is instructive to note the differences in SANS diameters between analyses for systems at 10 M HNO_3 and no metal. For samples of similar composition in the data set including zirconium, the average SANS diameter is less than 14 Å, while in the uranium data set the average SANS diameter is 16 Å. These deviations hint at the potential for systematic bias in aggregate size introduced in the analysis of SANS data.

Figure 4.6 shows that the average sizes of TBP aggregates determined by NMR diffusometry are comparable to those found using using SANS, suggesting that the form factor used in the analysis of the SANS data accurately reflects the physical reality of the system. Aggregate sizes determined using both methods should agree because both effectively relate the size of TBP aggregates to experimental measurements defined by the farthest reach of the butyl tails of the TBP molecules on a mass-average basis. In SANS, the calculated size of the aggregates is primarily determined by the strongly scattering hydrogen atoms in the butyl tails, which contrast with the deuterated solvent used in those experiments. Likewise, NMR diffusometry relates the speed of the protons adjacent to the butoxy oxygen of TBP

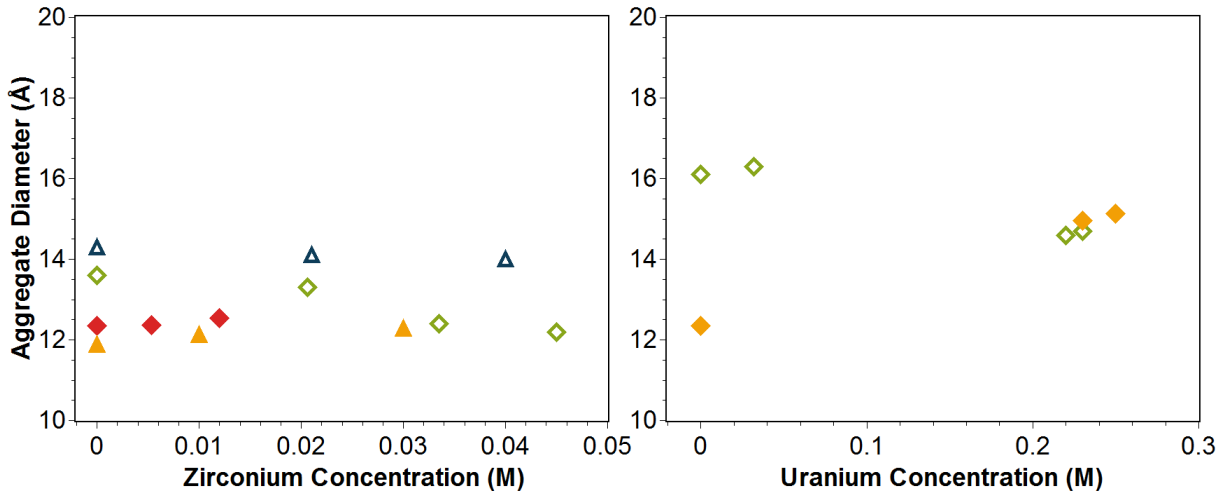

Figure 4.6: The sizes of TBP aggregates found using NMR and SANS are comparable for samples with varying zirconium, uranium, and HNO_3 concentrations. Triangle markers are samples at 5 M HNO_3. Diamond markers are samples at 10 M HNO_3. Filled markers indicate TBP aggregate diameters found by NMR spectroscopy. Unfilled markers indicate literature values for TBP aggregate diameters found by SANS[24, 27].

molecules to the sizes of the aggregates they compose. In certain systems, diffusion-derived aggregate sizes may be affected by association between the solvent and aggregate, similar to the well-known phenomenon of water forming a stable solvation shell around ionic solutes in aqueous solution. However, the strength of the interactions between the n-dodecane solvent and TBP aggregates are low enough that a decrease in diffusion due to solvation effects is not expected in this system. This is a common assumption in diffusion experiments involving nonpolar solvents and surfactants[104].

Furthermore, both methods find the mass-average size of TBP aggregates in solution. In SANS, the measured scattering intensity at a given value of the scattering vector, Q, is directly proportional to the number of scatterers making up each aggregate. In the TBP system, the primary scatterers are the hydrogen atoms in the TBP hydrocarbon tails, whose total scattering cross-section is substantially larger than the other components in the system. As a result, the contribution to the scattering signal is proportional to the number of TBP molecules making up each aggregate, indicating a mass dependence[105]. In diffusion NMR

spectroscopy of polydisperse species with identical chemical shifts, such as polymer systems made of a single monomer, the NMR-measured diffusion coefficient can be approximated as the mass-average diffusion coefficient[97]. The organic phase extraction samples measured in this work are examples of such polydisperse systems. Since diffusion can be directly related to size, this means that diffusion NMR analysis results in mass-averaged TBP aggregate sizes.

4.4.3 NMR Aggregate Sizes - Comparison Between Samples

The Wilke-Chang equation is a correlation based on the form of the more fundamental Stokes-Einstein equation. Values for the parameters used in the Wilke-Chang equation were determined through fitting diffusion data for 123 molecular solute-solvent systems[92]. As a result, the particle volumes determined using this equation are subject to a systematic bias that may be as high as 12% on average due to differences between the systems used in the parameterization of the Wilke-Chang equation and the TBP solvent extraction system explored here. However, the comparison of size trends within TBP systems is possible because the shapes of the solutes and solvent are substantially similar between samples.

Size trends indicate an increase in the average size of TBP aggregates with increasing metal concentration, as would be expected given the apparent saturation of the TBP extractant and the larger molecular volumes of the neutral metal salts compared to nitric acid and water. Saturation of the extractant is relevant because it indicates that changes in the average volumes of TBP aggregates are due to changes in the sizes of associated solutes and are not a result of concentration-dependent self-association of TBP monomers. Saturation of the TBP is indicated by the sample compositions, in which the combined concentrations of the polar solutes are greater than the concentration of TBP molecules.

In the nitric acid only and zirconium systems, the average TBP aggregation number is relatively constant at just below a value of two, while the aggregate volume increases with increasing zirconium concentration. The concentration of zirconium that could be reached in these samples was limited by third phase formation, which occurs at organic

phase zirconium concentrations just beyond the highest concentrations used here. Because the concentrations of zirconium in these samples are so low (less than 4% of the total polar solute concentration, or contained in as many as 1 in 10 TBP aggregates), this suggests that the increase in aggregate volume is not due solely to the increased volume of the metal salt relative the acid in identical TBP aggregates. Some TBP species formed in the presence of zirconium appear to also have a higher TBP aggregation number. However, this effect is difficult to quantify due to the very small contribution to the average TBP aggregate size by zirconium-containing species.

In contrast, the concentrations of uranium are as high as 40% of the total polar solute concentrations, corresponding to approximately 2 of every 3 TBP aggregates containing a uranyl cation. In these samples, the average TBP aggregate size is strongly impacted by the greater mass-average contribution of what seem to be large uranium-containing aggregates of up to four TBP. This value is very different from the aggregation number of two determined by traditional distribution studies under dilute uranium conditions[61], and indicates the formation of larger TBP species at high metal and acid concentrations.

4.4.4 Diffusion in the Third Phase

Diffusion NMR spectroscopy has been used to infer the microstructure of surfactant solutions based on the relative magnitudes of the diffusion coefficients of surfactant, oil, and water in ternary systems[104]. For a solution of oil in which water-containing micelles are dispersed, the diffusion coefficient of the oil is expected to be an order of magnitude higher than that of the water, and identical to the diffusion coefficient of the surfactant. Similarly, for a solution of water in which oil-containing micelles are dispersed, the diffusion coefficient of the water is expected to be higher than that of the oil and surfactant. In a bicontinuous system, where oil and water diffuse freely in surfactant liquid crystalline structures, the oil and water diffusion coefficients are high, while the surfactant diffusion coefficient is an order of magnitude lower.

The average diffusion coefficient of TBP-containing species in the third phase sample was found to be $3.45 \pm 0.07 \times 10^{-11}$ m^2/s. This value is an order of magnitude smaller than the average TBP diffusion coefficient of an *n*-dodecane solution containing only 20 v/v% TBP (*i.e.*, not pre-equilibrated with an acid solution), which was found to be $4.75 \pm 0.10 \times 10^{-10}$ m^2/s. The effects of interparticle interactions on these values are small compared to the effects that would be expected by the participation of TBP in a liquid crystalline-like phase. In a bicontinuous structure, like the interconnected-cylinder structure proposed by Ellis *et al.*[80], for the third phase formed in a different mixed extractant system containing various acids and TBP, it would be expected that the diffusion coefficient of TBP would be an order of magnitude slower than the diffusion coefficient of free TBP, that is, on the order of 10^{-11} m^2/s[104]. This is the case in an extraction system containing acid, TBP, and zirconium. The order of magnitude decrease in the rate of TBP diffusion observed in the third phase sample suggests that an analogy between third phase formation and the formation of liquid crystalline phases in surfactant systems may be applicable. This observation should be verified by measuring and comparing the *n*-dodecane and TBP diffusion coefficients in third phase samples using a technique like diffusion-ordered spectroscopy, which is used to separate the diffusion coefficients of the components of a mixture[106].

4.4.5 Aggregate Interactions

The effects of interparticle interactions on diffusion must be eliminated to determine the average sizes of TBP aggregates in solution from NMR diffusometry. The size and shape of the diffusing particles, and long- and short-range attractive or repulsive interactions all impact the change in the diffusion coefficient with solute fraction. The effects of interparticle interactions on the measured diffusion coefficients were determined in this work by fitting a line to a series of diffusion coefficients measured on dilution of a sample of an equilibrium organic phase with *n*-dodecane. Representative data and fitted lines for diluted samples are shown in Figure 4.7. Values of the interaction parameter, α, are given in Table 4.2. It was assumed as part of this analysis that TBP aggregation behavior in equilibrium organic phase

samples is unaffected by dilution. While clouding of the samples was initially observed on the addition of *n*-dodecane, this was found to disappear within an hour of sample preparation and no indication of precipitation or phase separation was observed. Because the polar solutes extracted by TBP (H_2O, HNO_3, $UO_2(NO_3)_2$, and $Zr(NO_3)_4$) are effectively insoluble in *n*-dodecane alone, it is reasonable to assume that these extracted solutes remain associated with TBP aggregates in solution on dilution with *n*-dodecane. Furthermore, the aggregates breaking apart would result in a deviation from linearity of the relationship between the diffusion coefficient and solute volume fraction. Relatively more small TBP aggregates would cause the slope to become steeper at low solute volume fractions because the average diffusion coefficient would be disproportionately increased. Conversely, if the TBP aggregates were coalescing to form larger aggregates on dilution, the relationship between diffusion coefficient and solute volume fraction would flatten at low solute volume fraction. The absence of phase separation, and the consistency of the linear relationship between solute volume fraction and diffusion coefficient support the assumption that sample dilution does not affect TBP aggregation in the organic phase.

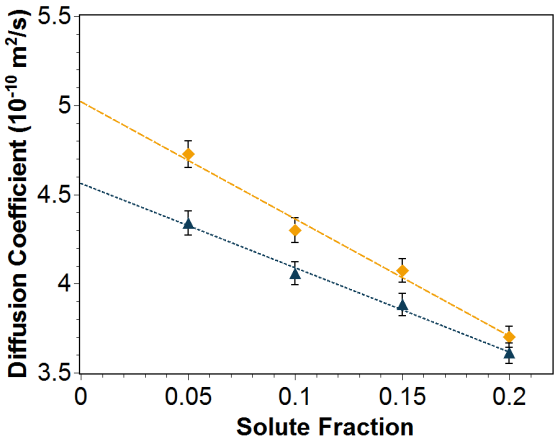

Figure 4.7: Representative data showing the effect of sample dilution on TBP diffusion coefficients. Diamond markers are for an organic phase sample in equilibrium with a 5 M HNO_3 only aqueous phase. Triangle markers are for an organic phase sample of 0.012 M $Zr(NO_3)_4$ in equilibrium with a 10 M HNO_3 aqueous phase.

Table 4.2: TBP aggregate infinite dilution diffusion coefficient, interaction parameter, and size results using diffusion NMR spectroscopy.

Sample	D_0[a] (m^2/s)	α[b]	*Agg. Vol.*[a] $(\AA^3)$	*Agg. Num.*[c]
5a	5.03×10^{-10}	-1.3 ± 0.1	878	1.7
Zr5b	4.85×10^{-10}	-1.31 ± 0.09	931	1.8
Zr5c	4.74×10^{-10}	-1.4 ± 0.2	969	1.8
10a	4.69×10^{-10}	-0.8 ± 0.1	984	1.8
Zr10b	4.67×10^{-10}	-0.97 ± 0.09	991	1.8
Zr10c	4.56×10^{-10}	-1.04 ± 0.06	1031	1.9
U10b	3.32×10^{-10}	-1.65 ± 0.07	1755	3.4
U10c	3.25×10^{-10}	-1.7 ± 0.1	1816	3.3

[a]Average uncertainty 2%; [b]Provided uncertainty corresponds to the fitting error; [c]Average uncertainty 3%

The α-values for all the sample compositions studied were negative, as would be expected to result from the combined effects of obstruction and electrostatic interactions. In a crowded system of diffusing particles, simple obstruction by other particles decreases the observed diffusion coefficient with increasing concentration. This effect results from the presence of other particles along a given particle's diffusion path, restricting the distance it can travel in the experimental diffusion time, Δ. Simple obstruction by other particles is modeled as a hard sphere potential. Multiple theoretical approaches for determining the concentration dependence of the self-diffusion coefficient of uniform hard spheres in dilute solution agree on an α-value within 10% of -2[107–109]. In the presence of attractive interparticle interactions, the α-value would be expected to be more negative. The α-values determined for the systems studied here are less negative, especially in the nitric acid only and zirconium systems. The difference is great enough that it is unlikely to be solely affected by the shapes of the particles, which may deviate from being spheres. In fact, obstruction effects are greater in dilute solutions of hard spherocylindrical particles, resulting in α-values between -2 and -2.5 depending on their length to width ratios[110]. The α-values of approximately -1 observed in nitric acid only and zirconium systems suggest that there are net repulsive interactions among TBP aggregates containing these solutes.

4.4.6 Repulsive Interactions: Ramifications for Scattering Interpretations

The majority of small angle scattering studies of extractant aggregation in the presence of polar solutes have used the Baxter model for sticky hard spheres to fit the scattering data. In the Baxter model, particles are modeled as spheres with interparticle interactions consisting of a combined hard sphere potential and an infinitely narrow attractive well potential at the sphere's surface[111]. In theory, the validity of the assumption of purely attractive interactions could be determined directly from the raw scattering data by looking at the scattering intensity at low angles corresponding to length scales similar in magnitude to the interparticle correlation distance. The intensity would be expected to increase relative the scattering attributable to the size and shape of the particles in systems with repulsive interparticles interactions, and decrease in systems with attractive interactions[112]. However, the scattering at low angles is dominated by the size and shape of the scattering particles, making this determination using scattering data alone difficult in these systems. The α-values determined by NMR diffusometry suggest that an improved small angle scattering model for systems of extracted polar solutes could include a long-range electrostatic repulsive potential in addition to a short-range attractive potential. Such a model has been used in the analysis of scattering data from systems of aggregating biological molecules[113].

4.4.7 Potential Explanation for Repulsive Interactions

Long range repulsive electrostatic interactions in these systems may result from interactions between charge-neutralizing nitrate anions in the polar cores of TBP aggregates. TBP extracts electrically neutral species. For the systems explored here, these species are water, nitric acid, zirconium nitrate, or uranyl nitrate. For each electrically neutral species there are areas of negative charge and areas of positive charge on the surfaces of the molecules and associated ions. The areas of negative charge are centered around the nitrate oxygen atoms, while the areas of positive charge are centered around the proton or cation. These areas of positive charge may interact with the negatively charged phosphoryl oxygen of the

TBP extractant, causing the TBP to remain associated with these areas of positive charge. The placement of TBP molecules around these areas could then present a steric hindrance to the close interaction of this positively charged surface with other charged species, and may screen these interactions. Depending on the specific placement of the TBP extractant around the neutral species, this may leave the areas of negative charge bare and available to interact by repulsive interactions. The arrangement of the negatively and positively charged areas on the surface of the neutral species, as well as the placement of the TBP molecules around these polar solutes will differ depending on the identity of the extracted species and may explain the origin of the observed repulsive interactions between TBP aggregates.

The apparent repulsive interactions among TBP aggregates also suggest a different driving force behind third phase formation than that proposed as a result of small angle scattering studies using the Baxter model. In those, it was suggested that the appearance of a third phase resulted from the condensation of sticky TBP aggregates in a process analogous to sedimentation, which is observed in traditional colloidal systems of discrete particles with surface attraction. Sedimentation is generally not observed in traditional colloidal systems when interparticle interactions are repulsive. For a system of TBP aggregates with repulsive interactions, the mechanism for third phase formation may be driven by the complex interplay among the affinity of TBP for a polar solute, the solubility of polar solute-containing TBP aggregates in the diluent, and the repulsive interactions between these aggregates. The first requirement for third phase formation is that solvation of the polar solute by TBP must be competitive with its solvation by water. A third phase will not form if a polar solute is not sufficiently extracted into the organic phase. Polar solute-containing TBP aggregates may then become insoluble in the diluent after a reaching a certain concentration, causing formation of the third phase. This insolubility may result from diluent-aggregate interactions that are more unfavorable than the interactions between identical species. This is similar to the mechanism suggested by Kertes which attributes third phase formation to poor solvation of extractant adducts by aliphatic hydrocarbon diluents[77]. These explanations contrast

with the mechanism of third phase formation suggested by the presence of attractive inter-aggregate forces, which is defined by favorable aggregate-aggregate interactions rather than poor diluent-aggregate interactions. Repulsive interactions between TBP aggregates in the third phase could then result in the formation of a Wigner glass-type structure. Wigner glasses are relatively dilute ordered phases in which repulsive interactions between particles fix the structure of the particles making up the phase[114].

4.5 Summary and Conclusions

Diffusion NMR spectroscopy can be used to determine aggregate sizes and interactions as a complementary method to powerful small angle scattering techniques for characterizing the structure of the organic phase in solvent extraction systems. Small angle scattering techniques rely on prior knowledge about the structures of samples to analyze scattering data and extract specific information about scattering particles. Diffusion NMR spectroscopy is an important method for obtaining this prior knowledge, if the effects of interparticle interactions on the diffusion coefficient can be effectively excluded. In the case of solvating extractant systems containing metals, we have found that there appears to be a repulsive component to interparticle interactions of TBP aggregates in solution. This suggests that the model used in the analysis of small angle scattering data in these systems in prior work could be improved by the inclusion of a repulsive potential. Assuming spherical aggregates, the aggregate sizes determined by diffusion NMR spectroscopy and SANS correspond well, indicating that these two methods are, as would be expected, measuring the same aggregate sizes by two very different experimental means. Finally, the diffusion coefficient of TBP in a third phase sample was found to be an order of magnitude slower than that of TBP in solution, showing that it is possible that the third phase results from the formation of a liquid crystalline phase.

4.6 Acknowledgements

This material is based upon work supported by the U.S. Department of Homeland Security under Grant Award Number, 2012-DN-130-NF0001. The views and conclusions contained in this document are those of the authors and should not be interpreted as representing the official policies, either expressed or implied, of the U.S. Department of Homeland Security.

CHAPTER 5

THE STRUCTURE OF TRIBUTYL PHOSPHATE SOLUTIONS: NITRIC ACID, URANIUM (VI), AND ZIRCONIUM (IV)

Modified from a paper submitted to the *Journal of Molecular Liquids*

Anna G. Baldwin[1], *Michael J. Servis*[2], *Yuan Yang*[3], *Nicholas J. Bridges*[4], *David T. Wu*[5], *Jenifer C. Shafer*[6]

5.1 Abstract

Diffusion, rheology, and small angle neutron scattering (SANS) data for organic phase 30 v/v % tributyl phosphate (TBP) samples containing varying amounts of water, nitric acid, and uranium or zirconium nitrate were interpreted from a colloidal perspective to give information on the types of structures formed by TBP under different conditions. Taken as a whole, the results of the different analyses were contradictory, suggesting that these samples should be treated as molecular solutions rather than colloids. This conclusion is supported by molecular dynamics (MD) simulations showing the existence of small, molecular aggregates in TBP samples containing water and nitric acid. Interpretation of TBP and nitric acid diffusion measurements from a molecular perspective suggest that nitric acid and metal species formed are consistent with the stoichiometric solvates that have traditionally been considered to exist in solution.

[1]Primary author and experimental researcher
[2]Co-author and computational researcher
[3]Co-author, NMR research scientist
[4]Co-author, Savannah River National Laboratory
[5]Co-author
[6]Corresponding co-author and advisor

5.2 Introduction

The Plutonium Uranium Reduction Extraction (PUREX) process has been used for over sixty years to recover uranium and plutonium from used nuclear fuel[3, 12], and is one of the most important and well-characterized solvent extraction systems currently in use[33, 115]. The PUREX process uses a 30 v/v % solution of the extractant tributyl phosphate (TBP, Figure 5.1), dissolved in an aliphatic hydrocarbon diluent such as kerosene, to preferentially extract tetravalent plutonium and hexavalent uranium from a 3 to 4 M nitric acid aqueous phase that includes fission products and other impurities[48–50]. Optimization of the PUREX process to improve the efficiency of this separation could help reduce the volume of radioactive waste produced, as well as lead to simplifications in the overall process design[47]. This requires making advancements in the molecular-scale understanding of the extraction of inorganic species by TBP.

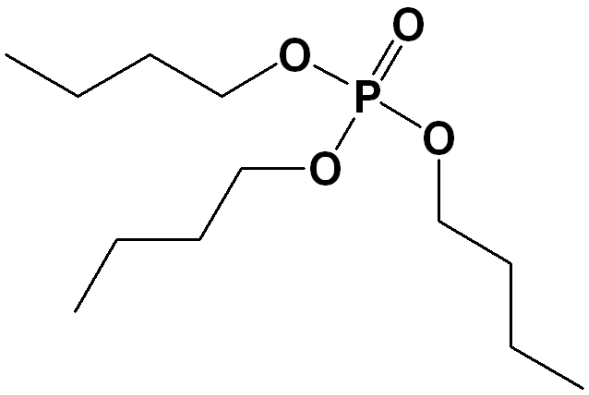

Figure 5.1: The molecular structure of the extractant tributyl phosphate (TBP).

Currently, an open debate exists over whether organic phases containing neutral solvating extractants such as TBP are best described as molecular solutions or solutions of colloidal aggregates. Traditionally, TBP organic phases containing inorganic solutes have been treated as molecular solutions composed of free extractant and discrete stoichiometric solvates in a diluent[19, 35, 39, 61, 116, 117]. Only extractants with long nonpolar hydrocarbon tails (8-20 methylene groups) and an ionic or highly polar head were thought to aggregate in sufficient

numbers to form colloidal, reversed micellar species in solution[22]. However, more recently, it has been suggested that TBP might also form reversed micellar species containing extracted water, acid, and metal[31, 118]. Like traditional surfactants with much longer hydrocarbon tails, TBP is surface-active. It is therefore possible that TBP forms structures in solution similar to those found in ternary water, oil, and surfactant microemulsions, which are known to form micelles and vesicles that are large enought to be considered colloidal[119–122]. This is the premise underlying the recent use of small angle scattering experiments to understand the structures formed by TBP in solution[118].

Since 2003, small angle X-ray and neutron scattering (SAXS and SANS) experiments have been used to characterize TBP species in both traditional[24–30] and nontraditional[123] solvent extraction samples containing water, and various acids and metals. For this work, we will only be considering the structure of TBP species in traditional samples. In order to interpret scattering data in prior work, these samples were assumed to consist of reversed micelles modeled as monodisperse hard spheres interacting through surface adhesion. This simplistic interparticle interaction model, developed by Baxter in 1968[111], was used to determine the sizes of TBP aggregates and the strength of the attractive interactions between them by varying the values of the aggregate diameter and stickiness parameter, τ^{-1}, until a good fit to the data by the model was achieved. The stickiness parameter is directly proportional to the strength of the attractive interactions between adhesive hard spheres, such that higher values of τ^{-1} correspond to stronger attractive interactions. The results for TBP aggregate sizes and interactions in SAXS and SANS investigations are consistent for different metals and inorganic acids, suggesting that TBP aggregates consist of two to five TBP molecules interacting through a strong attractive surface potential with τ^{-1} values between approximately 6 and 12. Assuming a thin square well potential with a well width of 10% of the hard sphere diameter, this corresponds to well depths ranging from approximately 1.6 to 2.3 k_BT, with deeper well depths corresponding to samples with higher metal concentrations. The source of these attractive interactions has been attributed to van

der Waals forces between polarizable aggregate cores[25, 27].

The simplicity of the Baxter fluid model means that it is easy to use and does not require numerical methods to solve for the structure factor. The Baxter potential corresponds to the infinitely narrow and deep limit of the square well potential, where the finite attractive surface interactions between particles are described by the temperature-dependent stickiness parameter, τ^{-1}. The radial distribution function and osmotic equation of state for the Baxter fluid were first calculated analytically by Baxter in 1968 using the Percus-Yevick approximation[111]. The structure factor is calculated from the Fourier transformation of the total correlation function, defined in terms of the radial distribution function, and can be directly determined from these relationships. Since then, analytical and simulation results for the phase diagram, average cluster size, and percolation threshold for the Baxter fluid have been reported in the literature[111, 124–127]. Percolation refers to a phenomenon where transient, system-spanning clusters are formed. The percolation threshold is the minimum value of τ^{-1} at which the Baxter fluid is percolated for a given solute volume fraction.

This research group recently used diffusion nuclear magnetic resonance (NMR) spectroscopy to corroborate the results of prior small angle scattering experiments using organic phase TBP samples containing nitric acid and either tetravalent zirconium or hexavalent uranium[128]. The sizes of TBP aggregates determined from diffusion coefficient measurements agreed well with prior values of two to four TBP molecules per aggregate determined by small angle scattering. The nature of the interactions between TBP aggregates was evaluated by assuming that the TBP aggregates could be treated as particles moving through a continuum fluid using classical hydrodynamic theory[107–109, 129]. This analysis leads to the conclusion of an extended repulsive component to the interaction between aggregates, which conflicts with the strong attractive interactions found using SAXS and SANS. Given the comparable sizes of the nonpolar diluent and TBP aggregates, the assumption of continuum hydrodynamics may be suspect. The Wilke-Chang equation[92], which does not apply in the hydrodynamic regime, was used instead of the Stokes-Einstein equation[101] to relate

the diffusion coefficient to size because of the small sizes of aggregates determined previously by SANS. The Stokes-Einstein equation is a poor description of this relationship for small solutes.

The diffusion of infinitely dilute particles in solution can be understood in terms of theoretical models describing two distinguishable extremes of diffusive behavior[130]. One extreme applies to colloidal systems, and the other applies to molecular systems. Diffusion in colloidal systems is described by hydrodynamic theory, in which mesoscopic colloidal particles are treated as macroscopic spheres moving through a continuum fluid. The continuum approximation is valid for solutions in which the particles comprising the surrounding fluid are very small compared to the diffusing particle. In the hydrodynamic regime, the diffusion of a particle at infinite dilution is inversely proportional to its radius. This relationship is given by the Stokes-Einstein equation[101], shown in Equation 5.1, where k_B is Boltzmann's constant, T is the temperature of the sample, η is the viscosity of the solvent at T, and r is the hydrodynamic radius of the diffusing particle. The Stokes-Einstein equation is accurate to about 20% for dilute solutions in which the solute size is greater than or equal to five times the size of the solvent[101].

$$D_0 = \frac{k_B T}{6\pi\eta r} \tag{5.1}$$

In contrast, using Enskog theory, the diffusion of a hard sphere through a fluid comprising hard spheres of comparable size can be shown to be inversely proportional to the square of the radius[130]. In real systems, the diffusion of a molecular (non-mesoscopic) species at infinite dilution is better described by models approaching a square dependence, such as the Wilke-Chang correlation, given in Equation 5.2 for spherical particles, where χ is an empirical parameter related to the self-association of the solvent and M_B is the solvent molecular weight[92]. The Wilke-Chang correlation is accurate to about 10% for dilute solutions of small, nondissociating solutes[131].

$$D_0 = 3.1 \times 10^{-8} \frac{\sqrt{\chi M_B} T}{\eta r^{1.8}} \tag{5.2}$$

As described in our previous work, an expression for the concentration dependence of the diffusion of colloidal particles can be derived from hydrodynamic theory[128]. The diffusion coefficient of particles in the hydrodynamic regime increases with increasing solute volume fraction at low concentrations according to the linear relationship[99]:

$$D = D_0(1 - \alpha\varphi) \tag{5.3}$$

where α is a unitless interaction parameter combining contributions from the second virial coefficient of the particles and their hydrodynamic interactions, and φ is the solute volume fraction. For a system of hard spheres, multiple theoretical approaches have determined α to be approximately two[107–109, 129]. For a system of aggregating colloidal particles, α is greater than two[97]. In real colloidal systems whose speciation does not change with concentration, α is determined empirically by measuring the diffusion coefficient of particles at different dilutions. No similarly simple diffusion coefficient/concentration relationships exist for molecular solutes.

In this paper, we will assess the treatment of TBP aggregates as colloidal particles in single phase organic samples under PUREX-like conditions using both experimental and computational methods. First, the results of diffusion NMR spectroscopy, rheology, and SANS experiments will be interpreted by treating the aggregates as colloids, and compared with the results of molecular dynamics (MD) simulations. Each of these experimental methods has been used extensively in the characterization of colloidal solutions and complex fluids due to the relative ease of developing theoretical treatments for spherical particles in a continuum solvent and, in the case of SANS, radiation scattering by the correlations in positions of spherical particles. In contrast, the development of theory to describe diffusion, viscosity, and small angle scattering for interacting aggregates at a molecular scale in solution is more challenging because the interactions between each type of particle in the system must be explicitly addressed. Such complex systems often cannot be dealt with analytically, making computational methods such as MD simulation the most effective means of theoretically treating the dynamic and equilibrium properties of molecular solutions.

5.3 Experimental Section

5.3.1 Materials

All materials and solutions used here have been described elsewhere[128]. SANS samples were prepared with deuterated *n*-dodecane, obtained from C/D/N Isotopes (98 atom % D; Pointe-Claire, Quebec, Canada), in place of the unlabeled compound.

5.3.2 Sample Preparation and Characterization

Organic phase TBP samples containing 30 v/v % TBP dissolved in *n*-dodecane were prepared and characterized as described elsewhere[128]. Briefly, all single phase organic TBP samples were prepared using a 30% TBP organic phase (pre-equilibrated with 3 M HNO_3) contacted with an aqueous phase of equal volume containing 3 M HNO_3 and varying amounts of $UO_2(NO_3)_2$ or $Zr(NO_3)_4$. The exceptions were a sample of the 30% TBP solution that had not been contacted with any aqueous phase (TBPO), and a sample of the 30% TBP solution contacted with pure water (TBPW). The compositions of all samples characterized in this work are given in Table 5.1 (page 76). Metal concentrations were determined using radiotracers, while acid and water concentrations were determined by titration. All phase contacts took place at 21 ± 1 °C.

5.3.3 Diffusion Coefficient Measurements

The average diffusion coefficient of TBP in each sample was measured using the same 400 MHz NMR instrument, Bruker DIFF60 Z-diffusion probe, and pulsed-field gradient stimulated echo experiment with longitudinal eddy current delay (STE-LED) described elsewhere[128]. The diffusion of TBP was calculated by monitoring the attenuation of the peak corresponding to the proton on the carbon adjacent to the butoxy oxygen, at a chemical shift of approximately 4.3 ppm[95]. The diffusion of HNO_3 was calculated by monitoring the attenuation of the peak corresponding to the acidic proton, at a chemical shift of approximately 10.5 ppm. All experiments were performed at 27.0 ± 0.1 °C.

The infinite dilution diffusion coefficient for each sample was determined by measuring the diffusion coefficients of diluted samples with solute volume fractions between 0.12 and 0.3, and linearly extrapolating to a solute volume fraction of zero. This is the same approach used previously[128], except that the organic phase samples herein were diluted 4:1, 3:2, and 2:3 with *n*-dodecane, giving samples with approximate solute volume fractions of 0.3, 0.24, 0.18, and 0.12 in this work.

5.3.4 Viscosity Measurements

The viscosities of samples at different solute volume fractions were determined using a dilution procedure similar to that used for determining the infinite dilution diffusion coefficient. Sample Zr30 was diluted 4:1, 3:2, 2:3, and 1:4 with *n*-dodecane, giving samples with approximate solute volume fractions of 0.3, 0.24, 0.18, 0.12, and 0.06. Viscosity measurements of these samples were made using a ThermoScientific HAAKE Viscotester iQ rheometer with Peltier temperature controller and cylindrical double gap measuring geometry. In all experiments, a shear rate of 4000 s^{-1} was used. Samples were allowed to reach thermal and mechanical equilibrium at the experimental temperature, 25.1 $\pm$ 0.1 °C, after which the viscosity was measured with an integration time of 10 s.

5.3.5 SANS Measurements

All SANS measurements were performed at the general purpose SANS (GP-SANS) instrument at Oak Ridge National Laboratory's High Flux Isotope Reactor (HFIR). Organic phase TBP samples prepared with deuterated *n*-dodecane were loaded into cylindrical quartz cuvettes with a 2 mm path length (Hellma USA) for analysis. Two instrument configurations were used to cover a total scattering vector (q) range of 0.004 - 0.93 $Å^{-1}$. The two configurations used sample-to-detector distances of 12.8 m and 1.2 m, both with a wavelength of 4.75 Å and a detector offset of 0.4 m to maximize the sampled range of q at each setting. After azimuthal averaging of the raw 2-D scattering pattern, the data were reduced

Table 5.1: Initial aqueous phase and equilibrium organic phase compositions of systems characterized in this work. Samples analyzed by NMR, rheology, and SANS were taken from equilibrium organic phases.

Sample ID	*Initial Aqueous*			*Equilibrium Organic*				
	$[HNO_3]^a$ *(mol/L)*	$[Zr]^b$ *(mol/L)*	$[U]^b$ *(mol/L)*	$[TBP]^c$ *(mol/L)*	$[HNO_3]^a$ *(mol/L)*	$[H_2O]^a$ *(mol/L)*	$[Zr]^b$ *(mol/L)*	$[U]^b$ *(mol/L)*
TBPO	-	-	-	1.1	0	0.02	0	0
TBPW	0	0	0	1.1	0	0.41	0	0
N3	3.0	0	0	1.1	0.73	0.39	0	0
Zr05	3.0	0.050	0	1.1	0.61	0.37	0.0025	0
Zr10	3.0	0.10	0	1.1	0.66	0.36	0.0039	0
Zr20	3.0	0.20	0	1.1	0.63	0.37	0.0057	0
Zr30	3.0	0.30	0	1.1	0.67	0.37	0.0073	0
U10	3.0	0	0.10	1.1	0.54	0.27	0	0.095
U20	3.0	0	0.20	1.1	0.44	0.19	0	0.19
U30	3.0	0	0.30	1.1	0.36	0.14	0	0.27
U40	3.0	0	0.40	1.1	0.26	0.09	0	0.34

[a]Average uncertainty 2%; [b]Average uncertainty 3%; [c]Estimated uncertainty 2%

following standard procedures using routines developed at HFIR operating in Igor Pro by Wavemetrics. This includes corrections for detector response, background scattering by the empty sample cell, and calibration to direct beam with a calibrated attenuator for absolute scale[132]. All SANS experiments were run at 25.0 ± 0.1 °C.

5.3.6 SANS Data Analysis

The SANS scattering intensity of a monodisperse system of spherical particles can be expressed as[82, 133]:

$$I(q) = \varphi V_p \Delta\rho^2 P(q) S(q) \tag{5.4}$$

where φ is the solute volume fraction, V_p is the volume of a scattering particle, $\Delta\rho$ is the difference between the scattering length densities of the solvent and particles, $P(q)$ is the particle form factor, and $S(q)$ is the structure factor. The particle form factor is related to the shape of the scattering particle, while the structure factor reflects the nature of the interactions between particles. Consistent with prior small angle scattering experiments on solvent extraction systems, all samples were assumed to contain uniform particles made of TBP and polar solute molecules in a uniform solvent made of deuterated *n*-dodecane. The primary contribution to the scattering contrast is the difference in scattering probability between hydrogen in the TBP and deuterium in the *n*-dodecane solvent. The scattering length density for each type of molecule, $SLD_{mol,j}$, was calculated by summing the coherent neutron scattering lengths, b_i, for each constituent atom, i, divided by the molecular volume, V_{mol} (Equation 5.5). The scattering length density of the particles in each sample, SLD_{part}, was calculated by multiplying the scattering length density for each molecule type, $SLD_{mol,j}$, by its volume fraction in the particles, φ_j, where j corresponds to the molecule type (Equation 5.6)[134, 135]. The solvent scattering length density, that of deuterated *n*-dodecane, was taken as a constant for all samples.

$$SLD_{mol,j} = \sum_{i=1}^{n} \frac{b_i}{V_{mol}} \tag{5.5}$$

$$SLD_{part} = \sum_{j=1}^{n} \varphi_j \times SLD_{mol,j} \tag{5.6}$$

The experimental SANS data were fit by Equation 5.4 using the form factor for a spherical particle and the structure factor for the Baxter model[24, 32, 82, 136], and including a constant term for incoherent scattering, I_{inc}, which results primarily from the hydrogen in the sample. An optimized fit of the experimental data was produced by varying the particle diameter, interaction strength, and incoherent scattering terms to minimize the sum of the squared errors using the generalized reduced gradient algorithm for nonlinear optimization. For modeling purposes, the sphere diameter in the form factor function and the hard sphere diameter in the structure factor function were assumed to be equal (the HS diameter). The uncertainties in the measured intensities for all samples at all values of q was less than 2%. When the scattering data for samples N3, Zr30, and U40 were modeled using the SASfit software package, the relative standard deviations of the particle diameters and τ^{-1} were less than 1%[137]. The uncertainty in the fitted parameters for the remaining samples is assumed to be similar in magnitude. Errors resulting from the goodness-of-fit to the data or appropriateness of the model for the system were not addressed, which is consistent with prior work in the literature.[24–30]

5.3.7 Molecular Dynamics Simulations

The classical molecular dynamics potentials used to simulate TBP, *n*-dodecane, nitric acid and water have been previously reported[138]. Simulation compositions of the post-contact organic phase were chosen to correspond to extraction of 5 M HNO_3 by 20% TBP and 3 M HNO_3 by 30% TBP. Those compositions are given in Table 5.2.

Initial configurations were generated with the Packmol software[139]. Molecular dynamics simulations were performed using the GROMACS 4.5.5 software package[140]. The isobaric isothermal NPT ensemble with periodic boundary conditions and a leap-frog Verlet integrator were used for all simulations. Pressure was set to 1 bar with the Berendsen

Table 5.2: The experimental conditions (first two columns) and corresponding numbers of molecules used in simulation with a $10.5 \times 10.5 \times 10.5$ nm box.

% TBP	$[HNO_3]_{aq,i}$ *(mol/L)*	*# TBP*	*# n-dodecane*	$\# HNO_3$	$\# H_2O$
20	5	528	2368	477	94
30	3	789	2118	398	194

barostat and temperature to 300 K with the Berendsen thermostat during equilibration and the Nose-Hoover thermostat during sampling. Particle-Mesh Ewald summation was used for long-range electrostatic summation with a 15 Å cut-off for short range electrostatic and van der Waals interactions. The LINCS algorithm was used for constraining hydrogen-containing bonds to enable use of a 2 fs time step. Each system was run 10 times and values presented here are averages over those 10 runs. Each run consisted of a 10 ns equilibration time followed by a 50 ns production run where coordinates were recorded for analysis every 20 ps.

The hydrogen bonding definitions and cluster analysis of the hydrogen bonded species that we have previously reported for the TBP/water/nitric acid system were implemented. In the cluster analysis, TBP and polar solute molecules are counted as connected if at least one hydrogen bond exists between them. Clusters are defined as a group of connected molecules. To facilitate comparison with scattering and diffusion data, we computed the TBP aggregation number for each cluster, defined as the number of TBP in that cluster. The TBP aggregation number distribution is then the probability of a TBP occuring in a cluster with a given TBP aggregation number.

5.4 Results and Discussion

5.4.1 Diffusion Data - Colloidal Interpretation

The Stokes-Einstein equation and the Wilke-Chang correlation were used to determine the average hydrodynamic radii of TBP species in samples with different water, nitric acid, and metal concentrations. The infinite dilution diffusion coefficients (D_0) for the samples, derived from dilution experiments, were used to calculate the radii and corresponding particle

volumes, given in Table 5.3. The hydrodynamic radii calculated using the Stokes-Einstein equation substantially underestimate the sizes of the diffusing TBP species, yielding particle volumes less than that corresponding to a single TBP molecule (455 Å^3) in most cases. In contrast, particle volumes calculated using the Wilke-Chang correlation are consistent with the sizes of 2:1 TBP to metal complexes established in distribution studies[19]. These results show that the sizes of organic phase TBP species are best described as inversely related to the square of the radius and are in the molecular, rather than hydrodynamic, regime.

Table 5.3: The volumes of TBP species are realistic when calculated using the Wilke-Chang (W-C) correlation rather than the Stokes-Einstein (S-E) equation. Use of the Stokes-Einstein equation results in particle volumes less than that of a single TBP molecule (455 Å^3) for most samples.

Sample ID	D_0[a] *(m^2/s)*	*W-C Radius*[a] *(Å)*	*W-C Volume*[b] *(Å^3)*	*S-E Radius*[a] *(Å)*	*S-E Volume*[c] *(Å^3)*
N3	4.68×10^{-10}	6.30	1047	3.63	200
Zr05	4.65×10^{-10}	6.32	1058	3.65	204
Zr10	4.65×10^{-10}	6.32	1056	3.65	203
Zr20	4.72×10^{-10}	6.27	1031	3.60	195
Zr30	4.76×10^{-10}	6.23	1015	3.56	189
U10	4.23×10^{-10}	6.66	1237	4.01	270
U20	3.83×10^{-10}	7.03	1458	4.43	363
U30	3.50×10^{-10}	7.40	1700	4.85	479
U40	3.42×10^{-10}	7.49	1763	4.96	511

[a]Average uncertainty 2%; [b]Average uncertainty 3%; [c]Average uncertainty 6%

In the investigated TBP samples, α, the unitless interaction parameter, was determined by measuring the diffusion coefficients of TBP species in a series of samples diluted with *n*-dodecane and assuming that there were no significant changes in speciation. A line was fit to the resulting data, and values for D_0 and α were calculated. The α values for all samples fell between 0.89 and 1.28, which in our previous work we attributed to repulsive interactions between species[128]. An alternative explanation for this observed trend is that the results from hydrodynamic theory do not apply to this system, and a better treatment would involve explicit consideration of molecular scale solvent-solute interactions. Given the failure of the Stokes-Einstein equation when applied to our samples, this may be a better explanation for

the observed dependence of the diffusion coefficient on solute volume fraction.

5.4.2 Viscosity Data - Colloidal Interpretation

In classical hydrodynamic theory, the viscosity of colloidal systems increases with increasing particle concentration. This behavior is observed in water-in-oil microemulsions, where the viscosity dependence on solute volume fraction is well-described by the hard sphere model[141]. An empirical relationship between concentration and viscosity for concentrated solutions of hard spheres developed by Thomas is given in Equation 5.7, where η_{rel} is the viscosity of the system divided by that of the pure solvent, and φ is the volume fraction of the dispersed material[142]. The higher order terms in Equation 5.7 can be disregarded in dilute solutions (<0.02 solute volume fraction), where a linear dependence is observed. Equation 5.7 is valid for solute volume fractions of up to 0.6 in suspensions of spherical particles made of various materials, such as glass and polystyrene[142]. It has also been used successfully to describe the concentration dependence of the viscosity of an oil-in-water microemulsion[143] and a water-in-oil nanoemulsion[144]. Structures formed in TBP solvent extraction systems containing mineral acids and metals have often been described as water-in-oil microemulsions or reversed micelles[25, 27, 30, 31, 118, 145]. It would be expected that if such supramolecular species were being formed, the relationship in Equation 5.7 would be fulfilled, as is found in traditional surfactant systems.

$$\eta_{rel} = 1 + 2.5\varphi + 10.05\varphi^2 + 0.00273e^{16.6\varphi} \tag{5.7}$$

Data for the relative viscosities of a series of dilutions of sample Zr30 with *n*-dodecane at 25.1 ± 0.1 °C are plotted as points in Figure 5.2, with a line corresponding to Thomas' empirical expression for the viscosity of a hard sphere suspension. Again, it was assumed that TBP speciation is not substantially affected by dilution with *n*-dodecane. A measured *n*-dodecane viscosity of 1.35 cP was used to calculate the relative viscosities. The experimentally observed increase in viscosity with increasing solute volume fraction is much less than the exponential relationship expected for a system of hard spheres. This increase is also

less than the exponential relationship observed in any of sixteen oil-in-water and water-in-oil emulsion systems[146]. The deviation from colloidal behavior of TBP samples is consistent with the trends observed in the diffusion data, as would be expected given the close interrelationship between diffusion and viscosity in a fluid. The combined results from both data sets give further credence to the premise that the organic phase in the PUREX process and other TBP solvent extraction systems should be treated as a molecular solution.

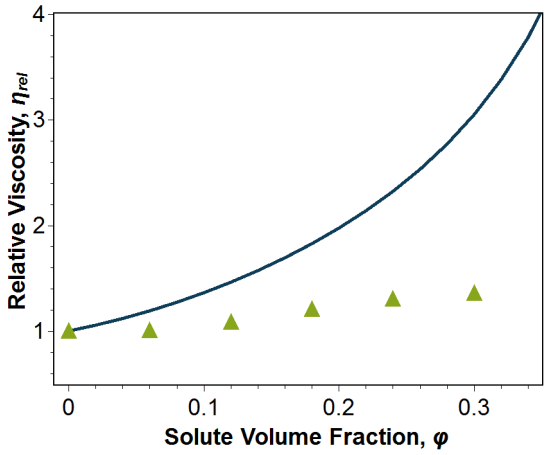

Figure 5.2: The dependence of the viscosity of a TBP organic phase containing zirconium on solute volume fraction (triangles) is not consistent with Thomas' empirical relationship for concentrated systems of hard spheres (line).

5.4.3 SANS Data - Colloidal Interpretation

5.4.3.1 SANS Indirect Method

There are two major ways to approach the analysis and interpretation of solution phase small angle scattering data: the direct and indirect methods[81, 86, 147]. In the direct method, a model describing the structure of scatterers in a sample is posited based on independent experimental or computational work and used to calculate a theoretical scattering pattern, which is then compared with experimental data. In the case of SANS, the scatterers are the atomic nuclei in the sample[134]. If the solution structure is known at an atomic level, as in the case of a trajectory calculated from an all-atom MD simulation, a theoretical

scattering pattern can be directly calculated from the known correlations between nuclei, and nuclear scattering cross sections[148]. If explicit correlations betweens scattering nuclei are not known, the direct method requires using a simplified model for the solution structure, e.g., assuming the existence of large scattering particles, in which the coherent neutron scattering cross sections of the atomic nuclei in a particle are evenly distributed across its volume. A scattering pattern, resulting from the difference in scattering probability between the particles and the surrounding medium, can then be calculated and fit to experimental data by varying the particle model parameters. This latter approach has been used successfully in colloidal systems[81, 86, 149], which can be modeled as particles dispersed in a solvent, and is less demanding than the former approach, which requires the development of rigorously validated forcefields.

In the indirect method, an attempt is made to reverse the Fourier transformation effected by the scattering experiment to recover the solution structure with a minimum of *a priori* assumptions. For a dilute solution of scattering particles, the indirect Fourier transformation (IFT) method can be used to recover the pair distance distribution function (PDDF) of the scattering particles, from which the sizes and shapes of the scattering particles can be inferred without the need to assume an intra-particle scattering (form factor) model[150, 151]. For concentrated solutions of scattering particles, the generalized indirect Fourier transformation (GIFT) method can be used to recover the PDDF of the scattering particles without the need for an intra-particle scattering model, by first assuming a particle interaction (structure factor) model[152, 153].

Ideally, the interpretation of small angle scattering data would rely on the use of both direct and indirect methods. An example of such an analysis is provided by Pedersen, in which the indirect method is used to choose an appropriate simplified scattering model for use in the direct method[82]. Consistent with this approach, the GIFT method was initially used to interpret our SANS data for sample U40. An accurate solution function calculated using GIFT is characterized by minimal oscillations and a small mean deviation

between the calculated and the experimental scattering patterns[151, 154]. A minimally-oscillating PDDF and low mean deviation indicate that the calculated PDDF both describes the experimental data well, and captures important structural information. However, we were unable to determine an accurate, stable solution for the indirect Fourier transformation of our SANS data using a monodisperse hard sphere structure factor. The use of a structure factor incorporating an attractive or repulsive interparticle potential would require making substantial assumptions about the nature of the attractive interactions between particles to limit the accessible parameter space, effectively eliminating the model-free aspects of the GIFT method. Because of these constraints, the GIFT method could not be used to interpret the SANS data in this work.

5.4.3.2 SANS Direct Method

Because we were unable to use an indirect method to aid in the selection of a simplified particle scattering model, it was necessary to select a model based on the shape of the scattering data. In colloidal systems, deconvolution of the contributions from the shapes of the particles, their polydispersity, and their interactions to the scattering intensity cannot be accomplished without additional independent information about the system[147]. Definitive independent information on the polydispersity and shapes of TBP species in solution does not exist, so the simplest model capable of describing the system—a model assuming monodisperse spheres interacting through the Baxter potential—was used. This model, used previously in small angle scattering investigations of TBP structure, requires only two parameters to describe the size of the scatterers and the nature of their interactions. These correspond to the HS diameter and τ^{-1}, the stickiness parameter, respectively.

A major benefit of the Baxter model is its ability to describe the very slight rise in the scattering intensity with decreasing q in the mid to low q range for all samples, as shown in Figure 5.3. This rise is the result of fluctuations in the density of scatterers. The trend at low q suggests that the hydrogen-containing TBP molecules are associated in solution, and precludes the use of a hard sphere model for particle interactions. The low q

data also undermine our previous finding of repulsive interactions between TBP species in solution, determined from diffusion measurements using an assumption of colloidal behavior. An example fit of this model to the SANS data for sample U40 is given in Figure 5.3. This figure shows that the model fits the data well at low to mid q values, but includes oscillations at high q that are not seen in the data.

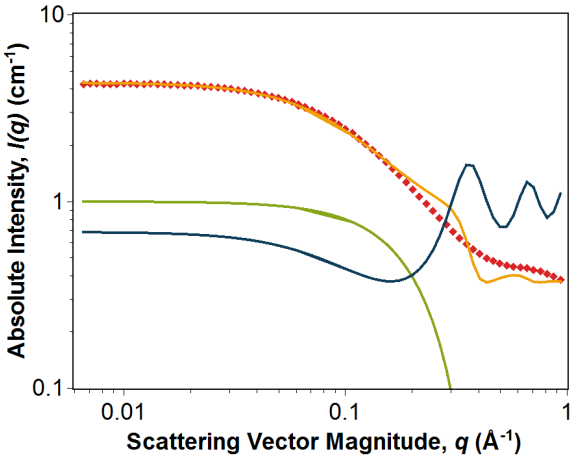

Figure 5.3: A model assuming that TBP species are monodisperse spheres interacting through the Baxter potential (Fitted $I(q)$: yellow line, $P(q)$: green line, $S(q)$: blue line) is able to describe experimental scattering for sample U40 (red diamonds) in the low to mid q region well. Deviations at high q result primarily from the absence of a correlation peak in the data. Experimental error bars are smaller than the markers.

The results of fitting the Baxter model to our SANS data are given in Table 5.4. A comparison of the diameters of TBP species determined using SANS and diffusion NMR spectroscopy for samples containing 20% and 30% TBP is provided in Figure 5.4. The average diameters of TBP species in all samples evaluated in this work range from 16.0 to 21.0 Å, while the values for τ^{-1} range from 4.20 to 7.59. As has been found in previous scattering work, the fitted particle diameters appear to increase with increasing uranium concentration[24]. The particle diameters remain constant with increasing zirconium concentration, which is not inconsistent with past observations of slowly decreasing particle diameter with increasing zirconium concentration[27]. Unlike in prior work, the strength of the attractive interactions between particles does not trend upward with increasing metal

concentration, although the values for τ^{-1} are similar in magnitude to those calculated previously (5-10). The τ^{-1} values calculated for each sample are so great that they exceed the percolation threshold for the Baxter fluid. The percolation threshold for each sample, given in Table 5.4, is the minimum value of τ^{-1} at which the Baxter fluid is percolated for a given solute volume fraction[125].

Table 5.4: Parameters used to fit the Baxter model to experimental SANS data, and the results of those fits.

Sample	Solute Fraction	$\Delta\rho^2$ cm^{-4}	HS Diameter[a] $\AA$	$\tau^{-1,a}$	$I_{inc}{}^a$ cm^{-1}	Perc. Threshold τ^{-1}
TBPO	0.302	4.29×10^{21}	16.0	4.20	0.407	2.75
TBPW	0.308	4.31×10^{21}	18.5	4.91	0.407	2.63
N3	0.339	3.95×10^{21}	20.4	7.08	0.388	2.09
Zr05	0.334	3.99×10^{21}	20.1	7.57	0.371	2.17
Zr10	0.336	3.97×10^{21}	21.0	7.41	0.401	2.14
Zr20	0.335	3.97×10^{21}	20.6	7.59	0.389	2.15
Zr30	0.337	3.95×10^{21}	20.5	7.29	0.419	2.13
U10	0.336	3.88×10^{21}	18.8	7.04	0.326	2.14
U20	0.337	3.78×10^{21}	20.3	6.56	0.382	2.13
U30	0.338	3.68×10^{21}	20.6	6.51	0.367	2.10
U40	0.339	3.61×10^{21}	20.8	6.51	0.368	2.10

[a]Estimated uncertainty 1%

5.4.3.3 Problems with Using the Baxter Model

When used to interpret scattering data for single phase organic TBP samples, the Baxter model yields problematic results. The τ^{-1} values calculated for all samples are so large that they exceed the threshold value beyond which the Baxter fluid has been found, both analytically and in Monte Carlo simulations, to percolate[125, 127]. According to the Noro-Frenkel law of corresponding states[155], this threshold holds for all systems of particles with equivalent reduced second virial coefficients interacting through a spherically symmetric short-ranged attraction, regardless of its form. Similar τ^{-1} values in the percolation region of the Baxter fluid have been calculated for TBP samples in prior scattering work. These τ^{-1} values were converted to the depth of an equivalent thin square well potential, which appeared to suggest a weaker attractive interaction. However, this transformation does not

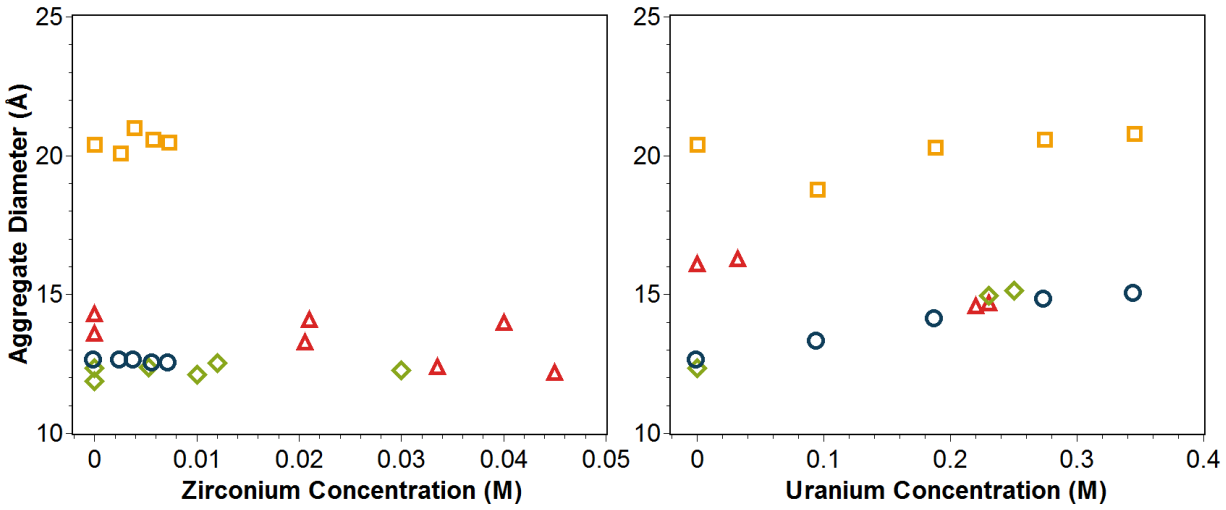

Figure 5.4: The SANS diameters for 30% TBP samples (yellow squares), found in this work, are approximately 1.5 times greater than those determined for 30% TBP samples by diffusion (blue circles), also determined here, 20% TBP samples by diffusion (red triangles)[128], and 20% TBP samples by SANS (green diamonds)[24, 27].

alter the percolated structures implied by these attractive interactions. The existence of percolated structures is contradicted by diffusion measurements.

The fast diffusion of TBP observed in all samples demonstrates that percolated structures are not formed, independent of assumptions about whether the diffusing species are colloidal. Diffusion coefficients of TBP species in undiluted metal and acid-containing samples (Figure Figure 5.8) are the same order of magnitude as that of a 30% TBP solution that has not been contacted with an aqueous phase (4.3×10^{-10} m^2/s), demonstrating that TBP forms small, discrete structures in solution. Thus, the attractive interactions between TBP species quantified using the Baxter model to interpret SANS data are likely much stronger than the true values for the system. The Baxter model appears to be a poor description of the weak van der Waals attractions between neutral TBP species, to which attractive interactions between TBP species have been previously attributed.

Additionally, the SANS diameters of TBP species in 30% TBP samples are consistently about 1.5 times larger at a given metal concentration than those determined using SANS for 20% TBP samples, and diffusion NMR spectroscopy diameters for both 20% and 30% TBP

samples. This trend is illustrated in Figure 5.4. A similar dependence of TBP aggregate diameter on TBP concentration in SANS experiments using the Baxter model has been observed previously in the literature[25]. Assuming spherical particles, the observed increase in particle diameter between 20% TBP and 30% TBP samples corresponds to a more than threefold increase in volume and, by extension, aggregation number. Such a large increase in size would result in significant differences in the measured TBP diffusion coefficients at different TBP concentrations, which is not observed. Specifically, the decrease in the TBP diffusion coefficient between polar solute-containing 20% and 30% TBP samples would be large compared to the decrease observed between uncontacted 20% and 30% TBP samples, in which TBP is known to form only small associated species[156–158]. These observations are also independent of assumptions about whether the diffusing species are colloidal.

Solutions of TBP in *n*-dodecane without any other solutes are known to contain TBP monomers and some associated species, mostly dimers and trimers. The distribution of TBP among these species does not change significantly between samples at 20% and 30% TBP. Consequently, the change in TBP diffusion coefficient with TBP concentration is small, decreasing from 4.8×10^{-10} m^2/s to 4.3×10^{-10} m^2/s between 20% TBP and 30% TBP solutions. The diffusion coefficient of TBP in an organic phase containing 0.006 M Zr decreases by nearly the same relative amount, from 3.8×10^{-10} m^2/s to 3.2×10^{-10} m^2/s, between 20% TBP and 30% TBP solutions. Similarly small decreases are observed in zirconium samples at different concentrations, and in the uranium samples, demonstrating that substantial changes in the average size of TBP species in 20% and 30% TBP samples do not occur. This suggests that the changes in particle size with TBP concentration determined by fitting the Baxter model to small angle scattering data are more likely an artifact of the model used rather than a reflection of real changes in TBP aggregate size. These model-independent diffusion results demonstrate that the Baxter model used to interpret SANS data in these TBP samples yields unphysical values for aggregate size and interaction strength.

5.4.4 Structures from Molecular Dynamics Simulations

Similar conclusions can be made from MD simulations of systems containing TBP, *n*-dodecane, water, and nitric acid. Figure 5.5 shows snapshots of the simulation boxes for the 20% (left) and 30% (right) TBP systems. Rather than a percolated network of spherical particles, as implied by the choice of the Baxter potential, simulation shows formation of small, discrete species. Figure 5.6 shows the two predominant species in solution, the 1:1 TBP:HNO_3 adduct and a 2:1 TBP:H_2O "bridged" species. In the 20% TBP system, several small pockets of water solvated by TBP can be observed. However, these are not numerous or large enough to significantly affect the average TBP aggregation number, which is dominated by the 1:1 TBP:HNO_3 adduct. The absence of water pockets in the 30% system is likely a reflection of the lower nitric acid concentration rather than the increased TBP volume fraction. In the 30% system, owing to the lower initial aqueous nitric acid concentration, the reduced ratio of acid to TBP means that there are fewer TBP-HNO_3 hydrogen bonds per TBP molecule. Therefore, more TBP are free to hydrogen bond to water, disrupting the formation of water pockets.

Hydrogen bonded clusters were measured from simulation to quantify the distribution of TBP among species in solution. The TBP aggregation number distributions for 30% TBP samples and 20% TBP systems are compared to evaluate the Baxter model scattering results indicating significant increases of up to three times the TBP aggregation number with a 50% increase in the TBP concentration. Figure 5.7 shows TBP aggregation number distributions for both systems. We computed the number weighted average TBP aggregation numbers, which were found to be nearly the same for both systems at 1.84 for 20% TBP and 1.87 for 30% TBP. This is consistent with our previously reported average TBP aggregation number of 1.7 for 20% TBP and 5 M HNO_3 found using diffusion NMR spectroscopy[128].

For both TBP volume fractions, nearly all of the TBP occur in a one-TBP cluster, most often the 1:1 TBP:HNO_3 adduct. The 1:1 TBP:HNO_3 species was observed 0.751 times per TBP in the 20% TBP 5 M HNO_3 simulation and 0.411 times per TBP in the 30% TBP

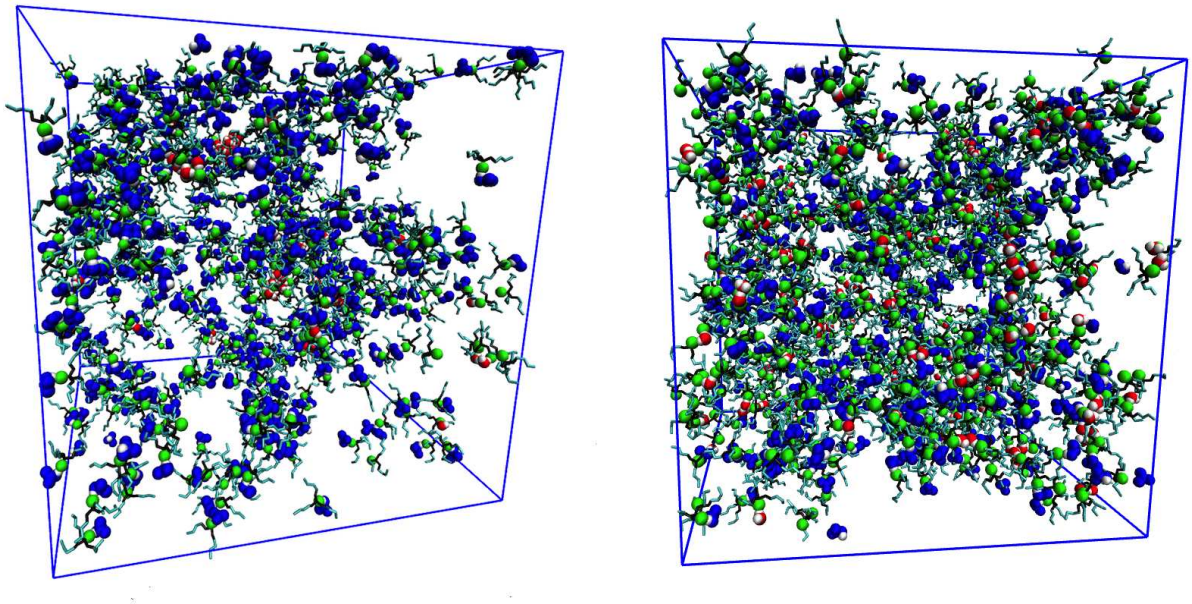

Figure 5.5: Simulation boxes for the 20% (left) and 30% (right) TBP simulations. The majority of TBP is observed to form 1:1 adducts with a single nitric acid molecule in both systems. TBP phosphoryl oxygen atoms are depicted as green spheres, with the phosphate group atoms as black lines and butyl tails as cyan lines. Water oxygen atoms are red with white hydrogen atoms. Nitric acid oxygen and nitrogen atoms are blue with white hydrogen atoms.

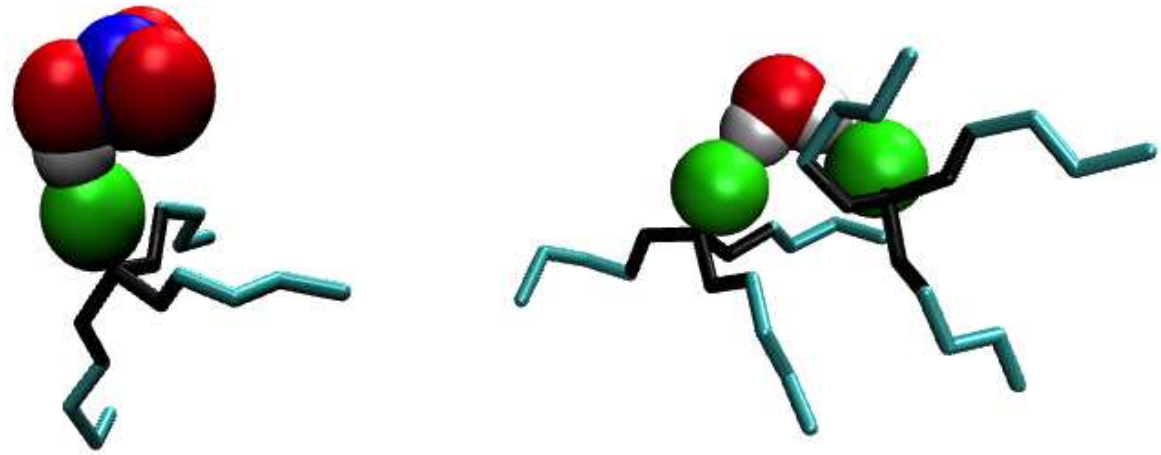

Figure 5.6: TBP is primarly found in small hydrogen bonded structures like the 1:1 TBP:HNO_3 adduct (right) and the 2:1 TBP:H_2O "bridged" species (left). Molecules are colored as described in Figure 5.5 with the exception of nitric acid oxygen atoms depicted here as red.

3 M HNO_3 simulation. The other most probable clusters were the TBP monomer, measured 0.065 times per TBP in the 20% system and 0.225 times per TBP in the 30% system, and the 2:1 TBP:H_2O "bridged" species, at 0.003 per TBP for 20% and 0.051 per TBP for 30%. The probabilities of TBP molecules existing in larger TBP aggregation number clusters decline rapidly with TBP aggregation number for both TBP volume fractions. Differences in TBP aggregation number that would indicate substantially different scattering particle volumes are not observed between the TBP volume fractions. The TBP aggregation number distribution in a nitric acid system shows that the organic phase appears to be a molecular solution made up of small, discrete species that occasionally associate to form short-lived larger aggregates of variable size. The Baxter fluid model does not describe the solution-phase structures observed in these simulations. The absence of a dependence of TBP aggregation number on solute volume fraction in nitric acid only simulations suggests that the dependence derived from using the Baxter model to interpret SANS data results from inadequacies in the model. The same SANS solute volume fraction dependence found in metal-containing systems is likely to result from the same inadequacies in the model rather than an unanticipated difference in physical behavior.

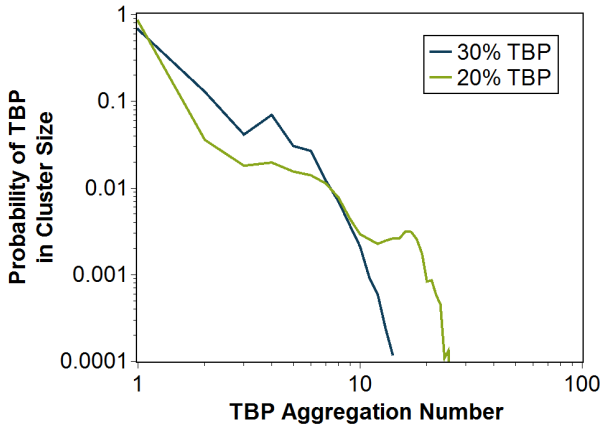

Figure 5.7: The probability of TBP occuring in a cluster with a given TBP aggregation number is plotted against the TBP aggregation number.

5.4.5 Diffusion Data - Molecular Interpretation

This section reinterprets the same set of TBP diffusion coefficients, considered earlier from a colloidal standpoint, from a molecular point of view. In the molecular regime, theoretical relationships between the concentration of a solute and its diffusion coefficient are not well-developed. Therefore, the observed relationship between diffusion coefficient and volume fraction cannot be easily interpreted as a reflection of the nature of solute-solute interactions, as in the hydrodynamic regime. Instead, the relationship between diffusion coefficient and volume fraction is impacted by solute-solute, solute-solvent, and solvent-solvent interactions[101]. At best, it can be stated that the previously described dependence of the diffusion coefficient on solute volume fraction is consistent with systems of associating solutes[159, 160].

Given the assumptions required to convert TBP diffusion coefficients to an aggregation number (no change in speciation on dilution, spherically shaped particles whose volumes are filled completely by the partial molar volumes of TBP and extracted solutes), it is useful to consider only the measured diffusion coefficients in undiluted samples to come to qualitative conclusions about the nature of TBP species in solution. The diffusion coefficient can be considered to be inversely proportional to aggregate size, assuming that changes in the interactions between species in solution have less of an impact on the diffusion coefficient than species size at a constant TBP concentration. This assumption is reasonable because interactions between neutral species in a nonpolar solvent are likely the result of weak van der Waals forces, and would not be expected to change significantly with solute composition at a given TBP concentration. This also allows us to consider the significance of nitric acid diffusion in these samples, which was measurable only in undiluted samples due to the low nitric acid concentrations. While average TBP diffusion coefficients include contributions from all possible TBP species, the average nitric acid diffusion coefficient only includes contributions from nitric acid/TBP species. These data are presented in Figure 5.8. For reference, the diffusion coefficient of TBP in an uncontacted 30% TBP sample is 4.3×10^{-10}

m^2/s.

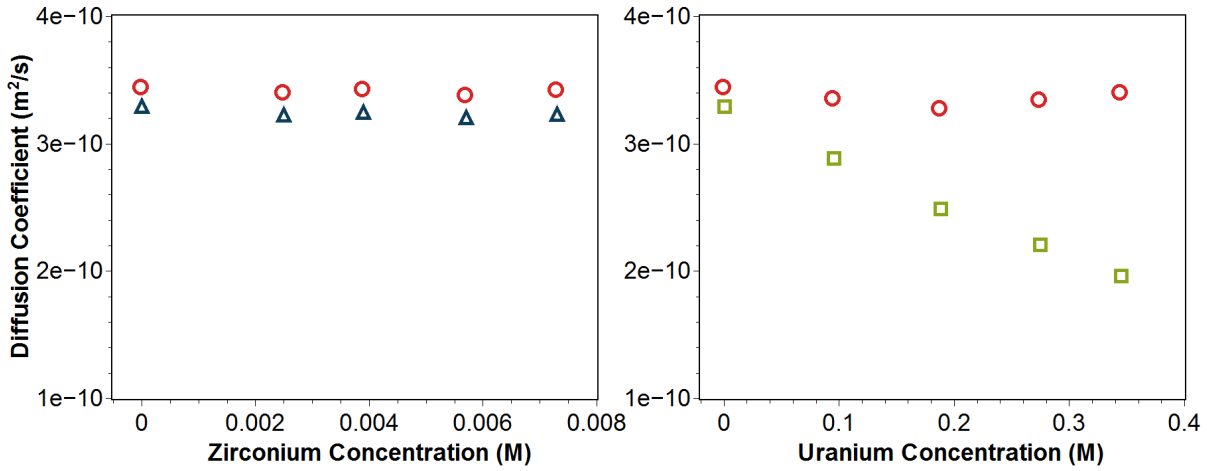

Figure 5.8: For 30% TBP samples, the change in the diffusion of nitric acid (red circles) with metal concentration is negligible, suggesting consistently sized aggregates. The change in TBP diffusion with metal concentration for samples containing zirconium (blue triangles) and uranium (green squares) is only appreciable in the uranium samples. Error bars are smaller than the markers.

The low metal concentrations in the zirconium samples make it difficult to interpret the diffusion data. The contribution of zirconium-containing TBP species to the average TBP diffusion coefficient is small compared to the contribution from water or acid species. Very generally, these data suggest that nitric acid-containing TBP species are marginally smaller than TBP species on average and that the sizes of nitric acid-containing species are constant. No strong conclusions can be made regarding the nature of the zirconium-containing species in solution because of the low zirconium concentration. However, the formation of a single nitric acid species with TBP agrees with the results of MD simulations presented previously.

In contrast, uranium concentrations are high enough that differences between nitric acid-containing species and uranium-containing species can be clearly observed. Again, the consistent nitric acid diffusion coefficients suggest that nitric acid-containing species are small and identically sized at all uranium concentrations. The average TBP diffusion coefficient decreases substantially with increasing uranium concentration, suggesting that uranium-containing species are larger than, and separate from, nitric acid-containing species. These

observations are consistent with a molecular, stoichiometric understanding of TBP extraction, in which 1:1 TBP:HNO_3 and 2:1 TBP:$UO_2(NO_3)_2$ adducts are considered to be dominant in solution.

5.5 Conclusions

In this work, it was demonstrated that TBP aggregates in solution do not behave as colloids, and that PUREX and some similar solvent extraction organic phases containing TBP should be treated as molecular solutions. When interpreted assuming that TBP forms colloidal species, diffusion, viscosity, and SANS data for 30% TBP samples containing nitric acid and uranium or zirconium yield contradictory or physically unrealistic results. The assumption that TBP forms reversed micelles interacting through surface adhesion is shown to be inconsistent with diffusion measurements and the results of MD simulations. Snapshots from these simulations illustrate what the small, molecular species formed by TBP in the presence of nitric acid and water look like. TBP aggregate size distributions derived from MD simulations show that the dominant hydrogen bonded species formed by water and nitric acid extracted by TBP are independent of TBP concentration. These data also show less common, larger transient clusters. Finally, the results of interpreting diffusion measurements assuming that TBP forms simple, molecular solutions are presented. These conclusions suggest that considering acids and metals extracted by TBP as molecular species is key to understanding the fundamental mechanisms underlying solvent extraction in certain types of TBP solvent extraction systems.

5.6 Acknowledgements

This material is based upon work supported by the U.S. Department of Homeland Security under Grant Award Number, 2012-DN-130-NF0001. The views and conclusions contained in this document are those of the authors and should not be interpreted as representing the official policies, either expressed or implied, of the U.S. Department of Homeland Security.

A portion of this research used resources at the High Flux Isotope Reactor, a DOE Office of Science User Facility operated by the Oak Ridge National Laboratory.

The authors would like to thank Dr. Ross J. Ellis for his insightful discussions about SAXS and SANS. We are also grateful to Dr. Jong K. Keum and Dr. Kenneth C. Littrell at ORNL for their assistance with our small angle scattering experiments, as well as Dr. Nathan Crawford and Thermo Fisher Scientific for providing instrument access and training for our rheology measurements.

Finally, the authors thank the Colorado School of Mines High Performance Computing center for computational resources.

CHAPTER 6
SUMMARY AND CONCLUSIONS

In this work, solvent extraction systems containing macroscopic concentrations of metals were investigated to understand the molecular-scale forces driving extraction in applied separations. Recently, it has been suggested that extraction by neutral solvating extractants in concentrated inorganic systems is governed by extractant aggregation rather than specific chemical interactions[31, 118]. To test this hypothesis, the extraction chemistries of solvating extractants from two different separations processes with applications in industrial-scale metal separations were considered.

The behavior of the PUREX process extractant, TBP, was explored under various conditions at high metal concentrations, including conditions similar to those found in industrial implementations of the PUREX process. The behavior of the extractant, TODGA, which has been considered for use in the ALSEP process, was explored in simple systems containing bulk amounts of lanthanides. Distribution studies characterizing the bulk extraction behavior of metals in these two solvent extraction systems were related to molecular-scale processes by comparison with the extraction behavior expected to result from a traditional solvation mechanism. Aggregation in the TBP system was characterized using diffusion NMR spectroscopy of 20% and 30% TBP samples. The latter samples were prepared under PUREX-like conditions. The results of diffusion, rheology, and small angle scattering experiments on TBP samples were compared with MD simulations to produce a comprehensive picture of TBP extracted species in solution. The following is a summary of this work in the context of the objectives and hypotheses presented in the introductory chapter.

Objective 1: Collect distribution data in TBP and TODGA solvent extraction systems under concentrated conditions that have not been previously characterized in the literature.

Hypothesis 1.1: The extraction of trace metals by TBP and lanthanides by TODGA adhere to a traditional solvation mechanism.

Hypothesis 1.2: The selectivity of TODGA for the light lanthanides results from outer coordination sphere effects.

Distribution data for the extraction of 11 trace metals by TBP in the presence of bulk uranium under PUREX extraction and stripping conditions were collected and published. Most metals followed the extraction behavior that would be expected based on a traditional understanding of extraction by solvation and the known affinity of TBP for uranium. The distribution ratios of these metals decreased with increasing uranium concentration under both extraction and stripping conditions. However, the distribution ratios of some low-valence transition metals were observed to increase with increasing uranium concentration, behavior that suggests an alternative extraction mechanism for these metals. One possible explanation for increased extraction of certain trace metals with increasing uranium concentration is co-extraction occurring through the formation of TBP colloidal aggreagates.

Distribution data for the extraction of bulk amounts of lanthanides by TODGA were collected at varying initial metal concentrations for light, middle, and heavy lanthanides. No anomalous extraction behavior was observed in the TODGA/lanthanide extraction system. Distribution ratios decreased exponentially with metal concentration, as is often observed in extraction systems as the extractant approaches saturation[34]. Distribution ratios increased across the lanthanide series as would be expected based on TODGA distribution studies of lanthanides at low concentrations. The amount of water co-extracted with each element was found to follow a pattern similar to that found for the extraction of the lanthanides across the

series. Because it has been established that water is not extracted in the inner coordination sphere of these metals, the similarity between these extraction patterns suggests that outer sphere effects may be responsible for the lanthanide selectivity of TODGA. One mechanism for this could be through the competing effects of increased extraction with the increase in charge density across the lanthanide series, and decreased solubility of TODGA extracted complexes with more co-extracted water.

Objective 2: Compare the results of diffusion NMR spectroscopy and SANS studies of organic phase TBP samples interpreted from a colloidal perspective.

Hypothesis 2.1: Like small angle scattering techniques, diffusion NMR spectroscopy can be used to characterize the nitric acid, uranium (VI) nitrate, and zirconium (IV) nitrate species extracted by TBP.

Diffusion NMR spectroscopy was used to measure the average diffusion coefficients of TBP species in samples similar to ones that had been characterized previously in the literature by small angle scattering. Dilution experiments were used to find the TBP infinite dilution diffusion coefficient for each sample, which was then related to the average volume of TBP species using the Wilke-Chang equation. The Wilke-Change volume was then converted to the diameter of an equivalent sphere for comparison to SANS results. The slope of the line relating the average TBP diffusion coefficient and TBP concentration in dilution experiments was assigned physical significance through comparison with colloidal systems. In colloidal systems, this slope is a reflection of the nature of the interactions between colloidal particles diffusing in a molecular solvent.

The average diameters of TBP aggregates from diffusion measurements were similar to those found previously using SANS, with TBP aggregation numbers for all samples of approximately two to four TBP molecules. However, the slope of the line relating the average TBP diffusion coefficient and TBP concentration in dilution experiments suggested that the interactions between TBP species were repulsive, rather than attractive as suggested in prior

small angle scattering experiments with TBP samples.

Objective 3: Assess the use of colloidal models to describe organic phase TBP samples by comparing the results of diffusion NMR spectroscopy, rheology, and SANS studies of samples under concentrated (PUREX-like) conditions.

Hypothesis 3.1: Nitric acid, uranium (VI) nitrate, and zirconium (IV) nitrate are extracted by TBP as colloidal species under PUREX-like conditions.

Identical TBP samples prepared under conditions similar to those found in the PUREX process were characterized by diffusion NMR spectroscopy, rheology, and SANS. When the results of these experiments were interpreted assuming that TBP forms colloidal aggregates, contradictory conclusions were reached about the sizes and interactions between aggregates. Diffusion measurements suggest that the average size of TBP species is not strongly impacted by TBP concentration, while SANS experiments suggest that TBP species are three times larger, by volume, in 30% TBP samples compared with 20% TBP samples. Diffusion measurements suggest repulsive interactions bewteen aggregates, while SANS experiments suggest attractive interactions. These contradictions are eliminated if assumptions about the colloidal nature of TBP species are discarded and these TBP samples are treated as molecular solutions. Such an approach is consistent with the results of MD simulations of TBP/nitric acid systems.

6.1 Future Directions

In this work, molecular-scale details about TBP and TODGA-extracted metal species have been eludicated, laying the groundwork for further experimental and theoretical investigations of these systems. The potential importance of outer sphere coordination to extractant selectivity was established through TODGA distribution studies. A series of experiments with inorganic TBP samples suggested that the treatment of TBP species as colloidal aggregates under PUREX-like and similar conditions may be unfounded. Future

work would focus on continuing experiments to further understand molecular-scale characteristics of TBP and TODGA extracted species, while extending some experimental methods used here to investigate other solvent extraction systems.

The experimental characterization of TBP and TODGA species in solution presented in this thesis is complicated by the complexity of the samples under investigation. Organic phase solvent extraction samples prepared by contacting an aqeuous phase containing acid or metal, and an organic phase containing at least one extractant and diluent are, by their nature, at least quaternary systems. In samples prepared by solvent extraction, the contribution of any single component to an experimental measurement is difficult to isolate due to its impact on the extraction of other components. As a result, systematic investigations of organic phase samples with, for example, a constant organic phase water concentration and changing acid or metal concentration, are uncommon in the recent literature.

The species formed by extractants in the presence of different solutes could be more clearly distinguished if organic phase samples were prepared by direct dissolution of the desired solutes. Incremental changes could then be made in the compositions of such simple binary or ternary samples to isolate the impact of each component. For example, diffusion and small angle scattering measurements of a TBP organic phase in which anhydrous uranyl nitrate is dissolved would not be impacted by the contributions of water and nitric acid species. Similarly, determining the solubility limits of anhydrous lanthanide nitrates in a TODGA organic phase would contribute to an understanding of the impact of water on the solubility of TODGA-solvated lanthanides. Understanding the extraction of water, acids, and metals in applied separations could be greatly bolstered by such fundamental studies of simple organic phase samples.

In addition, other experimental and computational characterization methods could be used to explore microscopic structures in solvent extraction systems. Sophisticated NMR techniques such as 3-D diffusion-ordered spectroscopy (DOSY) could be used to differentiate between species in the diffusion domain, eliminating many problems associated with sepa-

rating the diffusion coefficients of species with identical resonances in the traditional 2-D DOSY experiment. Monte Carlo simulations could be used to understand simple behavior in these systems, such as the rate of extractant exchange or the role that the number and directionality of binding sites plays in the structures formed in solution.

Finally, the same methods presented in this thesis could be used to characterize other solvent extraction systems. The use of theoretical relationships developed for colloidal systems to interpret small angle scattering and other experimental data is not limited to TBP. Such relationships have also been used in other extractant systems, with similarly limited justification. Diffusion NMR spectroscopy could corroborate the use of colloidal approaches in these systems where appropriate, giving further validity to the physical parameters dervied from such analyses. A series of diffusion experiments like those presented in this thesis could be performed, in which extractant diffusion coefficients in dilutions of a solvent extraction sample are measured and interpreted from a colloidal approach. These results could then be compared with the results of small angle scattering experiments to ensure that the assumption of colloidal behavior applies to a given solvent extraction system.

REFERENCES CITED

[1] R. M. Diamond and D. G. Tuck. Extraction of inorganic compounds into organic solvents. In *Progress in Inorganic Chemistry*, pages 109–192. John Wiley & Sons, Inc., 1960.

[2] J. Ruhoff and P. Fain. The first fifty critical days. *Mallinckrodt Uranium Division News*, 7(3 & 4):3–9, June 1962.

[3] C. F. Coleman and R. E. Leuze. Some milestone solvent extraction processes at the Oak Ridge National Laboratory. *J. Tenn. Acad. Sci.*, 53(3):102–107, 1978.

[4] M E Whatley and G L Bridger. Solvent extraction of solution containing rare earths. Preparation of thorium compounds from monazite by sulfuric acid decomposition and solvent extraction. Technical Report ISC-115, Ames Lab., IA, 30 June 1950.

[5] M. S. Gerber. A brief history of the PUREX and UO_3 facilities. Technical report, Westinghouse Hanford Company, 1993.

[6] G. M. Ritcey. Development of industrial solvent extraction processes. In *Solvent Extraction Principles and Practice, 2nd Ed.*, pages 277–339. Marcel Dekker, New York, 2004.

[7] K. J. Moody, I. D. Hutcheon, and P. M. Grant. *Nuclear Forensic Analysis*. CRC Press, 2005.

[8] L. A. Bromley. Thermodynamic properties of strong electrolytes in aqueous solutions. *AIChE J.*, 19(2):313–320, 1973.

[9] K. S. Pitzer. Thermodynamics of electrolytes. I. theoretical basis and general equations. *J. Phys. Chem.*, 77(2):268–277, 1973.

[10] K. S. Pitzer and G. Mayorga. Thermodynamics of electrolytes. II. activity and osmotic coefficients for strong electrolytes with one or both ions univalent. *J. Phys. Chem.*, 77 (19):2300–2308, 1973.

[11] C. L. Kusik and H. P. Meissner. Calculating activity coefficients in hydrometallurgy—a review. *Int. J. Miner. Process.*, 2(2):105–115, 1975.

[12] W. B. Lanham and T. C. Runion. Purex process for plutonium and uranium recovery. Technical Report ORNL-479(Del.), Oak Ridge National Laboratory, 1949.

[13] S. A. Ansari, P. Pathak, P. K. Mohapatra, and V. K. Manchanda. Chemistry of diglycolamides: promising extractants for actinide partitioning. *Chem. Rev.*, 112(3): 1751–1772, 2012.

[14] A. V. Gelis and G. J. Lumetta. Actinide Lanthanide Separation Process—ALSEP. *Ind. Eng. Chem. Res.*, 53(4):1624–1631, 2014.

[15] M. Husain, S. A. Ansari, P. K. Mohapatra, R. K. Gupta, V. S. Parmar, and V. K. Manchanda. Extraction chromatography of lanthanides using N,N,N',N'-tetraoctyl diglycolamide (TODGA) as the stationary phase. *Desalination*, 229(1–3):294–301, 2008.

[16] A. P. Zozulya and V. M. Peshkova. Investigation of complex formation in solution by the distribution method. *Russ. Chem. Rev.*, 29(2):101–118, 1960.

[17] E. R. Irish and W. H. Reas. The PUREX process — A solvent extraction reprocessing method for irradiated uranium. Technical Report HW-49483 A, Hanford Atomic Products Operation, 1957.

[18] J. Rydberg, G. R. Choppin, C. Musickas, and T. Sekine. Solvent extraction equilibria. In *Solvent Extraction Principles and Practice, 2nd Ed.*, pages 109–202. Marcel Dekker, New York, 2004.

[19] T. V. Healy and H. A. C. McKay. The extraction of nitrates by tri-*n*-butyl phosphate (TBP). part 2.—the nature of the TBP phase. *Trans. Faraday Soc.*, 52:633–642, 1956.

[20] Z. Zhu, Y. Sasaki, H. Suzuki, S. Suzuki, and T. Kimura. Cumulative study on solvent extraction of elements by N,N,N',N'-tetraoctyl-3-oxapentanediamide (TODGA) from nitric acid into *n*-dodecane. *Anal. Chim. Acta*, 527(2):163–168, 2004.

[21] Y. Marcus. Solvent extraction of inorganic species. *Chem. Rev.*, 63(2):139–170, 1963.

[22] Y. Marcus and A. S. Kertes. *Ion Exchange and Solvent Extraction of Metal Complexes*. John Wiley & Sons, Ltd., 1969.

[23] C. F. J. Colón, H. K. Moffat, and R. R. Rao. Modeling of liquid-liquid extraction (LLE) equilibria using Gibbs energy minimization (GEM) for the system TBP–HNO_3–UO_2–H_2O–diluent. *Solvent Extr. Ion Exch.*, 31(6):634–651, 2013.

[24] R. Chiarizia, K. L. Nash, M. P. Jensen, P. Thiyagarajan, and K. C. Littrell. Application of the Baxter model for hard spheres with surface adhesion to SANS data for the U(VI)—HNO_3—TBP—*n*-dodecane system. *Langmuir*, 19(23):9592–9599, 2003.

[25] S. Nave, C. Mandin, L. Martinet, L. Berthon, F. Testard, C. Madic, and T. Zemb. Supramolecular organisation of tri-n-butyl phosphate in organic diluent on approaching third phase transition. *Phys. Chem. Chem. Phys.*, 6(4):799–808, 2004.

[26] R. Chiarizia, M. P. Jensen, M. Borkowski, P. Thiyagarajan, and K. C. Littrell. Interpretation of third phase formation in the Th(IV)–HNO_3, TBP–n-octane system with Baxter's "sticky spheres" model. *Solvent Extr. Ion Exch.*, 22(3):325–351, 2004.

[27] R. Chiarizia, M. P. Jensen, P. G. Rickert, Z. Kolarik, M. Borkowski, and P. Thiyagarajan. Extraction of zirconium nitrate by TBP in n-octane: Influence of cation type on third phase formation according to the "sticky spheres" model. *Langmuir*, 20(25): 10798–10808, 2004.

[28] J. Plaue, A. Gelis, K. Czerwinski, P. Thiyagarajan, and R. Chiarizia. Small-angle neutron scattering study of plutonium third phase formation in 30% TBP/HNO_3/alkane diluent systems. *Solvent Extr. Ion Exch.*, 24(3):283–298, 2006.

[29] R. Chiarizia, M. P. Jensen, M. Borkowski, and K. L. Nash. A new interpretation of third-phase formation in the solvent extraction of actinides by TBP. In *Separations for the Nuclear Fuel Cycle in the 21st Century*, ACS Symposium Series, chapter 9, pages 135–150. American Chemical Society, Washington D. C., 2006.

[30] R. Chiarizia, A. Briand, M. P. Jensen, and P. Thiyagarajan. Sans study of reverse micelles formed upon the extraction of inorganic acids by TBP in n-octane. *Solvent Extr. Ion Exch.*, 26(4):333–359, 2008.

[31] K. Osseo-Asare. Aggregation, reversed micelles, and microemulsions in liquid-liquid extraction: The tri-n-butyl phosphate—diluent—water—electrolyte system. *Adv. Colloid Interface Sci.*, 37(1–2):123–173, 1991.

[32] C. Erlinger, L. Belloni, T. Zemb, and C. Madic. Attractive interactions between reverse aggregates and phase separation in concentrated malonamide extractant solutions. *Langmuir*, 15(7):2290–2300, 1999.

[33] A. Naylor and H. Eccles. Tri-n-butyl phosphate—The universal solvent for the nuclear fuel cycle. In *Proceedings of ISEC '88*, pages 31–36, Moscow, 1988. Vernadsky Institute of Geochemistry and Analytical Chemistry of the USSR Academy of Sciences.

[34] G. Petrich and Z. Kolarik. *The 1981 Purex Distribution Data Index.* Kernforschungszentrum Karlsruhe GmbH, 1981.

[35] K. Alcock, F. C. Bedford, W. H. Hardwick, and H. A. C. McKay. Tri-n-butyl phosphate as an extracting solvent for inorganic nitrates—I: Zirconium nitrate. *J. Inorg. Nucl. Chem.*, 4(2):100–105, 1957.

[36] D. Scargill, K. Alcock, and J. M. Fletcher. Tri-*n*-butyl phosphate as an extracting solvent for inorganic nitrates—II: Yttrium and the lower lanthanide nitrates. *J. Inorg. Nucl. Chem.*, 4(12):304–314, 1957.

[37] E. Hesford, H. A. C. McKay, and D. Scargill. Tri-*n*-butyl phosphate as an extracting solvent for inorganic nitrates—IV: Thorium nitrate. *J. Inorg. Nucl. Chem.*, 4:321–325, 1957.

[38] G. F. Best, H. A. C. McKay, and P. R. Woodgate. Tri-*n*-butyl phosphate as an extracting solvent for inorganic nitrates—III: The plutonium nitrates. *J. Inorg. Nucl. Chem.*, 4:315–320, 1957.

[39] K. Alcock, G. F. Best, E. Hesford, and H. A. C. McKay. Tri-*n*-butyl phosphate as an extracting solvent for inorganic nitrates—V: Further results for the tetra- and hexavalent actinide nitrates. *J. Inorg. Nucl. Chem.*, 6:328–333, 1958.

[40] T. Ishimori and K. Watanabe. Inorganic extraction studies on the system of tri-*n*-butyl phosphate—nitric acid. *Bull. Chem. Soc. Jpn.*, 33(10):1443–1448, 1960.

[41] D. F. Peppard, G. W. Mason, and J. L. Maier. Interrelationships in the solvent extraction behaviour of scandium, thorium, and zirconium in certain tributyl phosphate—mineral acid systems. *J. Inorg. Nucl. Chem.*, 3(3-4):215–228, 1956.

[42] H. Pollock. A stable diluent for Purex process extractants. Technical Report DP-294, Savannah River Laboratory, 1958.

[43] J. R. Flanary. Purex 1A column studies. Technical Report CF-52-4-13, Oak Ridge National Laboratory, 1952.

[44] R. M. Wallace and H. Pollock. Anomalous extraction of zirconium, niobium, and ruthenium by tributyl phosphate. Technical Report DP-308, Savannah River Laboratory, September 1958.

[45] V. Sagar, K. V. Chetty, and D. D. Sood. Extraction of plutonium (III) by TBP in presence of uranium. *Solvent Extr. Ion Exch.*, 18(2):307–317, 2000.

[46] I. Svantesson, I. Hagström, G. Persson, and J. O. Liljenzin. Distribution ratios and empirical equations for the extraction of elements in PUREX high level waste solution—I: TBP. *J. Inorg. Nucl. Chem.*, 41(3):383–389, 1979.

[47] S. Tachimori and Y. Morita. Overview of solvent extraction chemistry for reprocessing. In *Ion Exchange and Solvent Extraction: A Series of Advances*, volume 19, chapter 1, pages 1–63. CRC Press, 2010.

[48] J. M. McKibben. Chemistry of the Purex process. *Radiochim. Acta*, 36:3–15, 1984.

[49] D. O. Campbell and W. D. Burch. The chemistry of fuel reprocessing: Present practices, future trends. *J. Radioanal. Nucl. Chem.*, 142(1):303–320, 1990.

[50] K. L. Nash and J. C. Braley. Challenges for actinide separations in advanced nuclear fuel cycles. In *Nuclear Energy and the Environment*, chapter 3, pages 19–38. American Chemical Society, 2010.

[51] V. J. Reilly. The hydrolysis of tributyl phosphate and its effect on the Purex process. Technical Report ORNL-1138, Oak Ridge National Laboratory, 1951.

[52] E. K. Dukes. The formation and effects of dibutyl phosphate in solvent extraction. Technical Report DP-250, Savannah River Laboratory, 1957.

[53] A. A. Siczek and M. J. Steindler. The chemistry of ruthenium and zirconium in the PUREX solvent extraction process. *At. Energ. Rev.*, 16(4):575–618, 1978.

[54] R. J. Guenther, D. E. Blahnik, U. P. Jenquin, J. E. Mendel, L. E. Thomas, and C. K. Thornhill. Characterization of spent fuel approved testing material—ATM-104. Technical report, Pacific Northwest Laboratory, 1991.

[55] T. Izumida and F. Kawamura. Precipitates formation behavior in simulated high level liquid waste of fuel reprocessing. *J. Nucl. Sci. Technol.*, 27(3):267–274, 1990.

[56] G. Choppin, J. O. Liljenzin, J. Rydberg, and C. Ekberg. *Radiochemistry and Nuclear Chemistry*. Academic Press, 2013.

[57] M. A. Koehl, R. S. Rundberg, and J. C. Braley. Measured neutron flux parameters in the USGS TRIGA MARK I reactor. *J. Radioanal. Nucl. Chem.*, 306(1):31–38, 2015.

[58] C. Miyake, M. Hirose, T. Yoshimura, M. Ikeda, S. Imoto, and M. Sano. "The third phase" of extraction processes in fuel reprocessing, (I), formation conditions, compositions and structures of precipitates in Zr-degradation products of TBP systems. *J. Nucl. Sci. Technol.*, 27(2):157–166, 1990.

[59] D. J. Pruett. *Science and Technology of Tributyl Phosphate*, volume 3, chapter Extraction Chemistry of Fission Products, pages 81–122. CRC Press, 1990.

[60] P. G. M. Brown, J. M. Fletcher, and A. G. Wain. Nitrato nitrosylruthenium complexes and their extraction from nitric acid systems by tributyl phosphate. Part I. Laboratory studies. Technical Report AERE-C/R-2260, Atomic Energy Research Establishment (United Kingdom), 15 May 1957.

[61] E. Hesford and H. A. C. McKay. The extraction of nitrates by tri-n-butyl phosphate (TBP). Part 3.—Extraction at trace concentrations. *Trans. Faraday Soc.*, 54:573–586, 1958.

[62] P. Schatzberg. Solubilities of water in several normal alkanes from C_7 to C_{16}. *J. Phys. Chem.*, 67(4):776–779, 1963.

[63] Y. Marcus. *Ion Properties*. CRC Press, 1997.

[64] P. G. M. Brown, J. M. Fletcher, C. J. Hardy, J. Kennedy, D. Scargill, A. G. Wain, and J. L. Woodhead. The significance of certain complexes of ruthenium, niobium, zirconium and uranium in plant processes. In *Conference on the Peaceful Uses of Atomic Energy, Vol. 18*, pages 118–129, 1959.

[65] T. H. Siddall. Effects of structure of N,N-disubstituted amides on their extraction of actinide and zirconium nitrates and of nitric acid. *J. Phys. Chem.*, 64(12):1863–1866, 1960.

[66] Y. Sasaki, Y. Sugo, S. Suzuki, and S. Tachimori. The novel extractants, diglycolamides, for the extraction of lanthanides and actinides in HNO_3–n-dodecane system. *Solvent Extr. Ion Exch.*, 19(1):91–103, 2001.

[67] K. L. Nash. A review of the basic chemistry and recent developments in trivalent f-elements separations. *Solvent Extr. Ion Exch.*, 11(4):729–768, 1993.

[68] R. J. Ellis, D. M. Brigham, L. Delmau, A. S. Ivanov, N. J. Williams, M. N. Vo, B. Reinhart, B. A. Moyer, and V. S. Bryantsev. "Straining" to separate the rare earths: How the lanthanide contraction impacts chelation by diglycolamide ligands. *Inorg. Chem.*, 56(3):1152–1160, 2017.

[69] S. D. Reilly, A. J. Gaunt, B. L. Scott, G. Modolo, M. Iqbal, W. Verboom, and M. J. Sarsfield. Plutonium(IV) complexation by diglycolamide ligands—coordination chemistry insight into TODGA-based actinide separations. *Chem. Commun.*, 48(78):9732, 2012.

[70] S. Okumura, T. Kawasaki, Y. Sasaki, and Y. Ikeda. Crystal structures of lanthanoid(III) (Ln(III), Ln = Tb, Dy, Ho, Er, Tm, Yb, and Lu) nitrate complexes with N,N,N',N'-tetraethyldiglycolamide. *Bull. Chem. Soc. Jpn.*, 87(10):1133–1139, 2014.

[71] M. R. Antonio, D. R. McAlister, and E. P. Horwitz. An europium(III) diglycolamide complex: Insights into the coordination chemistry of lanthanides in solvent extraction. *Dalton Trans.*, 44:515–521, 2015.

[72] S. Tachimori, Y. Sasaki, and S. Suzuki. Modification of TODGA—n-dodecane solvent with a monoamide for high loading of lanthanides (III) and actinides (III). *Solvent Extr. Ion Exch.*, 20(6):687–699, 2002.

[73] P. N. Pathak, S. A. Ansari, S. V. Godbole, A. R. Dhobale, and V. K. Manchanda. Interaction of Eu^{3+} with N,N,N',N'-tetraoctyl diglycolamide: A time resolved luminescence spectroscopy study. *Spectrochim. Acta, Part A*, 73(2):348–352, 2009.

[74] G. Ferru, B. Reinhart, M. K. Bera, M. Olvera de la Cruz, B. Qiao, and R. J. Ellis. The lanthanide contraction beyond coordination chemistry. *Chem. - Eur. J.*, 22(20): 6899–6904, 2016.

[75] K. Osseo-Asare. Enhanced solvent extraction with water-in-oil microemulsions. *Sep. Sci. Technol.*, 23(12–13):1269–1284, 1988.

[76] R. G. Geier. PUREX process solvent: Literature review. Technical Report RHO-LD-74, Rockwell Hanford Operations, 1979.

[77] A. S. Kertes. Chemistry of the formation and elimination of a third phase in organophosphorus and amine extractant systems. In *Solvent Extraction Chemistry of Metals*, pages 377–400, London, 1965. Macmillan.

[78] P. R. V. Rao and Z. Kolarik. A review of third phase formation in extraction of actinides by neutral organophosphorus extractants. *Solvent Extr. Ion Exch.*, 14(6): 955–993, 1996.

[79] S. Nave, G. Modolo, C. Madic, and F. Testard. Aggregation properties of N,N,N',N'-tetraoctyl-3-oxapentanediamide (TODGA) in n-dodecane. *Solvent Extr. Ion Exch.*, 22 (4):527–551, 2004.

[80] R. J. Ellis, M. Audras, and M. R. Antonio. Mesoscopic aspects of phase transitions in a solvent extraction system. *Langmuir*, 28(44):15498–15504, 2012.

[81] B. Cabane. Small-angle scattering methods. In R. Zana, editor, *Surfactant Solutions: New Methods of Investigation*, volume 22 of *Surfactant Science Series*, pages 57–146. M. Dekker, New York, 1986.

[82] J. S. Pedersen. Analysis of small-angle scattering data from colloids and polymer solutions: Modeling and least-squares fitting. *Adv. Colloid Interface Sci.*, 70:171–210, 1997.

[83] G. Ferru, D. Gomes Rodrigues, L. Berthon, O. Diat, P. Bauduin, and P. Guilbaud. Elucidation of the structure of organic solutions in solvent extraction by combining molecular dynamics and X-ray scattering. *Angew. Chem. Int. Ed. Engl.*, 53(21):5346–5350, 2014.

[84] B. Qiao, G. Ferru, M. Olvera de la Cruz, and R. J. Ellis. Molecular origins of mesoscale ordering in a metalloamphiphile phase. *ACS Cent. Sci*, 1(9):493–503, 2015.

[85] M. K. Bera, B. Qiao, S. Seifert, B. P. Burton-Pye, M. Olvera de la Cruz, and M. R. Antonio. Aggregation of heteropolyanions in aqueous solutions exhibiting short-range attractions and long-range repulsions. *J. Phys. Chem. C*, 120(2):1317–1327, 2016.

[86] L. A. Feigin and D. I. Svergun. *Structure Analysis by Small-Angle X-Ray and Neutron Scattering*. Springer US, 1987.

[87] O. Glatter and R. May. Small-angle techniques. In *International Tables for Crystallography*, volume C, chapter 2.6, pages 89–112. Kluwer Academic Publishers, 2004.

[88] W. S. Price. Pulsed-field gradient nuclear magnetic resonance as a tool for studying translational diffusion: Part I. Basic theory. *Concepts Magn. Reson.*, 9(5):299–336, 1997.

[89] W. S. Price. Pulsed-field gradient nuclear magnetic resonance as a tool for studying translational diffusion: Part II. Experimental aspects. *Concepts Magn. Reson.*, 10(4): 197–237, 1998.

[90] Y. Cohen, L. Avram, and L. Frish. Diffusion NMR spectroscopy in supramolecular and combinatorial chemistry: An old parameter—new insights. *Angew. Chem.*, 44(4): 520–554, 2005.

[91] B. Lindman, O. Söderman, and H. Wennerström. NMR studies of surfactant systems. In *Surfactant Solutions: New Methods of Investigation*, volume 22 of *Surfactant Science Series*, pages 295–357. Marcel Dekker, New York, 1986.

[92] C. R. Wilke and P. Chang. Correlation of diffusion coefficients in dilute solutions. *AIChE J.*, 1(2):264–270, 1955.

[93] J. E. Tanner. Use of the stimulated echo in NMR diffusion studies. *J. Chem. Phys.*, 52(5):2523–2526, 1970.

[94] S. J. Gibbs and C. S. Johnson. A PFG NMR experiment for accurate diffusion and flow studies in the presence of eddy currents. *J. Magn. Reson.*, 93(2):395–402, 1991.

[95] SDBSWeb (National Institute of Advanced Industrial Science and Technology). SDBS no.: 2905. http://sdbs.db.aist.go.jp/sdbs/. Accessed: 27 June 2017.

[96] D. R. Caudwell, J. P. M. Trusler, V. Vesovic, and W. A. Wakeham. The viscosity and density of n-dodecane and n-octadecane at pressures up to 200 MPa and temperatures up to 473 K. *Int. J. Thermophys.*, 25(5):1339–1352, 2004.

[97] S. A. Willis, T. Stait-Gardner, A. S. Virk, R. Masuda, M. Zubkov, G. Zheng, and W. S. Price. Diffusion: Definition, description and measurement. In *Modern NMR Techniques for Synthetic Chemistry*, pages 125–176. CRC Press, 2015.

[98] L. M. M. Nazário, T. A. Hatton, and J. P. S. G. Crespo. Nonionic cosurfactants in AOT reversed micelles: Effect on percolation, size, and solubilization site. *Langmuir*, 12(26):6326–6335, 1996.

[99] F. Pitré, C. Regnaut, and M. P. Pileni. Structural study of AOT reverse micelles containing native and modified α-chymotrypsin. *Langmuir*, 9:2865–2860, 1993.

[100] W. van Megen and S. M. Underwood. Tracer diffusion in concentrated colloidal dispersions. III. Mean squared displacements and self-diffusion coefficients. *J. Chem. Phys.*, 91(1):552–559, 1989.

[101] E. L. Cussler. *Diffusion: Mass Transfer in Fluid Systems*. Cambridge University Press, 1997.

[102] W. M. Deen. *Analysis of Transport Phenomena*. Oxford University Press, 2012.

[103] W. Davis, J. Mrochek, and C. J. Hardy. The system: Tri-n-butyl phosphate (TBP)–nitric acid–water—I Activities of TBP in equilibrium with aqueous nitric acid and partial molar volumes of the three components in the TBP phase. *J. Inorg. Nucl. Chem.*, 28(9):2001–2014, 1966.

[104] B. Lindman and U. Olsson. Structure of microemulsions studied by NMR. *Ber. Bunsen-Ges.*, 100(3):344–363, 1996.

[105] I. Teraoka. *Polymer Solutions: An Introduction to Physical Properties*. John Wiley & Sons, 2002.

[106] G. A. Morris. Diffusion-ordered spectroscopy. In *eMagRes*. John Wiley & Sons, Ltd, 2007.

[107] S. Hanna, W. Hess, and R. Klein. Self-diffusion of spherical Brownian particles with hard-core interaction. *Physica A*, 111(1):181–199, 1982.

[108] N. Yoshida. Concentration dependence of the self-diffusion coefficient of hard spheres in solution. *Chem. Phys. Lett.*, 101(6):555–561, 1983.

[109] J. M. Rallison and E. J. Hinch. The effect of particle interactions on dynamic light scattering from a dilute suspension. *J. Fluid Mech.*, 167:131–168, 1986.

[110] H. Löwen. Brownian dynamics of hard spherocylinders. *Phys. Rev. E*, 50(2):1232–1242, 1994.

[111] R. J. Baxter. Percus-Yevick equation for hard spheres with surface adhesion. *J. Chem. Phys.*, 49(6):2770–2774, 1968.

[112] A. G. Kikhney and D. I. Svergun. A practical guide to small angle X-ray scattering (SAXS) of flexible and intrinsically disordered proteins. *FEBS Lett.*, 589(19 Pt A): 2570–2577, 2015.

[113] A. Stradner, H. Sedgwick, F. Cardinaux, W. C. K. Poon, S. U. Egelhaaf, and P. Schurtenberger. Equilibrium cluster formation in concentrated protein solutions and colloids. *Nature*, 432(7016):492–495, 2004.

[114] F. Sciortino, S. Mossa, E. Zaccarelli, and P. Tartaglia. Equilibrium cluster phases and low-density arrested disordered states: The role of short-range attraction and long-range repulsion. *Phys. Rev. Lett.*, 93(5):055701, 2004.

[115] H. A. C. McKay. TBP: Meeting-point of science and technology. In *Solvent Extraction Chemistry*, pages 185–194, Amsterdam, 1967. North-Holland Pub. Co.

[116] K. Alcock, S. S. Grimley, T. V. Healy, J. Kennedy, and H. A. C. McKay. The extraction of nitrates by tri-*n*-butyl phosphate (TBP). Part 1.—The system TBP + diluent + H_2O + HNO_3. *Trans. Faraday Soc.*, 52:39–47, 1956.

[117] A. M. Rozen. Problems in the physical chemistry of solvent extraction. In *Solvent Extraction Chemistry*, pages 195–235, Amsterdam, 1967. North-Holland Pub. Co.

[118] F. Testard, T. Zemb, P. Bauduin, and L. Berthon. Third-phase formation in liquid/liquid extraction: A colloidal approach. In *Ion Exchange and Solvent Extraction: A Series of Advances*, volume 19, chapter 7, pages 381–428. CRC Press, 2009.

[119] D. Langevin. Micelles and microemulsions. *Annu. Rev. Phys. Chem.*, 43(1):341–369, 1992.

[120] W. M. Gelbart and A. Ben-Shaul. The "new" science of "complex fluids". *J. Phys. Chem.*, 100(31):13169–13189, 1996.

[121] S. P. Moulik and B. K. Paul. Structure, dynamics and transport properties of microemulsions. *Adv. Colloid Interface Sci.*, 78(2):99–195, 1998.

[122] A. K. Rakshit and S. P. Moulik. Physicochemistry of W/O microemulsions: Formation, stability, and droplet clustering. In *Microemulsions: Properties and Applications*, volume 144 of *Surfactant Science*, pages 17–57. CRC Press, 2008.

[123] M. K. Bera, R. J. Ellis, B. P. Burton-Pye, and M. R. Antonio. Structural aspects of heteropolyacid microemulsions. *Phys. Chem. Chem. Phys.*, 16(41):22566–22574, 2014.

[124] R. O. Watts, D. Henderson, and R. J. Baxter. Hard spheres with surface adhesion: The Percus-Yevick approximation and the energy equation. In *Advances in Chemical Physics*, pages 421–430. John Wiley & Sons, Inc., 1971.

[125] Y. C. Chiew and E. D. Glandt. Percolation behaviour of permeable and of adhesive spheres. *J. Phys. A: Math. Gen.*, 16(11):2599–2608, 1983.

[126] G. Stell. Sticky spheres and related systems. *J. Stat. Phys.*, 63(5–6):1203–1221, 1991.

[127] M. A. Miller and D. Frenkel. Phase diagram of the adhesive hard sphere fluid. *J. Chem. Phys.*, 121(1):535–545, 2004.

[128] A. G. Baldwin, Y. Yang, N. J. Bridges, and J. C. Braley. Tributyl phosphate aggregation in the presence of metals: An assessment using diffusion NMR spectroscopy. *J. Phys. Chem. B*, 120(47):12184–12192, 2016.

[129] G. K. Batchelor. Brownian diffusion of particles with hydrodynamic interaction. *J. Fluid Mech.*, 74(1):1–29, 1976.

[130] R. O. Sokolovskii, M. Thachuk, and G. N. Patey. Tracer diffusion in hard sphere fluids from molecular to hydrodynamic regimes. *J. Chem. Phys.*, 125(20):204502, 2006.

[131] B. R. Bird, W. E. Stewart, and E. N. Lightfoot. *Transport Phenomena*. John Wiley & Sons, 2007.

[132] G. D. Wignall, K. C. Littrell, W. T. Heller, Y. B. Melnichenko, K. M. Bailey, G. W. Lynn, D. A. Myles, V. S. Urban, M. V. Buchanan, D. L. Selby, and P. D. Butler. The 40 m general purpose small-angle neutron scattering instrument at Oak Ridge National Laboratory. *J. Appl. Crystallogr.*, 45(5):990–998, 2012.

[133] I. Grillo. Small-angle neutron scattering and applications in soft condensed matter. In *Soft Matter Characterization*, pages 723–782. Springer Netherlands, 2008.

[134] A. Dianoux and G. Lander, editors. *Neutron data booklet*. OCP Science, 2003.

[135] Scattering length density - GISAXS. `http://gisaxs.com/index.php/Scattering_Length_Density`, 21 January 2015. Accessed: 15 June 2017.

[136] S. V. Menon, V. K. Kelkar, and C. Manohar. Application of Baxter's model to the theory of cloud points of nonionic surfactant solutions. *Phys. Rev. A*, 43(2):1130–1133, 1991.

[137] I. Breßler, J. Kohlbrecher, and A. F. Thünemann. SASfit: a tool for small-angle scattering data analysis using a library of analytical expressions. *J. Appl. Crystallogr.*, 48(Pt 5):1587–1598, 2015.

[138] M. J. Servis, D. T. Wu, and J. C. Braley. Network analysis and percolation transition in hydrogen bonded clusters: Nitric acid and water extracted by tributyl phosphate. *Phys. Chem. Chem. Phys.*, 19(18):11326–11339, 2017.

[139] L. Martinez, R. Andrade, E. Birgin, and J. Martinez. PACKMOL: A package for building initial configurations for molecular dynamics simulations. *J. Comp. Chem.*, 30:2157–2164, 2009.

[140] B. Hess, C. Kutzner, D. Spoel, and E. Lindhal. GROMACS 4: Algorithms for highly efficient, load balanced, and scalable molecular dynamics simulation. *J. Chem. Theory Comp.*, 4(3):435–447, 2008.

[141] M. Gradzielski and H. Hoffman. Rheological properties of microemulsions. In *Handbook of Microemulsion Science and Technology*, pages 357–386. CRC Press, 1999.

[142] D. G. Thomas. Transport characteristics of suspension: VIII. A note on the viscosity of Newtonian suspensions of uniform spherical particles. *J. Colloid Sci.*, 20(3):267–277, 1965.

[143] M. Gradzielski and H. Hoffmann. Charged o/w microemulsion droplets. *Prog. Colloid Polym. Sci.*, 93:167–174, 1993.

[144] P. Malo de Molina, M. Zhang, A. V. Bayles, and M. E. Helgeson. Oil-in-water-in-oil multinanoemulsions for templating complex nanoparticles. *Nano Lett.*, 16(12):7325–7332, 2016.

[145] K. Osseo-Asare. Third phase formation in solvent extraction: A microemulsion model. In *Metal Separation Technologies Beyond 2000 : Integrating Novel Chemistry with Processing*, pages 339–346. Minerals, Metals and Materials Society, 1999.

[146] R. Pal and E. Rhodes. Viscosity/concentration relationships for emulsions. *J. Rheol.*, 33(7):1021–1045, 1989.

[147] B. R. Pauw. Everything SAXS: Small-angle scattering pattern collection and correction. *J. Phys. Condens. Matter*, 25(38):383201, 2013.

[148] A. V. Shvetsov, A. E. Schmidt, D. V. Lebedev, and V. V. Isaev-Ivanov. Method for calculating small-angle neutron scattering spectra using all-atom molecular dynamics trajectories. *J. Synch. Investig.*, 7(6):1124–1127, 2013.

[149] M. H. G. Duits, R. P. May, A. Vrij, and C. G. De Kruif. Small-angle neutron scattering of concentrated adhesive-hard-sphere dispersions. *Langmuir*, 7(1):62–68, 1991.

[150] O. Glatter. A new method for the evaluation of small-angle scattering data. *J. Appl. Crystallogr.*, 10(5):415–421, 1977.

[151] K. Müller and O. Glatter. Practical aspects to the use of indirect Fourier transformation methods. *Makromol. Chem.*, 183(2):465–479, 1982.

[152] J. Brunner-Popela and O. Glatter. Small-angle scattering of interacting particles. I. Basic principles of a global evaluation technique. *J. Appl. Crystallogr.*, 30(4):431–442, 1997.

[153] B. Weyerich, J. Brunner-Popela, and O. Glatter. Small-angle scattering of interacting particles. II. Generalized indirect Fourier transformation under consideration of the effective structure factor for polydisperse systems. *J. Appl. Crystallogr.*, 32(2):197–209, 1999.

[154] G. Fritz and O. Glatter. Structure and interaction in dense colloidal systems: Evaluation of scattering data by the generalized indirect Fourier transformation method. *J. Phys. Condens. Matter*, 18(36):S2403, 2006.

[155] M. G. Noro and D. Frenkel. Extended corresponding-states behavior for particles with variable range attractions. *J. Chem. Phys.*, 113(8):2941–2944, 2000.

[156] D. M. Petković. Some correlations of trialkyl phosphates dimerization constants. *J. Inorg. Nucl. Chem.*, 30(2):603–609, 1968.

[157] D. M. Petković and Z. B. Maksimović. On association of trialkyl phosphates. *J. Inorg. Nucl. Chem.*, 38(2):297–300, 1976.

[158] M. J. Servis, C. A. Tormey, D. T. Wu, and J. C. Braley. A molecular dynamics study of tributyl phosphate and diamyl amyl phosphonate self-aggregation in dodecane and octane. *J. Phys. Chem. B*, 120(10):2796–2806, 2016.

[159] R. H. Stokes. Tracer diffusion in binary solutions subject to a dimerization equilibrium. *J. Phys. Chem.*, 69(11):4012–4017, 1965.

[160] K. R. Harris, P. J. Newitt, and Z. J. Derlacki. Alcohol tracer diffusion, density, NMR and FTIR studies of aqueous ethanol and 2,2,2-trifluoroethanol solutions at 25°C. *J. Chem. Soc., Faraday Trans.*, 94(14):1963–1970, 1998.

[161] E. L. Hahn. Spin echoes. *Phys. Rev.*, 80(4):580–594, 1950.

APPENDIX A
SELECTED METHODS

An overview of selected methods used in the course of this thesis is presented here.

A.1 Diffusion NMR Spectroscopy

Diffusion NMR spectroscopy is used to measure the self-diffusion (also called tracer diffusion) of molecules in a liquid sample. In a basic pulsed-field gradient (PFG) diffusion experiment, a liquid sample is placed in a gradient coil capable of generating a linear magnetic field gradient along the $z-$axis of the sample, as shown in Figure A.1. A series of RF and magnetic field gradient pulses is applied to the sample as shown, for example, in Figure 4.3. The strength of the applied magnetic field gradient is varied for a certain number of steps (often 16 or 32), and at each gradient strength an NMR spectrum is acquired. The decay in the NMR signal intensity of a component with increasing gradient strength is related to the self-diffusion coefficient of that component by the Stejskal-Tanner equation[88]:

$$S(G) = S(0)\, e^{-\gamma^2 \delta^2 G^2 D\left(\Delta - \frac{\delta}{3}\right)} \tag{A.1}$$

where S is the intensity of the NMR signal at a given magnetic field gradient strength (G), γ is the gyromagnetic ratio of the nucleus being observed, δ is the gradient pulse length, Δ is the diffusion time, and D is the diffusion coefficient. Usually, the maximum gradient strength is chosen to correspond to at least 95% decay of the NMR signal intensity.

The basis for the PFG diffusion experiment was first suggested by the discovery of the spin-echo and stimulated-echo signals by Hahn in 1950[161]. Hahn discovered that the application of two 90° RF pulses to a sample in sequence resulted in a spontaneous NMR signal, which peaked after an amount of time, τ, equal to the separation of the centers of the two pulses (Figure A.2). This spontaneous NMR signal is referred to as the spin-echo, and results from rephasing of the tranverse magnetization by the second RF pulse. The spin-echo

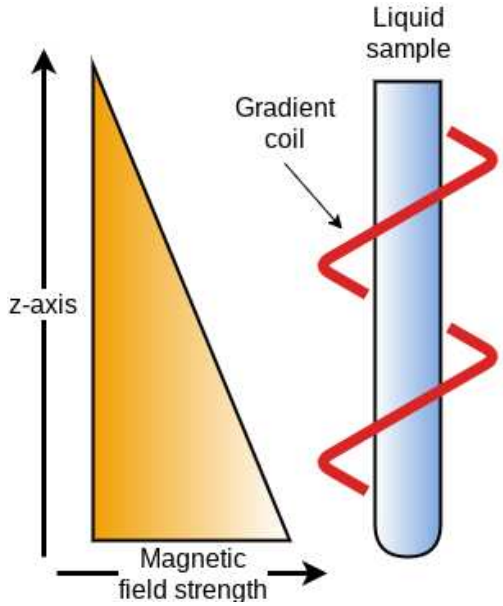

Figure A.1: In the PFG diffusion experiment, the sample is placed in a gradient coil that applies a linear magnetic field gradient along the $z-$axis of the sample.

signal is greatest for short pulse separations, and decays with longer separations due to decoherence introduced by spin-spin relaxation. Hahn also reported a stimulated-echo signal, correponding to a spontaneous NMR signal that results from the application of three 90° RF pulses to a sample (Figure A.3). The amplitude of the stimulated-echo signal is weighted by spin-lattice relaxation, which makes its use attractive for samples in which fast spin-spin relaxation makes the spin-echo signal undetectable.

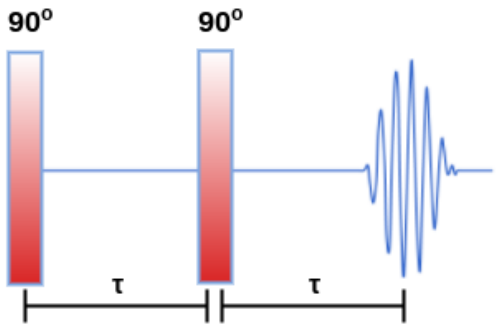

Figure A.2: The spin-echo pulse sequence and timing of the spin-echo signal.

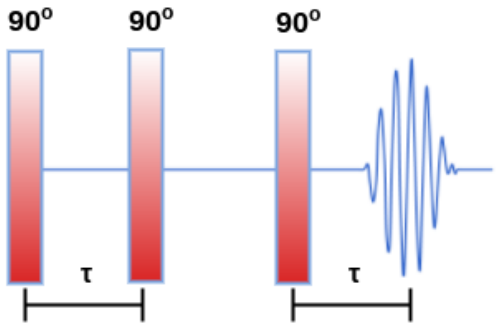

Figure A.3: The stimulated-echo pulse sequence and timing of the stimulated-echo signal.

A second concept important to the PFG diffusion experiment is the relationship between the magnetic field experienced by a nucleus and its Larmor frequency. This relationship is given in Equation A.2, where ω is the angular (Larmor) frequency of the precession of the magnetic moment of a nucleus with a gyromagnetic ratio of γ in the presence of a magnetic field of strength B.

$$\omega = \gamma B \tag{A.2}$$

When a magnetic field gradient is applied along the $z-$axis of a sample, the Larmor frequencies of nuclei in equivalent chemical environments are defined by their location along the $z-$axis of the sample.

The PFG diffusion experiment combines two magnetic field gradient pulses with a spin-or stimulated-echo pulse sequence, as in the stimulated-echo pulse sequence of Figure 4.3. The first gradient pulse effectively "marks" the location of nuclei along the $z-$axis of the sample and dephases the transverse magnetization. The second gradient pulse rephases the transverse magnetization. Rephasing is complete only if the nuclei do not move along the $z-$axis in the time between the gradient pulses. In the absence of movement, the echo signal amplitude is maximized. The echo signal amplitude is also maximized in the absence of a magnetic field gradient. At a constant magnetic field gradient pulse strength, the echo signal decreases with increasing displacement of the nuclei in the sample along the $z-$axis, which is related to their average rate of diffusion. Similarly, for nuclei moving at a constant rate,

the NMR signal intensity decreases with increasing gradient strength as shown in Figure 4.5. These relationships are contained in the Stejskal-Tanner equation.

A.2 Small Angle X-ray and Neutron Scattering

Small angle x-ray and neutron scattering (SAXS and SANS) are used to probe nanoscale (approximately 1 to 100 nm) structures in liquid and solid samples. X-rays are scattered by electrons, while neutrons are scattered by atomic nuclei. The pattern of scattered radiation in a SAXS or SANS experiment results from the distribution of scatterers in a sample. The mathematical principles used to understand both x-ray and neutron experiments are identical, although only liquid state SANS data are presented in this thesis. This appendix describes the scattering of both types of radiation at small angles in liquid state samples.

In a basic small angle scattering (SAS) experiment, a beam of monoenergetic radiation is passed through a thin liquid sample of known path length. Radiation deflected by the sample is detected by a 2-D detector placed on the other side of the sample from the radiation source, as shown in Figure A.4. The SAS experiment is run until the photon or neutron counting statistics-derived error estimates for all pixels in the detector are small. The resultant 2-D scattering pattern is then reduced by making various detector and background corrections, and converting the counts to an absolute scattering intensity (also known as the differential scattering cross-section) through calibration to a known source. This reduced 2-D scattering pattern can then be azimuthally averaged to produce a 1-D scattering pattern, where the $y-$axis is the absolute scattering intensity and the $x-$ axis is the magnitude of the scattering vector, q. The scattering vector magnitude is related to the scattering angle by Equation A.3, where θ is twice the scattering angle and λ is the wavelength of the radiation. The relationship between q and the approximate length scale, d, being probed in a sample is given by Equation A.4. The final 1-D scattering pattern can be interpreted using the direct or indirect methods, which are described in section 5.4.3.

$$q = \frac{4\pi \sin\theta}{\lambda} \tag{A.3}$$

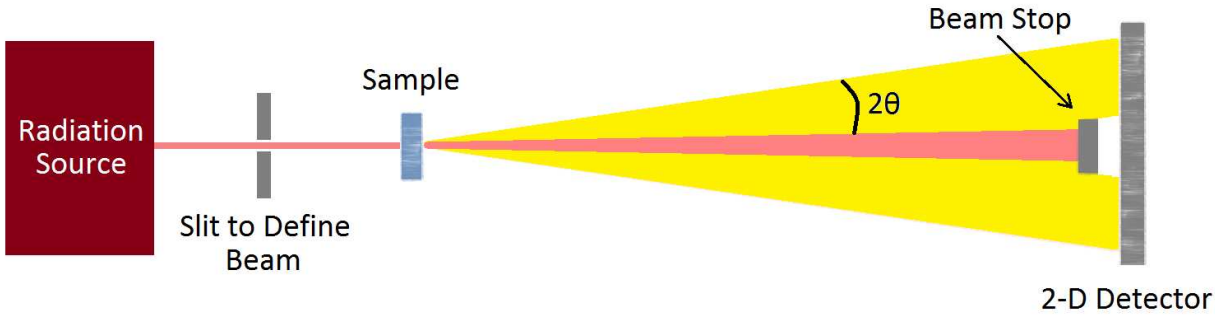

Figure A.4: In an SAS experiment, a beam of radiation is passed through a sample and deflected radiation is collected.

$$q = \frac{2\pi}{d} \tag{A.4}$$

APPENDIX B

SUPPORTING INFORMATION

The supporting information referenced in Chapter 2 is presented here.

* * *

The following figures show distribution ratio data for Mo, Zr, Ru, La, and Sm under PUREX extraction and stripping conditions at varying dibutyl phosphate concentrations.

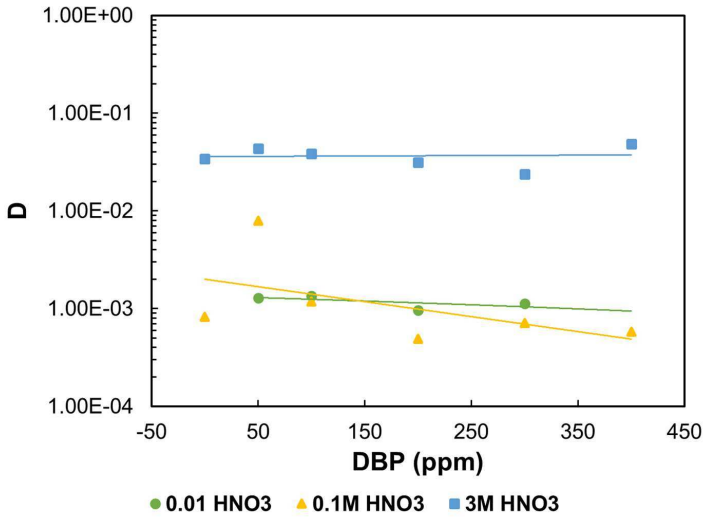

Figure S1: Variation in zirconium (IV) extraction with DBP concentration in an organic phase containing 30% TBP, *n*-dodecane and varying trace metals. Colors reflect different aqueous phase nitric acid concentrations.

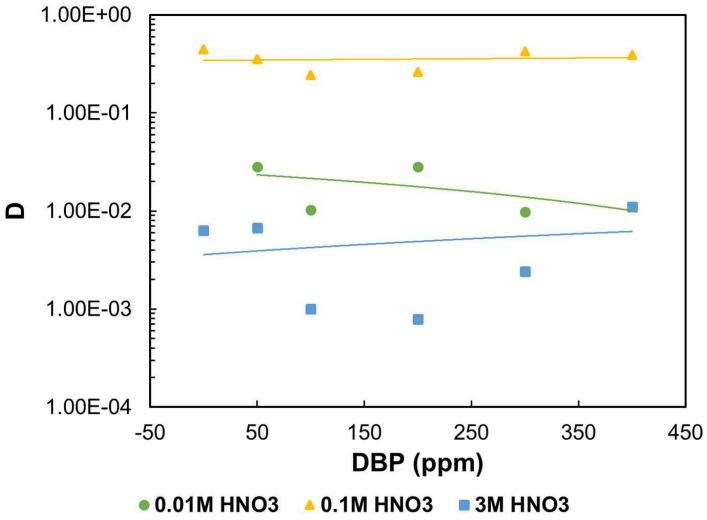

Figure S2: Variation in ruthenium (III) (as ruthenium nitrosyl) extraction with DBP concentration in the organic phase containing 30% TBP, *n*-dodecane and varying trace metals. Colors reflect different aqueous phase nitric acid concentrations.

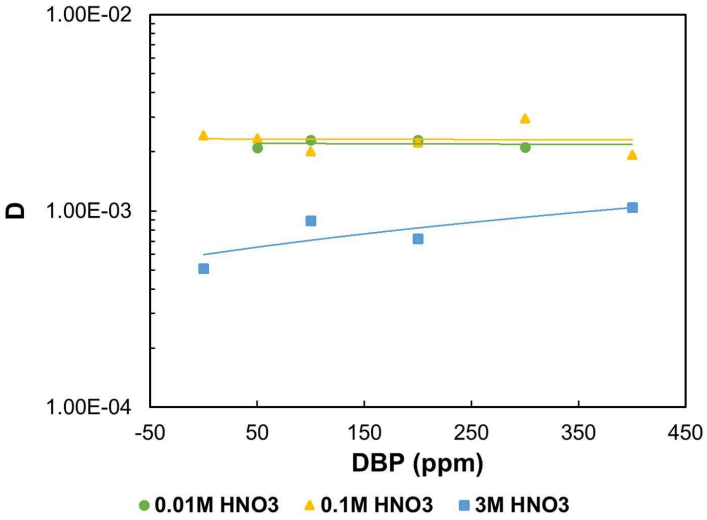

Figure S3: Variation in lanthanum (III) extraction with DBP concentration in the organic phase containing 30% TBP, *n*-dodecane and varying trace metals. Colors reflect different aqueous phase nitric acid concentrations.

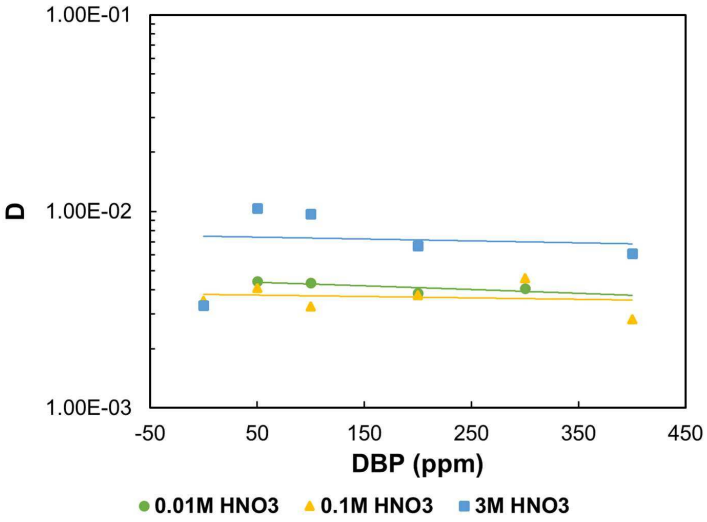

Figure S4: Variation in samarium (III) extraction with DBP concentration in the organic phase containing 30% TBP, *n*-dodecane and varying trace metals. Colors reflect different aqueous phase nitric acid concentrations.

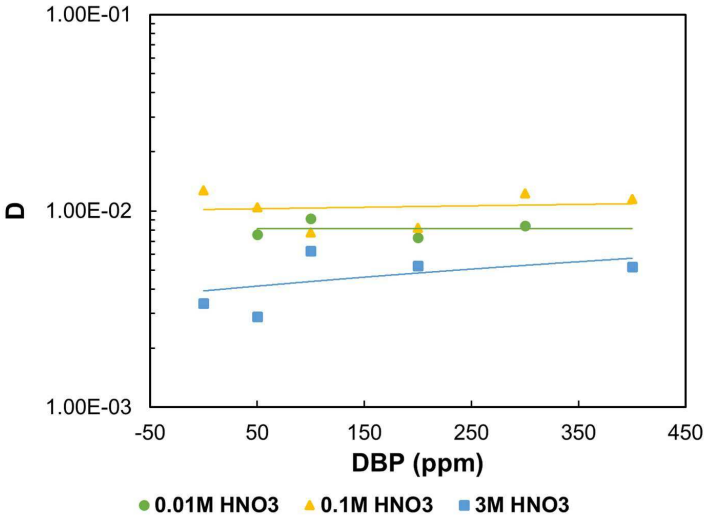

Figure S5: Variation in molybdenum (VI) (as molybdate) extraction with DBP concentration in the organic phase containing 30% TBP, *n*-dodecane and varying trace metals. Colors reflect different aqueous phase nitric acid concentrations.

APPENDIX C

COPYRIGHT PERMISSIONS

Copyright permissions from the publisher and co-authors of articles included in this thesis as Chapter 2, Chapter 4, and Chapter 5 are reproduced here.

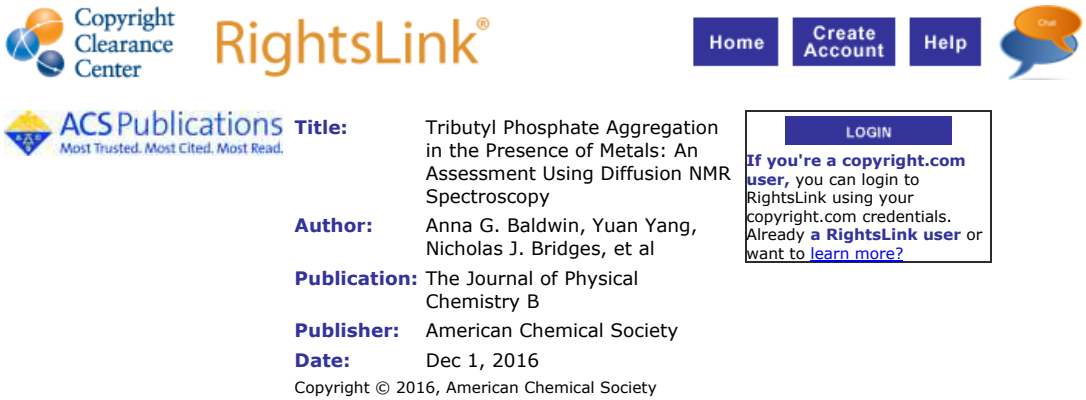

Copyright Clearance Center RightsLink®

Home | Create Account | Help

ACS Publications
Most Trusted. Most Cited. Most Read.

Title: Tributyl Phosphate Aggregation in the Presence of Metals: An Assessment Using Diffusion NMR Spectroscopy

Author: Anna G. Baldwin, Yuan Yang, Nicholas J. Bridges, et al

Publication: The Journal of Physical Chemistry B

Publisher: American Chemical Society

Date: Dec 1, 2016

Copyright © 2016, American Chemical Society

LOGIN

If you're a copyright.com user, you can login to RightsLink using your copyright.com credentials. Already **a RightsLink user** or want to learn more?

PERMISSION/LICENSE IS GRANTED FOR YOUR ORDER AT NO CHARGE

This type of permission/license, instead of the standard Terms & Conditions, is sent to you because no fee is being charged for your order. Please note the following:

- Permission is granted for your request in both print and electronic formats, and translations.
- If figures and/or tables were requested, they may be adapted or used in part.
- Please print this page for your records and send a copy of it to your publisher/graduate school.
- Appropriate credit for the requested material should be given as follows: "Reprinted (adapted) with permission from (COMPLETE REFERENCE CITATION). Copyright (YEAR) American Chemical Society." Insert appropriate information in place of the capitalized words.
- One-time permission is granted only for the use specified in your request. No additional uses are granted (such as derivative works or other editions). For any other uses, please submit a new request.

BACK | CLOSE WINDOW

Copyright © 2017 Copyright Clearance Center, Inc. All Rights Reserved. Privacy statement. Terms and Conditions.
Comments? We would like to hear from you. E-mail us at customercare@copyright.com

Copyright Clearance Center RightsLink®

Home | Create Account | Help

ACS Publications
Most Trusted. Most Cited. Most Read.

Title: Distribution of Fission Products into Tributyl Phosphate under Applied Nuclear Fuel Recycling Conditions

Author: Anna G. Baldwin, Nicholas J. Bridges, Jenifer C. Braley

Publication: Industrial & Engineering Chemistry Research

Publisher: American Chemical Society

Date: Dec 1, 2016

Copyright © 2016, American Chemical Society

LOGIN

If you're a copyright.com user, you can login to RightsLink using your copyright.com credentials. Already **a RightsLink user** or want to learn more?

PERMISSION/LICENSE IS GRANTED FOR YOUR ORDER AT NO CHARGE

This type of permission/license, instead of the standard Terms & Conditions, is sent to you because no fee is being charged for your order. Please note the following:

- Permission is granted for your request in both print and electronic formats, and translations.
- If figures and/or tables were requested, they may be adapted or used in part.
- Please print this page for your records and send a copy of it to your publisher/graduate school.
- Appropriate credit for the requested material should be given as follows: "Reprinted (adapted) with permission from (COMPLETE REFERENCE CITATION). Copyright (YEAR) American Chemical Society." Insert appropriate information in place of the capitalized words.
- One-time permission is granted only for the use specified in your request. No additional uses are granted (such as derivative works or other editions). For any other uses, please submit a new request.

BACK | CLOSE WINDOW

Copyright © 2017 Copyright Clearance Center, Inc. All Rights Reserved. Privacy statement. Terms and Conditions.
Comments? We would like to hear from you. E-mail us at customercare@copyright.com

Anna Baldwin <abaldwin@mymail.mines.edu>

Copyright Permissions for Thesis

2 messages

Anna G. Baldwin <abaldwin@mymail.mines.edu> Mon, Jul 17, 2017 at 3:56 PM
To: Jenifer Shafer <jshafer@mines.edu>

Hello Dr. Shafer,

In order for me to use previously published or submitted articles as chapters in my thesis, I am required to obtain written permission from all co-authors. This may be in the form of an email.

I would greatly appreciate if you would respond to this email granting me permission to use the following articles as chapters in my thesis:

Tributyl Phosphate Aggregation in the Presence of Metals: An Assessment Using Diffusion NMR Spectroscopy
Anna G. Baldwin, Yuan Yang, Nicholas J. Bridges, and Jenifer C. Braley
The Journal of Physical Chemistry B 2016 120 (47), 12184-12192
DOI: 10.1021/acs.jpcb.6b09154

Distribution of Fission Products into Tributyl Phosphate under Applied Nuclear Fuel Recycling Conditions
Anna G. Baldwin, Nicholas J. Bridges, and Jenifer C. Braley
Industrial & Engineering Chemistry Research 2016 55 (51), 13114-13119
DOI: 10.1021/acs.iecr.6b04056

The Structure of Tributyl Phosphate Solutions: Nitric Acid, Uranium (VI), and Zirconium (IV)
Anna G. Baldwin, Michael J. Servis, Yuan Yang, Nicholas J. Bridges, David T. Wu, and Jenifer C. Shafer

Thank you!
Anna G. Baldwin

Jenifer Shafer <jshafer@mines.edu> Mon, Jul 17, 2017 at 4:53 PM
To: Anna Baldwin <abaldwin@mymail.mines.edu>

HI Anna,

You have my permission.

Thank you!

Jen

Anna Baldwin <abaldwin@mymail.mines.edu>

Copyright Permissions for Thesis

4 messages

Anna G. Baldwin <abaldwin@mymail.mines.edu> Tue, Jul 11, 2017 at 9:47 AM
To: Yuan Yang <yuanyang@mines.edu>

Hello Yuan,

I hope your summer is going well!

In order for me to use previously published or submitted articles as chapters in my thesis, I am required to obtain written permission from all co-authors. This may be in the form of an email.

I would greatly appreciate if you would respond to this email granting me permission to use the following articles as chapters in my thesis:

Tributyl Phosphate Aggregation in the Presence of Metals: An Assessment Using Diffusion NMR Spectroscopy
Anna G. Baldwin, Yuan Yang, Nicholas J. Bridges, and Jenifer C. Braley
The Journal of Physical Chemistry B 2016 120 (47), 12184-12192
DOI: 10.1021/acs.jpcb.6b09154

The Structure of Tributyl Phosphate Solutions: Nitric Acid, Uranium (VI), and Zirconium (IV)
Anna G. Baldwin, Michael J. Servis, Yuan Yang, David T. Wu, and Jenifer C. Shafer

Thank you!
Anna G. Baldwin

Anna G. Baldwin <abaldwin@mymail.mines.edu> Tue, Jul 11, 2017 at 9:54 AM
To: Yuan Yang <yuanyang@mines.edu>

My apologies, the author list on the following article should read:

The Structure of Tributyl Phosphate Solutions: Nitric Acid, Uranium (VI), and Zirconium (IV)
Anna G. Baldwin, Michael J. Servis, Yuan Yang, Nicholas J. Bridges, David T. Wu, and Jenifer C. Shafer

Thank you!

Anna G. Baldwin
[Quoted text hidden]

Yuan Yang <yuanyang@mines.edu> Tue, Jul 11, 2017 at 3:05 PM
To: Anna Baldwin <abaldwin@mymail.mines.edu>

Hi Anna,

I am doing great and taking vacation right now in China.

Glad to hear that you are going to defend. Good Luck!

> Anna Baldwin has my permission to use the following articles as chapters in her thesis:
>
> **Tributyl Phosphate Aggregation in the Presence of Metals: An Assessment Using Diffusion NMR Spectroscopy**
> Anna G. Baldwin, Yuan Yang, Nicholas J. Bridges, and Jenifer C. Braley
> The Journal of Physical Chemistry B 2016 120 (47), 12184-12192
> DOI: 10.1021/acs.jpcb.6b09154
>
> **The Structure of Tributyl Phosphate Solutions: Nitric Acid, Uranium (VI), and Zirconium (IV)**
> Anna G. Baldwin, Michael J. Servis, Yuan Yang, David T. Wu, and Jenifer C. Shafer

Best,
Yuan Yang

Sent from my iPad
[Quoted text hidden]

Anna G. Baldwin <abaldwin@mymail.mines.edu> Wed, Jul 12, 2017 at 12:45 PM
To: Yuan Yang <yuanyang@mines.edu>

Thank you for getting back to me so quickly even though you're traveling!

Best,
Anna
[Quoted text hidden]

Anna Baldwin <abaldwin@mymail.mines.edu>

Copyright Permissions for Thesis

3 messages

Anna G. Baldwin <abaldwin@mymail.mines.edu> Tue, Jul 11, 2017 at 9:48 AM
To: "Michael John Servis (mservis@mymail.mines.edu)" <mservis@mymail.mines.edu>

Hello Michael,

I hope your summer is going well!

In order for me to use previously published or submitted articles as chapters in my thesis, I am required to obtain written permission from all co-authors. This may be in the form of an email.

I would greatly appreciate if you would respond to this email granting me permission to use the following articles as chapters in my thesis:

The Structure of Tributyl Phosphate Solutions: Nitric Acid, Uranium (VI), and Zirconium (IV)
Anna G. Baldwin, Michael J. Servis, Yuan Yang, David T. Wu, and Jenifer C. Shafer

Thank you!

Anna G. Baldwin

Anna G. Baldwin <abaldwin@mymail.mines.edu> Tue, Jul 11, 2017 at 9:53 AM
To: "Michael John Servis (mservis@mymail.mines.edu)" <mservis@mymail.mines.edu>

My apologies, the author list on the following article should read:

The Structure of Tributyl Phosphate Solutions: Nitric Acid, Uranium (VI), and Zirconium (IV)
Anna G. Baldwin, Michael J. Servis, Yuan Yang, Nicholas J. Bridges, David T. Wu, and Jenifer C. Shafer

Thank you!
Anna G. Baldwin
[Quoted text hidden]

Michael Servis <mservis@mymail.mines.edu> Mon, Jul 17, 2017 at 11:53 AM
To: "Anna G. Baldwin" <abaldwin@mymail.mines.edu>

My summer is going well. Thanks for asking.

I give permission to use the paper as a chapter in your thesis.

Good luck with your defense.

Best,

Michael
[Quoted text hidden]
--
Michael Servis
PhD Student, Nuclear Engineering
J. C. Braley Research Group
Colorado School of Mines

Anna Baldwin <abaldwin@mymail.mines.edu>

Copyright Permission for Thesis

2 messages

Anna G. Baldwin <abaldwin@mymail.mines.edu> Mon, Jul 17, 2017 at 3:54 PM
To: David Wu <dwu@mines.edu>

Hello Dr. Wu,

I hope you are enjoying your summer abroad!

Thank you for your comments on the TBP paper! They really helped me to clarify some ambiguities in the text, and fixed some important errors. Your input was invaluable, and I'm very grateful. Since I'm using it as a chapter in my thesis, I have to obtain written permission from all co-authors. It can be granted in the form of an email.

I would greatly appreciate if you would respond to this email granting me permission to use the following article as a chapter in my thesis:

The Structure of Tributyl Phosphate Solutions: Nitric Acid, Uranium (VI), and Zirconium (IV)
Anna G. Baldwin, Michael J. Servis, Yuan Yang, Nicholas J. Bridges, David T. Wu, and Jenifer C. Shafer

Thank you!
Anna G. Baldwin

David Wu <dwu@mines.edu> Mon, Jul 17, 2017 at 4:03 PM
To: Anna Baldwin <abaldwin@mymail.mines.edu>

Hi Anna,

Glad to be helpful. Yes, I grant you permission to use the article below as a chapter in your thesis.

Best wishes,
David Wu
[Quoted text hidden]

Anna Baldwin <abaldwin@mymail.mines.edu>

Copyright Permissions for Thesis

4 messages

Anna G. Baldwin <abaldwin@mymail.mines.edu> Tue, Jul 11, 2017 at 9:45 AM
To: Nicholas.Bridges@srnl.doe.gov

Hello Nick,

In order for me to use previously published or submitted articles as chapters in my thesis, I am required to obtain written permission from all co-authors. This may be in the form of an email.

I would greatly appreciate if you would respond to this email granting me permission to use the following articles as chapters in my thesis:

Tributyl Phosphate Aggregation in the Presence of Metals: An Assessment Using Diffusion NMR Spectroscopy
Anna G. Baldwin, Yuan Yang, Nicholas J. Bridges, and Jenifer C. Braley
The Journal of Physical Chemistry B 2016 120 (47), 12184-12192
DOI: 10.1021/acs.jpcb.6b09154

Distribution of Fission Products into Tributyl Phosphate under Applied Nuclear Fuel Recycling Conditions
Anna G. Baldwin, Nicholas J. Bridges, and Jenifer C. Braley
Industrial & Engineering Chemistry Research 2016 55 (51), 13114-13119
DOI: 10.1021/acs.iecr.6b04056

The Structure of Tributyl Phosphate Solutions: Nitric Acid, Uranium (VI), and Zirconium (IV)
Anna G. Baldwin, Michael J. Servis, Yuan Yang, David T. Wu, and Jenifer C. Shafer

Thank you!
Anna G. Baldwin

Anna G. Baldwin <abaldwin@mymail.mines.edu> Tue, Jul 11, 2017 at 9:54 AM
To: Nicholas.Bridges@srnl.doe.gov

My apologies, the author list on the following article should read:

The Structure of Tributyl Phosphate Solutions: Nitric Acid, Uranium (VI), and Zirconium (IV)
Anna G. Baldwin, Michael J. Servis, Yuan Yang, Nicholas J. Bridges, David T. Wu, and Jenifer C. Shafer

Thank you!

Anna G. Baldwin
[Quoted text hidden]

Nicholas.Bridges@srnl.doe.gov <Nicholas.Bridges@srnl.doe.gov> Tue, Jul 11, 2017 at 6:25 PM
To: "Anna G. Baldwin" <abaldwin@mymail.mines.edu>

Anna

As one of the co-authors on the detail articles below, you have my permission to use the articles as part of your dissertation.

Nicholas Bridges

Sent from my iPhone
[Quoted text hidden]

Anna G. Baldwin <abaldwin@mymail.mines.edu> Wed, Jul 12, 2017 at 12:46 PM
To: Nicholas.Bridges@srnl.doe.gov

Thank you!

Anna
[Quoted text hidden]